Microstructure of Ion Irradiated Nickel and Nickel–Copper Alloys

Lu-Min Wang

December 1988

UWFDM-783

Ph.D. thesis.

FUSION TECHNOLOGY INSTITUTE

UNIVERSITY OF WISCONSIN

MADISON WISCONSIN

Microstructure of Ion Irradiated Nickel and Nickel–Copper Alloys

Lu-Min Wang

Fusion Technology Institute
University of Wisconsin
1500 Engineering Drive
Madison, WI 53706

http://fti.neep.wisc.edu

December 1988

UWFDM-783

Ph.D. thesis.

MICROSTRUCTURE OF ION IRRADIATED NICKEL AND NICKEL-COPPER ALLOYS

by

LU-MIN WANG

A thesis submitted in partial fulfillment of the
requirements for the degree of

DOCTOR OF PHILOSOPHY
(Materials Science)

at the

UNIVERSITY OF WISCONSIN-MADISON

1988

MICROSTRUCTURE OF ION IRRADIATED NICKEL AND NICKEL-COPPER ALLOYS

Lu-Min Wang

Under the supervision of Professor Richard Arthur Dodd

Pure nickel and three concentrated Ni-Cu alloys, namely, Ni-10Cu (at.%), Ni-25Cu and Ni-50Cu, with various oxygen (residual or pre-injected) and helium (pre-injected) contents have been irradiated with 14 MeV nickel or copper ions up to a peak damage level of ~ 100 dpa at the same homologous temperature of 0.45 T_m to study the effects of gas and copper concentrations on the formation of radiation induced defect clusters. The depth dependent microstructures of the damaged region in the irradiated samples have been analyzed by cross-section transmission electron microscopy techniques.

Pre-injection of a small amount (10 to 75 appm) of helium or oxygen have considerably enhanced void formation in the irradiated pure nickel. The residual oxygen has also been found to play an important role in promoting void formation. Lowering the total oxygen content of the nickel samples from 180 appm to 75 appm considerably reduced the void density and increased void size. The experimental results on the effect of oxygen in this study support recent theoretical models which predict that oxygen can stabilize voids by reducing the metal surface energy and that gas is necessary for voids to form in nickel.

The Ni-Cu alloys showed great resistance to void formation under the irradiation conditions. Without oxygen pre-injection, voids formed in irradiated Ni-10Cu only at the peak displacement damage level of ~ 100 dpa, but no voids were observed in Ni-25Cu and Ni-50Cu even at that damage level. Pre-injection of 100 appm oxygen promoted void formation in Ni-10Cu at ~ 10 dpa, but showed no effect in Ni-25Cu and Ni-50Cu samples. Most excess vacancies precipitated into dislocation loops in the irradiated Ni-Cu alloys regardless of the presence of pre-injected oxygen or small helium bubbles produced by helium pre-injection. The density of dislocation loops and helium bubbles in the irradiated Ni-Cu alloys increased with increasing copper content and their size decreased concomitantly with increasing copper content in the investigated composition range. The special swelling resistance of Ni-Cu alloys is attributed to trapping of gas atoms and vacancies by fine-scaled clusters of like atoms in the alloys during irradiation.

APPROVED:

December 9, 1988
Date

Professor Richard Arthur Dodd

ACKNOWLEDGEMENTS

On completion of this thesis, I would like to express my heartfelt thanks to the following individuals for their advice and assistance during the course of the study.

As my thesis advisor, Professor R.A. Dodd has provided me invaluable guidance and support throughout my graduate study years at the University of Wisconsin-Madison, without that, the completion of this thesis would be impossible. I dedicate this thesis to him. I also wish to show special appreciation to Professor G.L. Kulcinski for his invaluable advice and continuous encouragement.

I would like to thank Professor P.A. Quin, Dr. J.H. Billen, Mr. R.C. Schmidt and Mr. T. Rebholtz of the University of Wisconsin Nuclear Physics group for their assistance and advice on the use of the tandem accelerator facility. I would like to thank Mr. R. Casper for providing training on the operation of the transmission electron microscopes and for his effort in keeping the microscopes always in good operating condition.

My association with past and present fellow graduate students in the Radiation Damage Group at the University of Wisconsin-Madison has been a very rewarding experience. For their many valuable suggestions, discussions, assistance, and contributions to the completion of this thesis research as well as their unforgettable friendliness, I wish to thank Dr. D.B. Bullen, Dr. R.L. Sindelar, Dr. S.J. Zinkle, Dr. C.D.

Croessman, Dr. D.L. Plumton, Dr. J.J. Kai, Dr. L.E. Seitzman, Mr. D.H. Plantz, Mr. D.J. Pertzborn, Ms. R.D. Griffin, Mr. S.H. Han, Ms. S.N. Farrens, Mr. J.H. Liang, Mr. M.H. Hassan and Mr. M.H. Song.

I also wish to extend my appreciation to Mr. D. Bruggink, Mrs. P. Caliva and Ms. E. DuCharme for their assistance in preparing the manuscripts of the many reports generated during my thesis study.

Finally, I would like to thank my wife, Li Zhao, for her lasting understanding, patience and support, which have also been especially important to me in making the completion of this thesis possible.

This research was supported by the United States Department of Energy, Office of Fusion Energy.

TABLE OF CONTENTS

LIST OF FIGURES

LIST OF TABLES

CHAPTER 1

INTRODUCTION

In the proposed D-T nuclear fusion reactor, high energy neutrons will be produced by the reaction

$$ {}^{2}_{1}\mathrm{D} + {}^{3}_{1}\mathrm{T} = {}^{4}_{2}\mathrm{He}\ (3.52\ \mathrm{MeV}) + {}^{1}_{0}\mathrm{n}\ (14.08\ \mathrm{MeV}). \qquad (1.1) $$

The interactions between the fusion neutrons and the structural materials of a fusion device may cause serious material deterioration, thereby limiting the safety and the lifetime of the reactor. This problem of radiation damage has long been considered as the second most serious obstacle to the commercialization of fusion power[1], after the production and confinement of a D-T plasma.

During irradiation by fusion neutrons, there will be two elementary interactions[2,3] between the radiation and the lattice atoms in a crystalline material. First, the bombarding particles transfer recoil energy to the lattice atoms. This produces vacancy and interstitial concentrations in excess of thermal equilibrium levels. Secondly, the bombarding particles can cause nuclear reactions which may produce considerable concentrations of foreign elements within the material. In particular, the inert gas helium which is produced by (n,α)-reactions plays an important role in the behavior of metals and alloys since it can cause drastic property changes, even at very low concentrations. Some of the radiation induced point defects will escape vacancy-interstitial

recombination and precipitate into defect clusters, e.g. dislocation loops, voids and stacking fault tetrahedra, thus greatly altering the microstructure and physical properties of the material. Particularly, the precipitation of vacancies into 3-dimensional voids leads to the phenomenon of void swelling, in which case the dimensions of rigidly held components will increase during operation of the reactor. Although it is concluded recently by some researchers[3] that the lifetime of most fusion reactor components will be determined by ductility losses rather than by swelling, swelling due to void formation under irradiation is still a serious problem in the reactor design.

Since there are currently no experimental facilities that can generate the same irradiation environment as that which will be present in a commercial fusion reactor, the high-energy neutron irradiation effects have to be studied by using fission neutrons or high-energy electrons or ions. Accelerator-based ion irradiations can produce damage structures similar to that of high-energy neutrons, and the high displacement damage rates associated with heavy-ion irradiations allow high damage levels to be achieved in a very short time. The effects of helium gas on the damage structure evolution can also be studied in ion-irradiated metals by utilizing dual-ion irradiation[4-9] or by pre-injection of helium ions[6-9]. Therefore, although heavy-ion irradiation cannot be directly correlated to neutron irradiation, it is still a very useful tool for both detailed investigation of the effects of changing various experimental parameters (temperature, alloy composition, gas atom

concentration, etc.) on the radiation damage structure evolution and preliminary radiation studies on new alloy systems[10].

In this study, microstructures resulting from 14 MeV heavy-ion irradiation of pure nickel and several concentrated nickel-copper alloys, namely, Ni-10Cu (at.%), Ni-25Cu and Ni-50Cu, including the effects of residual oxygen and pre-injected helium and oxygen, have been investigated in detail using transmission electron microscopy (TEM) of cross-section specimens[10]. This method allows the entire ion damage region to be viewed at once, and has been concluded to be necessary whenever quantitative void swelling information is desired from ion irradiation studies[11].

The motivation for the study is originated as follows.

As a pure metal, nickel has been selected in many radiation induced void swelling studies[12] to avoid the complex analysis problems imposed by phase changes. The effects of helium, either pre-injected or co-implanted during heavy-ion irradiation of pure nickel have also been studied in detail previously. However, only two of those studies[13,14] investigated the depth-dependent microstructure produced in helium-pre-injected, heavy-ion irradiated samples utilizing the cross-section technique. The results of those studies indicated that the pre-injected helium can either promote[13] or suppress[14] void swelling depending on the experimental conditions, especially the concentration of the pre-injected helium. Moreover, none of the above mentioned studies has included investigation on the effect of oxygen. Oxygen is the most

common residual gas in metals and has been indicated to promote void formation both by theoretical analysis[15,16] and by some experiments on other materials[17-21]. Therefore, it seems that any quantitative consideration of the effect of gases on void formation would be incomplete without considering the effect of residual oxygen in the material. Unfortunately, no experiments had been reported in which the concentration of the residual gases has been varied in a controlled manner[22] prior to the present study. The study of pure nickel in this research also provides a comparison basis for the study of Ni-Cu alloys which have been irradiated under similar conditions to pure nickel.

The Ni-Cu system is one of the few alloy systems which forms a complete solid solution over the entire composition range[23] (though a miscibility gap at lower temperatures ($\leq$ 322 °C) is included in the Cu-Ni phase diagram[24] based on a thermodynamic calculation[25], it has not been experimentally verified because of the low temperature). While voids can easily be produced in pure copper[26] and pure nickel[12], the Ni-Cu alloys have been shown to be very resistant to void formation under neutron[26], ion[27,28] and electron[29] irradiations. In fact, no voids have ever been observed in concentrated Ni-Cu alloys containing more than 10% alloying element (copper or nickel). However, the data-base for the irradiation of concentrated Ni-Cu alloys (> 10% alloying element) before this study was quite small and the cause of the suppressed void formation in the Ni-Cu alloys remained uncertain. In the literature, neutron irradiations were only carried out to very low dose (0.01 dpa)[26];

most ion irradiations were done by using low energy (0.1-0.3 MeV) ions[27-29], where the free surface effects on void formation[11] were important since the damaged region is too thin[30]. Only three samples of Ni-Cu alloys (Ni-20Cu, Cu-20Ni and Cu-2Ni) have been irradiated by high energy (46.5 MeV) ions and no cross-section analysis has been done. Although many samples have been irradiated in the HVEM (high voltage electron microscope) by 1 MeV electrons[31], the value of the results is also limited because electron irradiation in the HVEM cannot produce displacement cascades[32], which are formed in both neutron and heavy-ion irradiations. Finally, no comparison work has been done to study the gas effect in irradiated Ni-Cu alloys. Although Ni-Cu alloys are unlikely to be used as structural materials in the proposed future fusion reactor, such a simple system merits further work in view of the considerable importance attached to the understanding and control of void formation.

The objectives of the present research are, first, to investigate the effect of oxygen (both residual and pre-injected) and helium (pre-injected) on void formation in pure nickel, then to investigate the effect of copper concentration on defect cluster formation characteristics of Ni-Cu alloys in the presence of oxygen and helium atoms.

Figure 1.1 shows the Cu-Ni phase diagram where the compositions and the irradiation temperatures used in this study are indicated. It should be noted that all the heavy-ion irradiations in this study have been performed at the same homologous temperature of 0.45

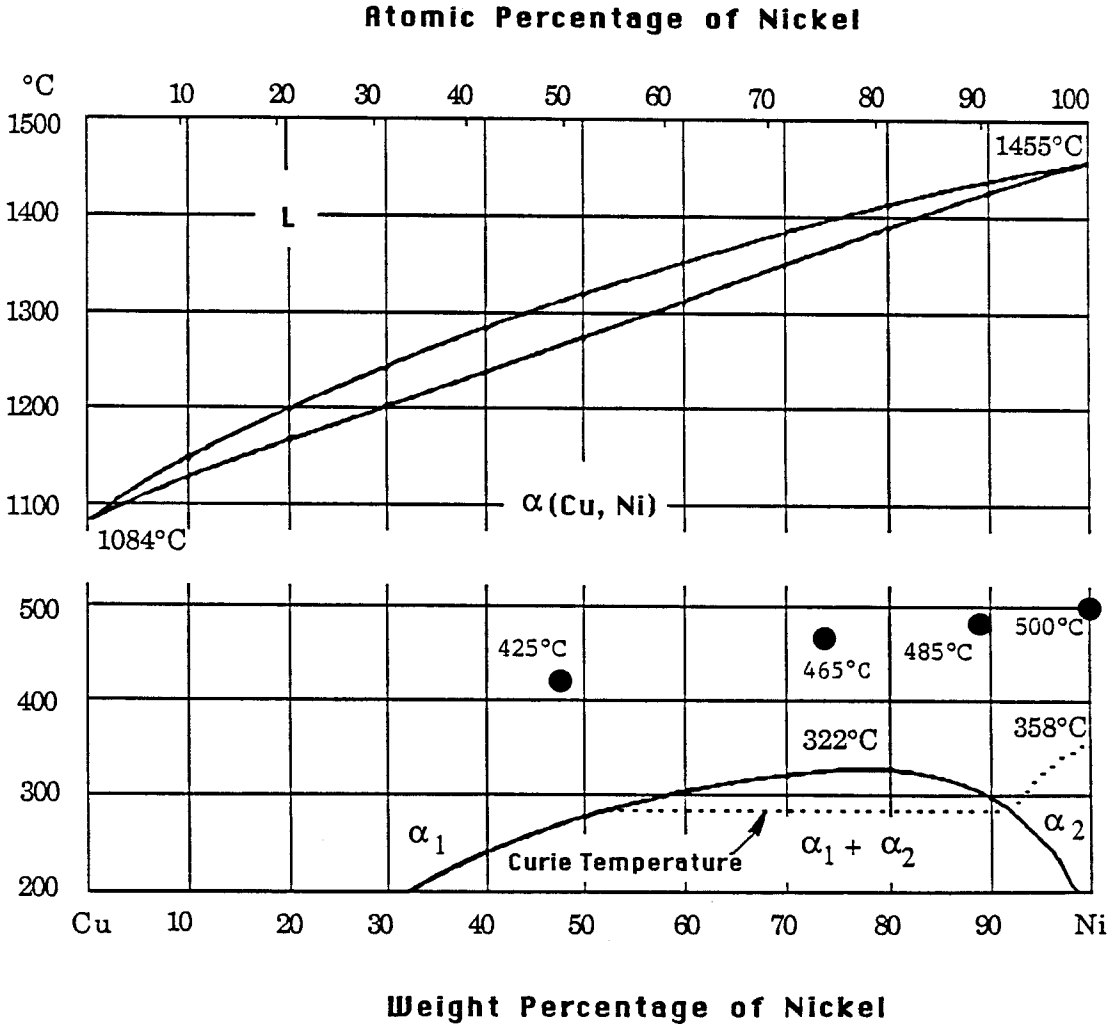

● irradiation performed in this study

Figure 1.1 Phase diagram of Cu-Ni system[24] with the compositions and irradiation temperatures used in this study indicated by the ● 's.

T_m, because voids are known to form only in the temperature range of 0.3-0.6 T_m. At lower temperatures, vacancies are not mobile enough to move together to form voids and most of them will recombine with a mobile interstitial atom. When the temperature is higher than 0.6 T_m, the equilibrium vacancy concentration is very high, which makes the vacancy supersaturation insufficient for void nucleation and growth.

The rest of this thesis is organized as follows. Chapter 2 gives a brief review on the general radiation damage theory, but concentrating on the topic of void formation. Chapter 3 reviews relevant previous experimental work on pure nickel, pure copper and Ni-Cu alloys. Chapter 4 describes the detailed experimental procedure performed in this study, while the experimental results and their discussion are given in Chapters 5 and 6 respectively. Chapter 7 gives a general summary and the conclusions of this research.

References for Chapter 1

1. G.L. Kulcinski, in: Radiation Effects and Tritium Technology for Fusion Reactors (Proc. Int. Conf. Gatlinburg, 1975), USERDA Report CONF-750989 (1976) 1-17.

2. G.L. Kulcinski, Contemp. Phys. 20 (1979) 417.

3. H. Ullmaier, Nuclear Fusion 24 (1984) 1039.

4. H.E. Kissinger, J.L. Brimhall, E.P. Simonen and L.A. Charlot, Battelle Report PNL-2495, UC-25 (1978).

5. J.L. Brimhall, IEEE Transactions on Nuclear Science, NS-28, No. 2 (April, 1981) 1308.

6. S.C. Agarwal, G. Ayrault, D.I. Potter, A. Taylor and F.V. Nolfi, Jr., J. Nucl. Mater. 85 & 86 (1979) 653-657.

7. N.H. Packan and K. Farrell, J. Nucl. Mater. 85 & 86 (1979) 677-681.

8. N.H. Packan, K. Farrell and J.O. Stiegler, J. Nucl. Mater. 78 (1978) 143-155.

9. J.A. Spitznagel, F.W. Wiffen and F.V. Nolfi, J. Nucl. Mater. 85 & 86 (1979) 629.

10. S.J. Zinkle and R.L. Sindelar, Nucl. Inst. and Meth. B16 (1986) 154.

11. S.J. Zinkle, Ph.D. Thesis, University of Wisconsin-Madison (1985).

12. D.B. Bullen, UWFDM-488, University of Wisconsin-Madison (Oct., 1982).

13. K. Farrell, N.H. Packan and J.T. Houston, Rad. Effects 62 (1982) 39-52.

14. D.B. Bullen, Ph.D. Thesis, University of Wisconsin-Madison (1984).

15. W.G. Wolfer, J. Nucl. Mater. 122 & 123 (1984) 367.

16. S.J. Zinkle, W.G. Wolfer, G.L. Kulcinski and L.E. Seitzman, Phil. Mag. A55 (1987) 127.

17. L.D. Glowinski et al., J. Nucl. Mater. 61 (1976) 29.

18. M.J. Makin et al., in: Radiation Effects in Breeder Reactor Structural Materials, Eds. M.L. Bleiberg and J.W. Bennett (TMS-AIME, New York, 1977) pp. 645-665.

19. S.C. Agaswal, D.I. Potter and A. Taylor, Met. Trans. 9A (1978) 569.

20. B.A. Loomis and S.B. Gerber, J. Nucl. Mater. 97 (1981) 113.

21. R.L. Sindelar, Ph.D. Thesis, University of Wisconsin-Madison (1985).

22. A.J.E. Foreman, in: Proceedings BNES on Dimensional Stability and Mechanical Behavior of Irradiated Metals and Alloys, Brighton, England (1983).

23. M. Hansen, Constitution of Binary Alloys, 2nd Ed., McGraw-Hill Book Company, New York, 1958.

24. Metals Handbook, 8th edition, American Society for Metals, Vol. 8, 1973, p. 294.

25. L. Elford, F. Muller and O. Kubaschwski, Ber. Bunsenges. Physik. Chem. 73 (1969) 601.

26. J.L. Brimhall and H.E. Kissinger, Rad. Effects 15 (1972) 259.

27. D.J. Mazey and F. Menzinger, J. Nucl. Mater. 48 (1973) 15.

28. K-H. Leister, Ph.D. Thesis, Kernforschungszentrum Karlsruhe (1983).

29. P. Dauben and R.P. Wahi, Progress Report No. 2 (1981-1984), Reports of the Hahn-Meitner-Institute.

30. S.J. Zinkle and R.W. Knoll, UWFDM-578, University of Wisconsin-Madison (1984).

31. P. Barlow, Ph.D. Thesis, University of Sussex (1977).

32. P. Barlow et al., Phil. Mag. 36 (1975) 565.

CHAPTER 2

THEORETICAL BACKGROUND

A. Radiation-Produced Point Defects and dpa Calculation

During irradiation of crystalline solids, the implanting energetic particles (e.g. neutrons, heavy ions or electrons) will collide with lattice atoms and transfer energy to them. As noted by Olander[1], the energy transferred (T) from a non-relativistic particle with kinetic energy E and mass M_1 to a stationary particle of mass M_2 is given by

$$T = \frac{1}{2} E \Lambda (1 - \cos \theta) \tag{2.1}$$

where θ is the scattering angle in the center-of-mass coordinate system and Λ is given as

$$\Lambda = \frac{4 M_1 M_2}{(M_1 + M_2)^2} \quad . \tag{2.2}$$

Electrons in the MeV range must be considered as relativistic particles. In that case, the maximum energy transferred is given by Dienes and Vineyard[2] as:

$$T_{max} = \frac{2 (E + 2m_0c^2) E}{Mc^2} \tag{2.3}$$

where m_0 is electron rest mass, M is the mass of a target atom and c is the velocity of light.

When the recoil energy imparted on a target atom exceeds a certain value, the so-called threshold or displacement energy (E_d)[3], the target atom leaves its regular site; it becomes displaced and comes to rest as an interstitial atom. Its original lattice site has become the site of a vacancy. Therefore, a Frenkel defect pair (vacancy-interstitial atom pair) is created. The displacement energy depends on the metal or alloy, the crystal structure and direction of displacement.

An atom which has been displaced directly by a bombarding particle is known as a "primary knock-on atom", or PKA, which may have an energy from the eV to keV range. PKAs with relatively lower energies can not displace other atoms and will lose their energy due to various inelastic interactions which cause only very localized heating of the lattice. But the more energetic PKAs may create one or a number of secondary knock-ons. Each of these secondary knock-ons, when given enough energy, may in turn displace other atoms. The result of this displacement cascade is the formation of many Frenkel pairs in the crystalline material. The density of the Frenkel pairs along the path of the incident particle depends very strongly on the energy of the particle as well as the type of particle and can be expressed by[4]:

$$N_d(E) = N_0 \int \Phi(E)\, \sigma(E)\, K(E,T)\, \nu(T)\, dT \qquad (2.4)$$

where N_0 is the atomic density of the crystal, $\Phi(E)$ is the flux of the incident particles with energy E, $\sigma(E)$ is the collision cross section between the incident particle and the matrix atoms, $K(E,T)$ is the

probability of the production of a PKA with kinetic energy T through collision, and $\nu(T)$ is the number of matrix atoms which are subsequently displaced by the PKA.

Large displacement cascades are produced during fast neutron and ion irradiations. Due to the large Rutherford collision cross section between the incident ion and the lattice atoms, ion irradiation results in a displacement cascade which is more dense than that found for neutron irradiation. However, because of the limited range of a charged particle in a metal crystal (as compared to a neutron), the spatial distribution of displacement cascades produced by ion irradiation is limited to only a few microns from the surface. And also, because the ion-atom collision cross section increases with decreasing ion velocity, the displacement damage rate for ion irradiation is depth-dependent. The displacement rate and, in turn, the number of Frenkel pairs produced near the end of ion range is greater than those at the surface by a factor of 5-10.

Energetic electrons (> 0.5 MeV) can also cause atomic displacements in crystalline materials. But since the mass of an electron is so small, electrons may transfer at most a few percent of their energy to a metallic lattice atom, so that the displacement damage is limited to a few Frenkel pairs per collision. Therefore, high energy electron irradiations only produce an isolated point defect damage structure, as opposed to the dense Frenkel pairs produced by the displacement cascades in fast neutron and ion irradiations, even if the fluences of the incident particles are the same.

In order to compare the potential damage levels under irradiations of different particles with various energies, a theoretical unit known as dpa (displacement per atom) was established and has been widely used. The unit is a measure of the cumulative effect of an irradiation which causes displacements. A dose of 1 dpa means that, on the average, each lattice atom in the crystal has been displaced once during the irradiation. The dpa unit does not account for dose rate effects, Frenkel pair recombination in the cascade region, the spatial rearrangements of point defects due to thermally assisted migration, or the effect of transmutation reactions which occur under neutron irradiation. Nevertheless, it is a useful unit for calculating first order effects that will be expected in various irradiation environments.

To calculate the dpa profile of an ion-irradiated metal, the depth distribution of energy deposition from incident ions has to be determined first. Lindhard, Scharff and Schoitt, as well as others[5-9] have developed the most widely used and accepted model for determining energy loss of an ion slowing down in an amorphous solid. The model is known as LSS theory. The LSS theory assumes total separability for electronic and nuclear scattering energy loss mechanisms and assumes that the electronic energy loss is proportional to the velocity of the incident ions. The nuclear stopping cross section is calculated from a screened Thomas-Fermi statistical model of the atom. This theory is applicable to many target-projectile combinations over a wide energy range, but breaks down for moderately low ion energies.

When the nuclear and electronic stopping powers are known, the number of displacements per atom (dpa) at a depth x can be calculated using a modified Kinchen-Pease model proposed by Torrens and Robinson[10,11]

$$N_d(x) = \frac{J}{N}\frac{K S_D(x)}{2E_d} \quad \text{(dpa)} \tag{2.5}$$

where J is the incident ion fluence, N is the atomic density of the target, $S_D(x)$ is the energy available for displacements (damage energy) at the depth x, K is the displacement efficiency which accounts for events that do not lead to displacements, and E_d is the spatial averaged threshold energy for displacement . Early computer modeling of the cascade structure indicated that the displacement efficiency was independent of the incident particle energy[10], with a value of K=0.8. That number has been used as a standard value over the years for dpa calculations. However, recent experimental and theoretical studies have shown that K is strongly dependent on energy, with K decreasing for increasing recoil energy[12]. For high energy (≥ 1 MeV) neutron or heavy-ion irradiation of FCC metals, K=0.3 is probably a more appropriate value to use. That would reduce many previously cited damage levels by a factor of 3/8. Nevertheless, the damage values in this study will still be derived from the K=0.8 assumption to be consistent with the previous decade of ion irradiation studies.

It should also be mentioned here that the final position of an incident ion in a target material has a statistical nature, i.e., ions having

exactly the same initial incident energy do not always follow the same path, resulting in some particular spatial distribution of ions in the solid. The ion distribution function depends on the ion and target species, incident ion energy and the angle of incidence. The final distribution of displacement damage is the average result of all the incident ions.

A computer code based on LSS theory developed by Brice[13] was used in several previous 14 MeV heavy-ion irradiation studies[14-16] to calculate both ion damage profile and injected ion distribution. However, the damage ranges calculated by computer codes based on LSS theory have been shown to be 15-40 % shorter than the damage regions observed in TEM cross-section studies[14-20]. This has been explained by diffusional spreading and the possible over-estimation of the electronic stopping loss factor for heavy-ion irradiations[15]. Recently, a Monte Carlo computer code, TAMIX[21], has been developed to calculate the damage and ion distributions in ion irradiated materials. This code is based on a modified Kinchen-Pease model and simulates the ion transport process in solids statistically. Its results agree closely with those calculated using Brice code. In this study, the TAMIX code has been used to estimate the ion distribution and the ion fluences needed for producing the desired displacement damage at a certain depth in the target. Figure 2.1 (a) and (b) show the comparison of the Brice result with the TAMIX result for dpa and ion concentration distributions in 14 MeV nickel ion irradiated pure nickel (the depth profile of 5 MeV oxygen ions is included in the TAMIX calculation). Figure 2.2 (a) and (b) show the

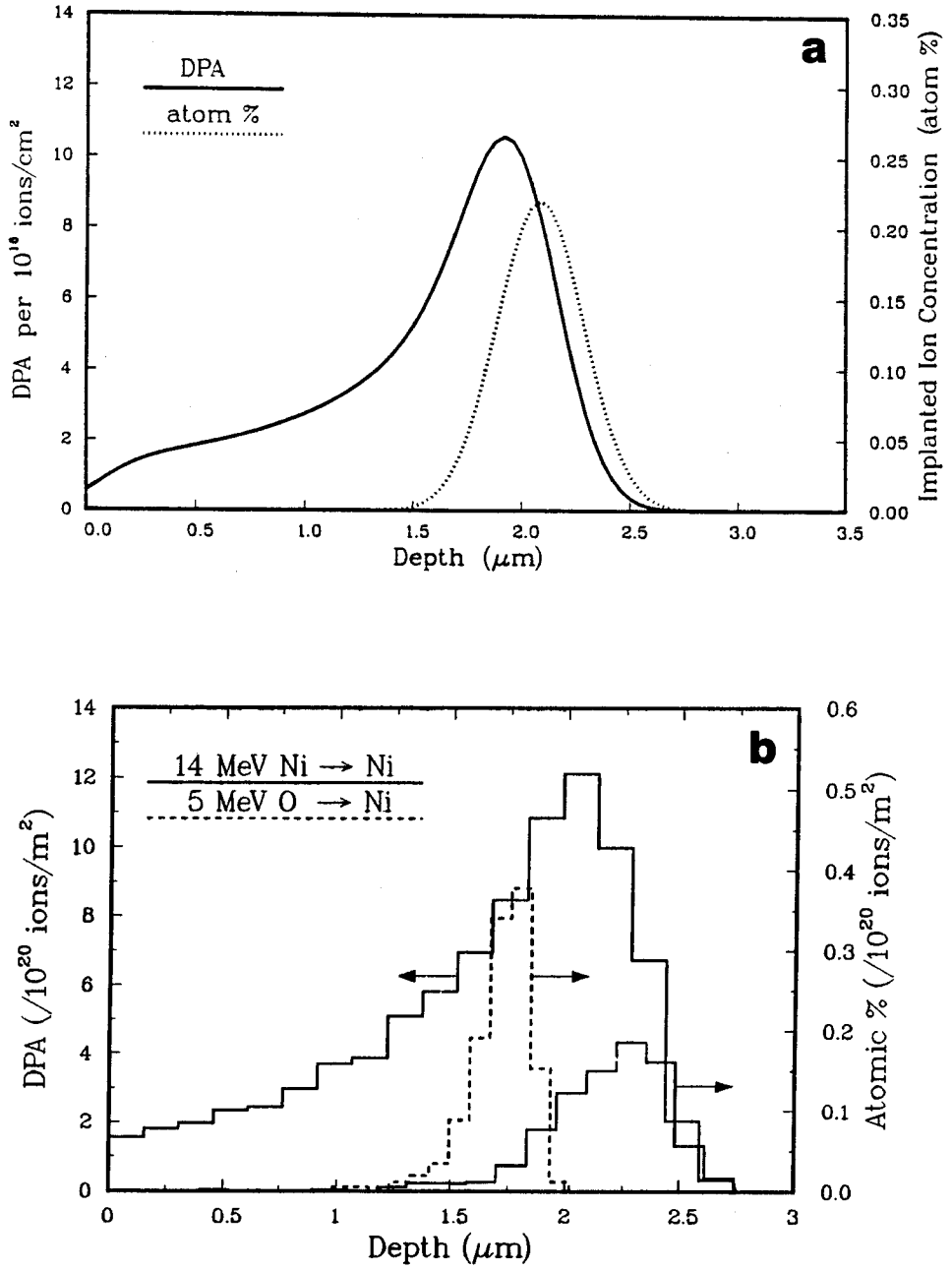

Figure 2.1 Displacement damage and implanted ion concentration versus depth from the irradiated surface for 14 MeV nickel ion irradiated pure nickel, calculated using (a) the Brice code[13] (b) the TAMIX code[21] (1000 ion histories, the distribution of 5 MeV oxygen ions is also included).

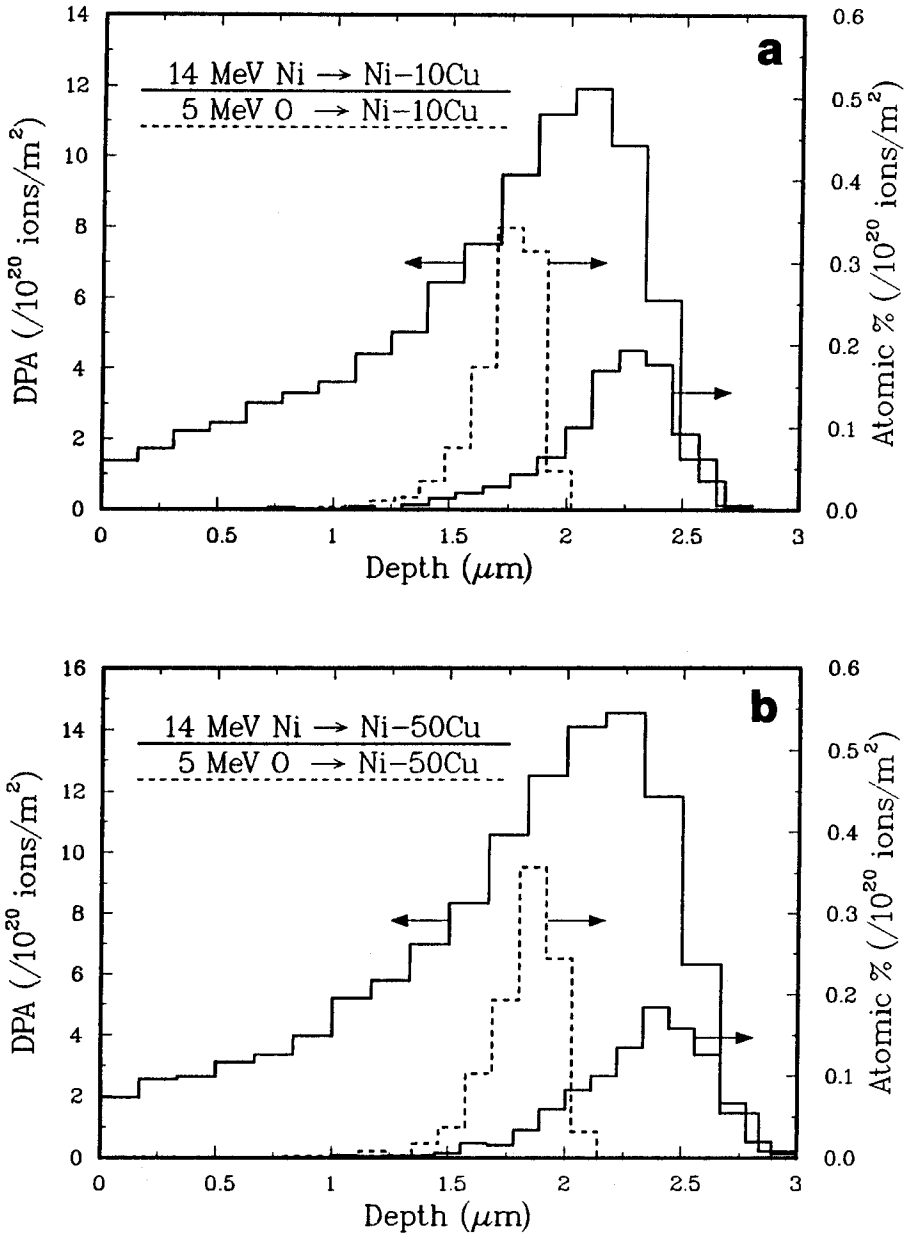

Figure 2.2 Displacement damage (by 14 MeV nickel ions) and implanted ion concentrations (14 MeV nickel ions and 5 MeV oxygen ions) versus depth in irradiated (a) Ni-10Cu and (b) Ni-50Cu, calculated using the TAMIX code[21] (1000 ion histories).

results of similar TAMIX calculations for 14 MeV nickel ion irradiated Ni-10Cu and Ni-50Cu respectively (both include the depth profile of 5 MeV oxygen ions). Some other TAMIX results relevant to the experiments performed in the present study are included in Chapter 4. In the calculations, the effective displacement energies, E_d, used for nickel and copper atoms are 40 eV[3] and 29 eV[15] respectively.

B. Radiation-Induced Void Swelling

The production of point defects can cause the concentrations of vacancies and interstitials in an irradiated metal to be much higher than the normal thermal equilibrium concentrations. Under certain conditions, some of those point defects will escape vacancy-interstitial recombination and form defect clusters. During irradiation, interstitials can rapidly aggregate to form dislocation loops, thereby increasing the dislocation density of annealed metals. Also, interstitial atoms have a stronger attraction to edge-type dislocation sinks than vacancies (dislocation bias) due to their greater relaxation strain[22,23]. As a result, there is a higher flux of vacancies arriving at neutral sinks, which may lead to void formation. The overall effect of the production of voids in metals used in reactor is that the material will swell and possibly distort rigidly held components, thereby promoting early failure.

Since the first void was observed in steel by Cawthorne and Fulton[24] in 1966, voids have been observed in over a dozen elements and scores of alloys[4]. The general conditions under which voids are formed

seem to be well known. Voids are known to form only in the temperature range of 0.3-0.6 T_m. At lower temperatures, vacancies are not mobile enough to come together forming voids and most of them will recombine with a mobile interstitial atom (interstitials generally become mobile in metals at very low temperatures, i.e. below 50 K, while vacancies are mobile only for temperatures $\geq 0.25\ T_m$[25]). When the temperature is higher than 0.6 T_m, the equilibrium vacancy concentration is very high, making the vacancy supersaturation in metals insufficient for void nucleation and growth. It is also known that void swelling is dependent on the damage rate, damage level, gas and other impurity contents in the metal, and other factors[4].

The basic theories for void nucleation and growth, as well as the effects of gases and other impurities on void formation are briefly reviewed in this section.

B.1. Void Nucleation Theory

The first approach to void nucleation theory was made by Harkness et al.(1969)[26,27]. They utilized an equation applicable to nucleation of voids only in the presence of a vacancy supersaturation and did not consider the interstitials which are produced simultaneously with those vacancies during irradiation. Better models that dealt with the effect of irradiation on void nucleation were developed independently by Katz and Wiedersich[28] and Russell (1971)[29], and they are collectively known as WKR theory. The theory was further refined later by Russell

(1978)[30], Wolfer and Si-Ahmed (1982)[31] and has been considered to be the classical theory for void nucleation. The WKR theory considers void nucleation in the presence of both supersaturations of vacancies and interstitials during irradiation. According to this theory, whether or not a void will nucleate is governed not simply by point defect concentrations, but by the ratio of the arrival rates of vacancies and interstitials at neutral sinks. Void nucleation is possible only when the rate of arrival of vacancies is larger than that of interstitials. The arrival rates of defects at a neutral sink are proportional to the product of their mobility and concentration. Since interstitials have higher mobility and the concentrations of interstitials and of vacancies are equal originally, the presence of some other sinks that preferentially attract interstitials are required for void nucleation. As mentioned before, dislocations are this type of sink.

Russell[30] has noted that there are several mechanisms by which void nucleation can occur: (a) homogeneous nucleation of vacancy and interstitial clusters, (b) heterogeneous nucleation on single gas atoms or gas atom clusters, (c) co-precipitation of vacancies, interstitials and gas atoms, (d) direct nucleation from the vacancy-rich core of displacement cascades, and (e) nucleation in the presence of surface active impurities.

The basic assumptions of the classical WKR theory for homogeneous void nucleation are that an incubation period or a lag time exists, during which a subcritical cluster population forms; this period is then followed by a steady-state nucleation period, during which a

constant population of clusters grows beyond a critical size per unit time. An individual cluster overcomes the nucleation barrier at the critical size only as a result of growth fluctuations. Once it crosses the barrier its further growth becomes more deterministic and growth fluctuations become negligible. The second important assumption of the classical and homogeneous nucleation theory concerns the termination of the nucleation period and the cessation of the steady-state nucleation rate. This termination is generally believed to be caused by a depression of the supersaturation of the clustering species. For a continuous irradiation, the increasing void density is believed to eventually reduce the vacancy supersaturation and thereby stop the cluster flux across the nucleation barrier. Although it is difficult to precisely specify the required reduction, Russell[30] suggested that a lowering of the vacancy supersaturation by a factor of ten will suffice to terminate void nucleation.

In the original WKR theory, only monatomic point defects were considered as mobile species. However, it was pointed out later that the migration energy of divacancies can be significantly lower than that of monovacancies for many cubic metals[31]. Furthermore, the binding energy of divacancies is sufficiently large for a significant fraction of them to remain bound, even at high temperatures. As a result, the product of divacancy concentration and diffusion coefficient can be as large as the corresponding product for monovacancies. This factor has

been considered in the WKR theory modification made by Wolfer and Si-Ahmed[31].

Quantitative predictions of the WKR theory did not agree with experimental results. Nevertheless, some of the qualitative predictions of the model are still appropriate[32].

In the classical approach to void nucleation, the critical size and the nucleation barrier are determined mainly by the supersaturations, the internal energy of the cluster, and by the diffusion coefficients of the mobile species. The subcritical cluster population below the critical size was considered to have no direct influence on the critical size and the nucleation barrier. The latter assumption has been shown to be incorrect[33]. Another theoretical approach to void nucleation, which abandoned the above assumption, has been developed recently by Wolfer and Wehner in 1985[33,34]. In that model, the void size is treated as a continuous variable, and a new Fokker-Plank equation[35] is used to describe the vacancy cluster distribution. Their results depend rather critically on the value of the sink-averaged interstitial bias factor. Void number densities that are in close agreement with measured values are obtained when appropriate bias factor parameters are used. Wehner and Wolfer have also shown[33] that void nucleation is an evolutionary process with no steady-state regime. Therefore, it appears that the basic assumption contained in the WKR model is not valid.

B.2. Void Growth Theory

The most widely used model for the growth of voids in an irradiation environment was initially proposed by Harkness and Li[36] (1971) and was further improved by Wiedersich[37] (1972) and by Brailsford and Bullough[38] (1972). The model is based on the formalism of chemical rate theory.

The basic assumption of rate theory is that a discrete, random array of sinks for point defects can be approximated by an appropriate continuum of sinks. This replacement of a set of discrete sinks with a continuum means that the derived rate equations will contain an implied spatial averaging over distances greater than the average sink spacing and an average over a time interval greater than the average cascade lifetime[39]. The essential hypothesis of the analysis is that the metal already contains void embryos and sinks for interstitials. Since the irradiation produces the same number of free vacancies and interstitials, the depletion of interstitials by those sinks will lead to a net flow of vacancies to the unbiased sinks (i.e. voids) and hence to void growth. Rate equations may be written to describe the point defect production, migration and loss to sinks. The strengths of the various sinks, including voids, grain boundaries, dislocations, surfaces, have been analyzed in detail by Brailsford et al.[40,41]. Once the point defect concentrations (C_v and C_i) are obtained from the rate equations[42], the void growth rate can then be calculated by (assuming no divacancy contribution)[43]:

$$\frac{dr_v}{dt} = \frac{\Omega}{r_v} \{ Z_v^v (r_v) D_v [C_v - C_v^e (r_v)] - Z_i^v (r_v) D_i C_i \} \quad (2.6)$$

where Ω is the atomic volume, r_v is the void radius, $Z_{v,i}$ is the void capture efficiency of interstitials or vacancies, $D_{v,i}$ is the diffusion coefficient for interstitials or vacancies, and $C_v^e(r_v)$ is the thermal vacancy concentration at the void,

$$C_v^e (r_v) = C_v^e \exp [(\frac{2\gamma}{r_v} - p_g) \frac{\Omega}{kT}] \quad (2.7)$$

where C_v^e is the bulk thermal vacancy concentration, γ is the surface tension and p_g is the gas pressure in the void.

Voids were originally considered to be neutral sinks. However, Wolfer and coworkers[34,43,44] have shown that small, bare voids have a strong bias toward interstitial absorption due to an image force interaction. This would obviously prohibit void nucleation and growth. Therefore, a void surface coating consisting of a shell of impurity atoms which changes the bias of the void was suggested to be necessary for void nucleation and growth.

Mansur and Wolfer[44] have also investigated the effect of incorporating mobile divacancies into void nucleation and growth equations. Divacancies were shown to have a fairly substantial influence on void swelling, causing increases in swelling at low temperatures and decreases at the peak swelling temperature.

Wolfer[32] compared the void nucleation and growth theories with an extensive data base on high-fluence swelling in austenitic alloys and showed that they were in good qualitative agreement. He concluded that swelling as a function of dose can be divided into an initial transient period of low swelling rate, followed by a steady-state, higher-swelling rate regime as shown in Figure 2.3. As shown in the figure, the transient period is composed of several regimes of increasing length. First, a short period for the point defects to reach their stationary concentrations, this is a part of the longer time lag regime for void nucleation. Then there is a period of void nucleation to reach a certain void number density at a given irradiation temperature. After that, the void sink strength approaches the value of the dislocation sink strength. Steady-state swelling commences when the void and dislocation sink strengths become equivalent. At very high doses, the dislocation sink strength may drop below the void sink strength. This results then in a saturation of swelling which is often observed in ion-bombardment studies.

B.3 Gas Effects on Void Formation

As mentioned in Chapter 1, during irradiation by fusion neutrons helium will be produced in metals mainly due to the (n,α) reactions, such as[45]

$$ {}^{A}_{Z}M + {}^{0}_{1}n^{f} = {}^{A-3}_{Z-2}M' + {}^{4}_{2}He \text{ (several MeV)}. \qquad (2.8) $$

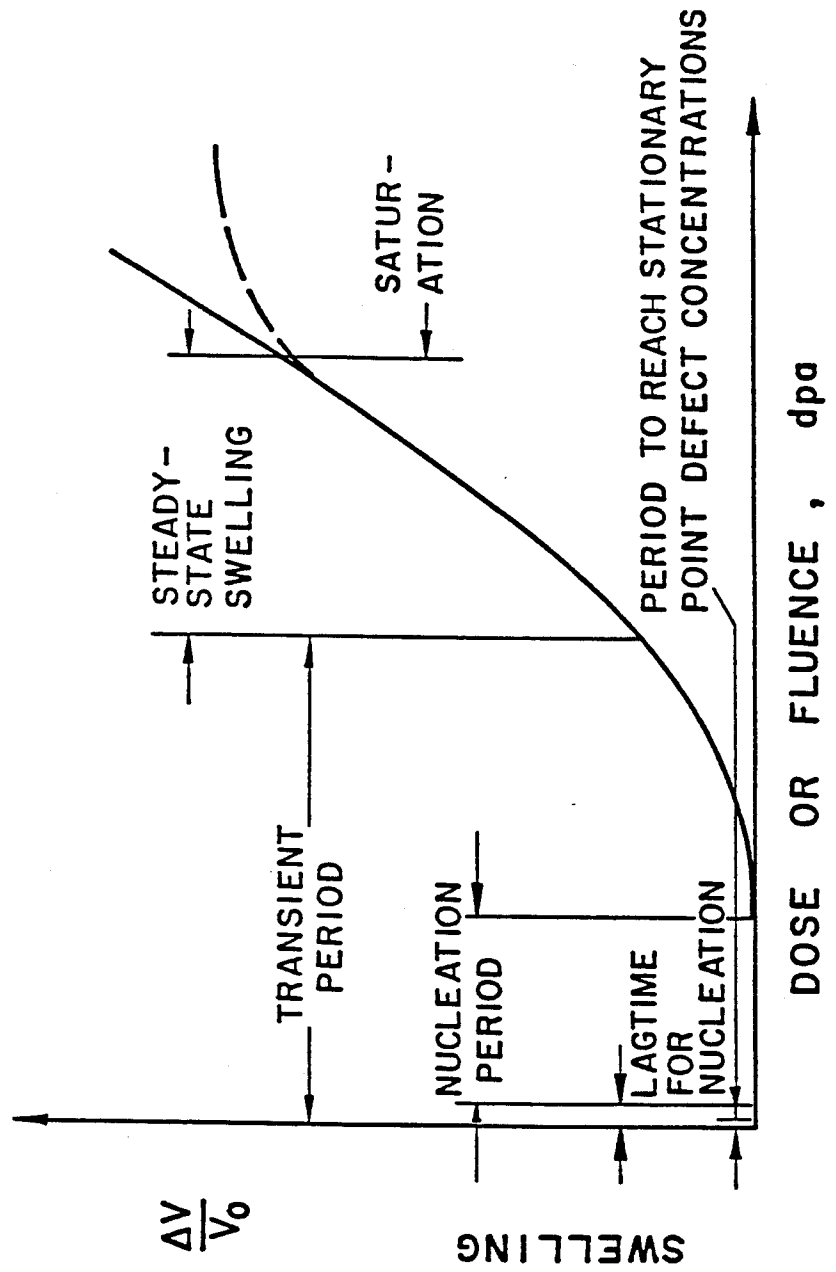

Figure 2.3 General form of swelling versus dose with the various stages involved[32].

The appm helium/dpa ratio for potential fusion reactor materials could be as high as about 15[45].

Among the various deleterious effects of helium on the material properties, the ductility losses observed in tensile, creep and fatigue tests are supposed to be the most critical. It is now generally agreed that the high temperature ductility losses are due to helium bubbles on the grain boundaries; such bubbles form under almost all external conditions because of the vanishingly small solubility of helium in metals[45].

The major concern about helium in this thesis, however, is its effect on void formation.

It has been found in reactor irradiations or ion bombardment experiments with helium injections that[45-47]: (1) helium usually increases the concentration and decreases the size of voids; (2) helium reduces the dose level for the first appearance of voids; (3) helium allows voids to exist at higher temperatures. It is generally believed that helium enhances the void nucleation process because the gas pressure in the gas-filled gas-vacancy clusters minimizes the thermal reemission of vacancies from the cavity[48]. Also, according to equation (2.7), when the gas pressure inside a vacancy cluster increases, the thermal equilibrium vacancy concentration near the void will be lowered, this will permit void growth at higher temperatures than without gas[42].

Some ion irradiation experiments[14,49] have shown that large pre-injected or co-injected helium levels can almost totally suppress swelling. This was explained by either over-nucleation of copious very

small cavities[14] or increased vacancy-interstitial recombination due to the trapping of vacancies by co-implanted helium atoms[50].

It should be noted here that the method by which helium is introduced into the matrix strongly influences void swelling[48]. Swelling increases in the following order: pre-injection at room temperature, pre-injection at elevated temperatures, co-implantation with heavy ions in dual ion irradiation. Void size varies in the same order, while void density decreases with the above order.

Besides helium, other gases, mainly hydrogen and oxygen, may also play important roles in promoting void formation[14,51]. Hydrogen will be continuously produced during neutron irradiation as a result of (n,p) transmutation reactions, while oxygen and other reactive gases are often introduced into metals during fabrication. According to Wolfer[32], reactive gases such as hydrogen and oxygen can become chemisorbed on subcritical-sized void surfaces, thereby reducing the surface energy and the activation barrier for void nucleation.

Recently, Zinkle et al.[15,52] developed a vacancy cluster stability model to predict the most stable vacancy cluster morphology in FCC metals. In this model, the relative energy of the void is compared with other vacancy clusters, namely, the perfect circular dislocation loop, the faulted (Frank) loop, and the stacking fault tetrahedron. Calculations using this model[15,53,54] indicated that a void is thermodynamically unstable in copper, nickel and stainless steels since the other types of vacancy clusters have lower energies per vacancy for all the cluster

sizes. However, the void can be stabilized by surface energy reductions. These reductions can be achieved by chemisorption of oxygen onto the metal surface. Knowing the fraction of oxygen which chemisorbs and the surface coverage required permits the determination of the minimum oxygen concentration needed to promote void stability. Figure 2.4 and 2.5 show the effect of surface energy on void stability, and the minimum oxygen concentration needed for void stability in nickel, respectively. The calculations were performed by Seitzman[53], using the above model and the best known material parameters. In the calculation of minimum required oxygen concentration for void stability shown in Figure 2.5, the void densities and radii used are taken from Wehner and Wolfer's data for a damage rate of 10^{-3} dpa/s[33]. At low temperatures a greater oxygen concentration is needed for void stabilization as shown in the figure, due to the higher void densities at those temperatures.

B.4. Effect of Alloying Elements and Impurities on Void Formation

It has been established that alloys do behave differently as regards void formation during irradiations. Early studies on stainless steel have shown that the threshold fluence for void formation is much higher than that found in a pure metal such as nickel[55]. It is also well established that voids do not form as readily in impure nickel[56] and aluminum[57] as in the corresponding highly pure metal. Also, it is well known from experimental studies that void swelling depends on solute type and concentration, i.e. solute atoms can either retard or accelerate void

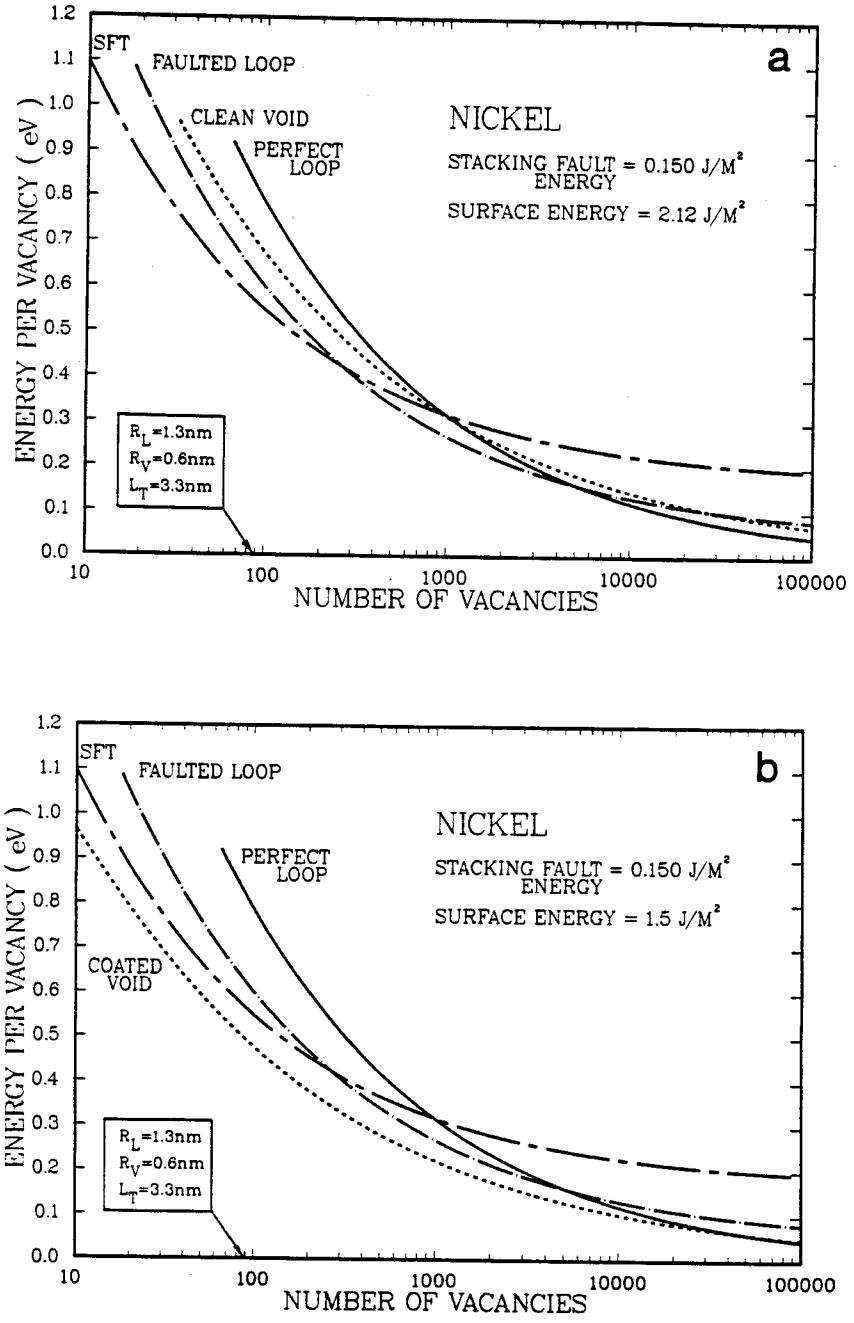

Figure 2.4 Comparison of the stability of different vacancy cluster species versus cluster size in nickel with a surface energy of (a) 2.12 J/m^2 and (b) 1.5 J/m^2, calculated by Seitzman[53].

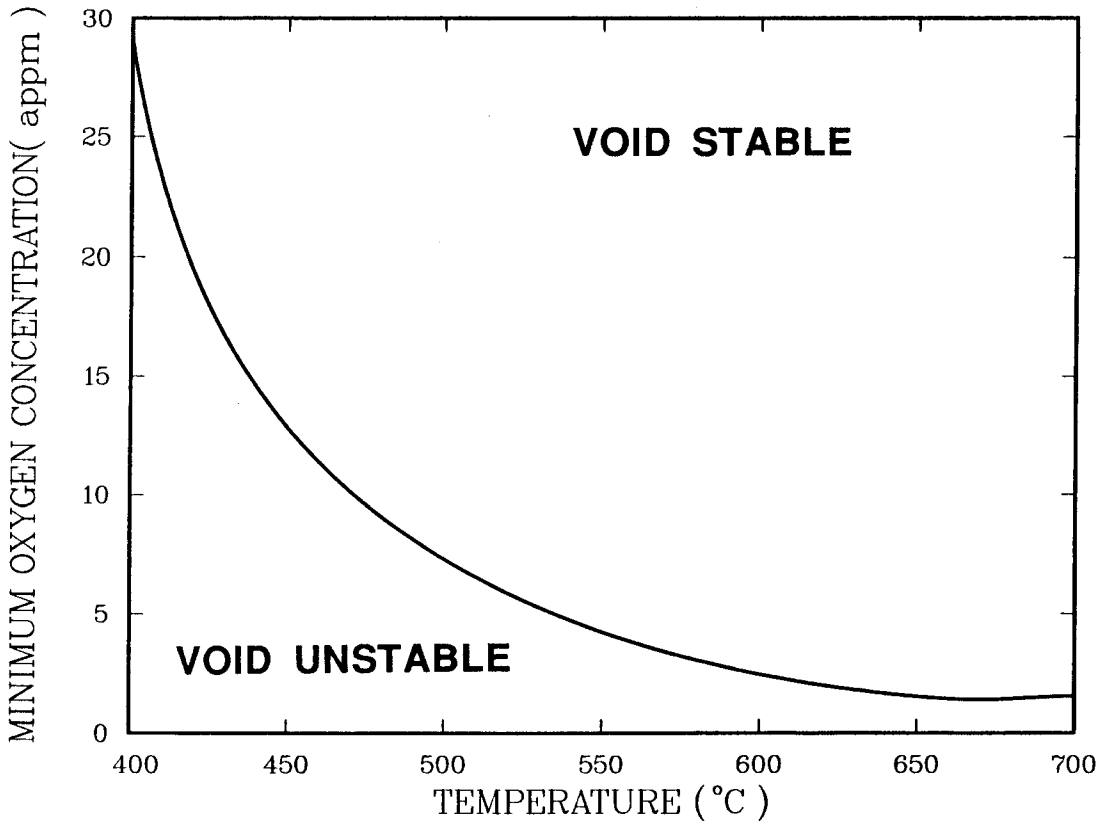

Figure 2.5 Minimum oxygen concentration to stabilize the void in nickel as a function of temperature, calculated by Seitzman[53].

nucleation and growth. Small changes in the concentrations of matrix alloying elements can lead to very significant changes in swelling[42].

There are several explanations to account for the observed alloying effects on void swelling[58]. Alloying can lower the stacking fault energy, so making the formation of three dimensional voids less energetically favorable. Alloying either lowers or raises the melting point thereby shifting the homologous temperature of the material to above or below the void formation temperature regime. The alloying constituents and impurities in the material can trap point defects resulting in a greater probability for mutual annihilation. According to Mansur[42], this point defect trapping may be pictured under suitable definitions as equivalent to changing vacancy and interstitial diffusion coefficients. The alloying element or impurities can also combine with gas atoms, such as oxygen, making them unavailable for void nucleation. During irradiation, solute may segregate to point defect sinks and thereby affect void nucleation and growth by altering the sink capture efficiencies[59]. Lastly, precipitate particles in alloys will also influence the void formation process, because there are strong interactions between point defects and those particles. According to Russell[60], point defects are annihilated at the interface between incoherent precipitate particles and the matrix, and are trapped at the interface between coherent particles and the matrix.

Various theoretical models have been established to model the effects of solute atoms and precipitates on void swelling. Detailed reviews can be found in the literature[42,61-63].

C. Mass Transport and Phase Stability under Irradiation

Irradiation of metals and alloys with neutrons, electrons and heavy ions may introduce up to 10 J/mol of energy in the form of atomic displacements. This energy, which is in the form of vacancies, self-interstitials and cores of displacement cascades is then available to produce a range of mass transport and phase changes in addition to the defect cluster formation in irradiated metals. These processes include: radiation-enhanced diffusion, irreversible segregation of solute to or away from dislocations and interfaces, precipitation of phases which are not thermally stable, dissolution of thermally stable phases, disordering of ordered precipitates, rendering crystalline phases amorphous. The theories for these changes have been developed during the last decade and have been reviewed in detail by Russell[60] in 1984. Only a very brief summary on some of the most important mechanisms is given below.

C.1. Radiation-Enhanced Diffusion

Thermal diffusion in substitutional alloys usually occurs by the interchange of position between atoms and adjacent vacant sites. Diffusion under irradiation may also take place by the motion of self-interstitials which are not present under equilibrium conditions. The irradiation enhancement of vacancy and interstitial concentrations will then give a corresponding increase of diffusion coefficients[64,65].

Diffusion under irradiation will occur through one of the following three mechanisms[66]: (1) vacancy (substitutional) site exchange with a neighboring atom; (2) an interstitial atom jumping to a neighboring interstice; (3) interstitialcy motion, which forces a substitutional atom into an interstice with the interstitial atom taking the vacant substitutional site. Interstitial type diffusion occurs in alloys with significant atomic size difference, while interstitialcy type diffusion occurs in alloys with similar solute/solvent sizes[67]. Among the three mechanisms, vacancy diffusion dominates at all temperatures where the irradiation-produced vacancies are mobile.

C.2. Radiation-Induced Solute Segregation

Under irradiation there are net fluxes of vacancies and interstitials to various sinks such as dislocations, internal interfaces and free surfaces. If there is a preferential coupling of certain alloying elements to these fluxes, irradiation-induced solute segregation will occur.

Solute segregation has a number of important consequences. Precipitates may form in locally enriched areas even though the precipitated phase is unstable at the average matrix composition. Conversely, precipitates which are stable at the average matrix composition may dissolve in depleted regions. Non-equilibrium surface compositions may alter the activation energy for the nucleation of voids or precipitated phases. In addition, the ability of a void surface to accept

point defects depends on its composition. A local alteration in surface composition may give significant changes in void nucleation and growth.

Irradiation-induced segregation is a complex physical phenomenon for which no complete physical model exists. Three kinetic models, namely, size factor, dilute solute/defect binding , and the inverse Kirkendall effect, have been developed and discussed in detail in the literature[60]. Here, only the size effect model will be discussed, because segregation in irradiated Cu-Ni alloys has been shown to be in agreement with the predictions drawn from this model (see Chapter 3).

According to the size model, self interstitials in BCC and FCC metals exist in a "dumbbell" configuration where two atoms share a single lattice site[68]. The dumbbell configuration has a lower strain energy when an undersized solute atom is included in it. The small atom would tend to remain part of the dumbbell, which would migrate by interchanging solvent atoms. The dumbbell will tend to migrate toward point defect sinks during irradiation, which leads to a preferential segregation of the undersized solute atoms around sinks.

C.3. Phase Stability under Irradiation

The phase transformations occurring under irradiations may be classified as either radiation-enhanced or radiation-induced[69]. Radiation-enhanced precipitation refers to transformations in which equilibrium is reached more quickly than in thermally aged specimens. Radiation-induced precipitation means transformations which will

revert back to the original phase when the sample is annealed after irradiation.

Solute segregation can cause precipitation at point defect sinks when the solute concentration there exceeds the solubility limit, but it cannot produce a phase which would not normally appear at that temperature without irradiation[70]. It was concluded that radiation-induced solute segregation can only shift the phase diagram laterally. Therefore, there must be other mechanisms responsible for the appearance of phases which are not thermally stable. This topic is beyond the scope of this thesis.

It has been shown by Martin[71] that radiation-induced segregation may also destabilize a stable solid solution to cause spinodal-like decompositions (periodic concentration fluctuations). The physical basis of the instability proposed by Martin is that a local increase in solute concentration due to solute segregation attracts vacancies. In turn, more interstitials are annihilated in the vacancy rich region, which would increase the local solute concentration yet more. Recently, Krisnan and Abromeit[72] presented a theory for radiation-induced spinodal type instabilities in concentrated alloys. The physical basis of the theory is the existence of a bias in vacancy-interstitial recombination which would enrich certain kinds of alloying element at certain regions through interstitial diffusion. In this way, a spatially periodic structure would be built up. The model yielded a temperature and dose rate independent

concentration fluctuation wavelength, which was stated to be in agreement with experimental observations.

D. Special Effects during Ion Irradiation

Several special effects which occur during ion irradiations should be considered when comparing results of ion irradiations to those of neutron irradiations:

(1) The displacement rates associated with heavy-ion bombardment studies are usually several orders higher than neutron irradiation, resulting in increased point defect recombination and a lower ratio of thermally emitted versus in-flowing vacancies. This high displacement rate effect on swelling is equivalent to conducting the irradiation at a lower temperature with lower displacement rates, because the temperature range of swelling is determined by a balance between point defect recombination, loss to sinks (including voids) and thermal emission of vacancies from voids[15]. That means heavy-ion irradiations shift the swelling regime to higher temperatures compared to neutron irradiations. The magnitude of the temperature shift of the swelling peak can be obtained by using a theory established by Bullough and Perrin[73].

(2) The energetic heavy ions used to create displacement damage in metals come to rest in the form of excess interstitial atoms in the matrix without a vacancy partner. These injected interstitials can cause decreased or complete suppression of void swelling, as shown both

experimentally and theoretically[74-76]. The effect is more pronounced at lower temperatures where the point defect recombination is important. In a heavy-ion irradiation, the peak in the damage profile overlaps the ion deposition profile, meaning that there is an excess of interstitials in the damage peak. Therefore, using the swelling data obtained from the peak damage region is not appropriate.

(3) It has been shown theoretically that point defect concentrations approach the thermal equilibrium values at the free surface if the surface is a good absorber of point defects[42]. As a result, a void denuded zone should exist near free surfaces. This effect of free surface is important in ion irradiations, especially when the ion energy is low, because the damage zone is limited to only a few microns or less below the incident surface. This effect is also important in electron irradiations performed in the HVEM, where the sample foil has to be very thin. According to Garner and Thomas[77], the width of the surface void denuded zone depends on temperature and displacement rate, being on the order of 0.5-1.0 μm for displacements rates typical of ion or electron irradiation.

(4) Since the point defect concentrations produced by ion irradiation is depth dependent, point defects may diffuse down the concentration gradient and cause a broadened point defect profile compared to the calculated damage profile using computer codes such as the Brice code. It is predicted that diffusional spreading will decrease void swelling at the damage peak and cause void swelling at depths

greater than would otherwise be expected[78]. Evidence of this diffusional spreading effect has been found in several studies[75,78-80].

In view of the effects caused by injected interstitials, free surfaces and diffusional spreading, it seems that the cross-section TEM analysis technique should as a rule be used whenever quantitative void swelling information is desired from ion irradiation studies[15], because only by this method can the depth dependent damage structure be studied accurately.

References for Chapter 2

1. D.R. Olander, Fundamental Aspects of Nuclear Reactor Fuel Elements, Ch. 17, ERDA Technical Information Document, TID-26711-PI, 1976.

2. G.J. Dienes and G.H. Vineyard, in: Radiation Effects in Solids, Chap. 2, pp. 6-55, Interscience, New York, 1957.

3. ASTM Standard E521, Annual Book of ASTM Standards, Part 45.

4. G.L. Kulcinski, Contemp. Phys. 20 (1979) 417-447.

5. J. Lindhard, V. Nielsen and M. Scharff, Mat. Fys. Medd. Dan. Vid. Selsk. 63, No. 10 (1968).

6. J. Lindhard, M. Scharff and H.E. Schoitt, Mat. Fys. Medd. Dan. Vid. Selsk. 33, No. 14 (1963).

7. J. Lindhard, V. Nielsen, M. Scharff and P.V. Thomsen, Mat Fys. Med. Dan. Vid. Selsk. 33, No.10 (1963).

8. K.B. Winterbon, P. Sigmund and J.B. Sanders, Mat. Fys. Medd. Dan. Vid. Selsk. 37, No. 14 (1970).

9. J. Lindhard and M. Scharff, Phys. Rev. 124 (1961) 128-130.

10. I.M. Torrens and M.T. Robinson, in: Radiation-Induced Voids in Metals, Edited by J.W. Corbett and L.C. Ianniello, U.S.A.E.C. Technical Information Center, CONF-710601, 1972, p. 739.

11. M.T. Robinson, Nuclear Fusion Reactors, British Nuclear Energy Society, London, 1970, p. 364.

12. J.H. Kinney, M.W. Guinan and Z.A. Munir, J. Nucl. Mater. 122 & 123 (1984) 1028-1032.

13. D.K. Brice,"Ion Implantation Range and Energy Deposition B Codes COREL, RASE4 and DAMG 2", SAND-7500622, Sandia National Laboratory, ALbuguergue, NM, July 1977.

14. D.B. Bullen, Ph.D. Thesis, University of Wisconsin-Madison (1984).

15. S.J. Zinkle, Ph.D. Thesis, University of Wisconsin-Madison (1985).

16. J.B. Whitley, Ph.D. Thesis, University of Wisconsin-Madison (1978).

17. K. Farrell, N.H. Packan and J.T. Houston, Rad. Effects 62 (1982) 39-52.

18. O.S. Oen, J. Narayan and T.S. Noggle, in Applications of Ion Beams to Metals, S.T. Picraux, E.P. Eer Nisse and F.L. Vook (Eds.), 1974, pp. 639-650.

19. J.B. Roberto and J. Narayan, in: Fundamental Aspects of Radiation Damage, CONF-751006-Pl, 1975, pp. 120-126.

20. J. Narayan, O.S. Oen and T.S. Noggle, J. Nucl. Mater. 71 (1977) 160-170.

21. S. Han, Ph.D. Thesis, University of Wisconsin-Madison (1988).

22. R. Bullough and R.C. Perrin, in: Radiation Damage in Reactor Materials, Vol.II, IAEA, Vienna (1969), p. 233.

23. J. Gittus, Irradiation Effects in Crystalline Solids, Applied Science Publ. Ltd., Barking, Essex, England (1978).

24. C. Cawthorne and E.J.Fulton, Nature 216 (1967) 575-576.

25. J.W. Corbett, Electron Radiation Damage in Semiconductors and Metals, Solid State Physics Supplement 7, Academic Press (1966).

26. S.D. Harkness and Che-Yu Li, in: Radiation Damage in Reactor Material, Vol.II, IAEA 230 (1969) 189-214.

27. S.D. Harkness, J.A. Tesk and Che-Yu Li, Nuclear Appli. and Tech. 9 (1970) 24-30.

28. J.L. Katz and H. Wiedersich, J. Chem. Phys. 55 (1971) 1414.

29. K.C. Russell, Acta Met. 19 (1971) 753.

30. K.C Russell, Acta Met. 26 (1978) 1615-1630.

31. W.G. Wolfer and A. Si-Ahmed, Phil. Mag. A 46 (1982) 723-736.

32. W.G. Wolfer, J. Nucl. Mater. 122 & 123 (1984) 367-378.

33. M.F. Wehner and W.G. Wolfer, Phil. Mag. A52 (1985) 189-205.

34. W.G. Wolfer et al., in: Proc. of Intern. Conf. on Rad. Effects in Breeder Structural Materials, M.L. Bleiburg and J.W. Bennett (Eds.), 1977, p. 841.

35. W.F. Wehner and W.G. Wolfer, Phys. Rev. A28 (1983) 3003.

36. S.D. Harkness and Che-Yu Li, Met. Trans. 2 (1971) 1457.

37. H. Wiedersich, Rad. Effects 12 (1972) 111-125.

38. A.D. Brailsford and R. Bullough, J. Nucl. Mater. 44 (1972) 121-135.

39. W.G. Wolfer, L.K. Mansur and J.A. Sprague, in: Rad. Effects in Breeder Reactor Structural Materials, Scottsdale, Arizona, 1977, p. 841.

40. A.D. Brailsford, R. Bullough and M.R. Hayns, J. Nucl. Mater. 60 (1976) 246.

41. A.D. Brailsford, J. Nucl. Mater. 60 (1976) 257.

42. L.K. Mansur, Nucl. Tech. 40 (1978) 5-34.

43. W.G. Wolfer and M.H. Yoo, ORNL/TM-5398 (May, 1975).

44. L.K. Mansur and W.G. Wolfer, J. Nucl. Mater. 69 & 70 (1978) 825-829.

45. H. Ullmaier, Nuclear Fusion 24 (1984) 1039.

46. K. Farrell, P.J. Maziasz, E.H. Lee and L.K. Mansur, in: Fundamental Aspects of Helium in Metals (Proc. Int. Symp., Julich, 1982), H. Ullmaier (Ed.), Rad. Effects 78 (1983) 1-417.

47. N.H. Packan and K. Farrell, Nucl. Technol. 3 (1983) 392.

48. K. Farrell, Rad. Effects 53 (1980) 175-194.

49. N.H. Packan and K. Farrell, J. Nucl. Mater. 85 & 86 (1979) 677.

50. A. Kumar and F.A. Garner, in: Proc. of the 12th Int. Symp. on Effects of Radiation on Materials, Williamsburger, June 18-29, 1984.

51. R.L. Sindelar, Ph.D. Thesis, University of Wisconsin-Madison, 1985.

52. S.J. Zinkle, L.E. Seitzman and W.G. Wolfer, Phil. Mag. A 55 (1987) 111-125.

53. L.E. Seitzman, L.M. Wang, R.A. Dodd and G.L. Kulcinski, J. Nucl. Mater. 141-143 (1986) 738-742.

54. L.E. Seitzman, Ph.D. Thesis, University of Wisconsin-Madison (1988).

55. E.E. Bloom, ORNL-TM-3492, 1971.

56. J.L. Brimhall, H.E. Kissinger and G.L. Kulcinski, BNWL-SA-3921, 1971.

57. J.O. Stiegler, K. Farrell, C.K.H. DuBoss and R.T. King, in: Radiation Damage in Reactor Materials, Vol.2, p. 215, I.A.E.A., Vienna,1969.

58. J.L. Brimhall and H.E. Kissinger, Rad. Effects 15 (1972) 259.

59. A. Si-Ahmed and W.G. Wolfer, J. Nucl. Mater. 102 (1981) 143.

60. K.C. Russell, Progress in Materials Science, 28 (1984) 229-434.

61. A. Si-Ahmed, Ph.D. Thesis, University of Wisconsin-Madison (1981).

62. P.R. Okamoto, N.Q. Lam and H. Wiedersich, in: Proc. of the Workshop on Correlation of Neutron and Charged Particle Damage, J.O. Stieger(Ed.), ORNL(June 1976), CONF-760673, p. 111.

63. W.G. Wolfer, F.A. Garner and L.E. Thomas, ASTM STP 782 (1982) 1023.

64. R. Sizmann, J. Nucl. Mater. 69-70 (1978) 386.

65. Y. Adda, M. Beyeler and G. Brebec, Thin Solid Films 25 (1975) 107-156.

66. H. Wiedersich, in Phase Stability during Irradiation (1981), p.23.

67. H. Wiedersich, P.R. Okamoto and N.Q. Lam, J. Nucl. Mater. 83 (1979) 98.

68. H.G. Haubold and D. Martinson, J. Nucl. Mater. 69-70 (1978) 644.

69. P. Wikes, J. Nucl. Mater. 83 (1979) 166-175.

70. K.C. Russell, J. Nucl. Mater. 83 (1979) 176.

71. G. Martin, Phys. Rev. B21 (1980) 2122.

72. K. Krishnan and C. Abromeit, J. Phys. F.14 (1984) 1103.

73. R. Bullough and R.C. Perrin, in: Irradiation Effects on Structural Alloys in Nuclear Reactor Applications, ASTM STP 484 (1970) 317.

74. A.D. Brailsford and L.K. Mansur, J. Nucl. Mater. 71 (1977) 110.

75. B. Badger, Jr., D.L. Plumton, S.J. Zinkle, R.L. Sindelar, G.L. Kulcinski, R.A. Dodd and W.G. Wolfer, ASTM STP 870 (1985) 297-316.

76. F.A. Garner, J. Nucl. Mater. 117 (1983) 177.

77. F.A. Garner and L.E. Thomas, in: Effects of Radiation on Substructure and Mechanical Properties of Metals and Alloys, ASTM STP 529 (1973) 303-325.

78. L.K. Mansur and M.H. Yoo, J. Nucl. Mater. 85 & 86 (1979) 523.

79. K. Farrell, N.H. Packan and J.T. Houston, Rad. Effects 62 (1982) 39.

80. C.H. Henager, Jr., J.L. Brimhall and E.P. Simonen, Rad. Effects 36 (1978) 49.

CHAPTER 3

REVIEW OF THE RELEVANT PREVIOUS EXPERIMENTS

A. Void Formation in Irradiated Pure Nickel

Shortly after the first finding of voids in neutron irradiated austenitic stainless steel by Cawthorne and Fulton[1], Brimhall and Mastel[2] reported the observation of voids in neutron irradiated pure nickel in 1968. Since then, numerous experimental work has been done on the topic of void formation in pure nickel as well as in other pure metals such as copper, aluminum, iron, vanadium etc., because it would help to gain an understanding of the basic mechanism in the absence of complex microstructures or phase changes. The methods used to introduce voids in pure nickel include irradiations by fast and thermal neutrons, heavy and light ions, and electrons. Most of the irradiations on pure nickel have already been reviewed by Whitley[3] and Bullen[4] with the irradiation conditions and the void parameters tabulated. In this section, first, a brief summary on the results of the previous neutron and electron irradiations of pure nickel will be given, then a somewhat more detailed review on the heavy-ion irradiated nickel, especially those with helium ions injected, follows.

Voids have been noted to form in neutron irradiated nickel over a temperature range from 260 °C (0.3 T_m) to 850 °C (0.65 T_m) when irradiated above a fluence of $5x10^{17}$ n/cm^2 [2,5-19] (as a crude estimate of damage, 10^{22} n/cm^2 corresponds to 5 dpa in EBR-II[20]). Lowering the

helium production from transmutation reactions by enriching with the Ni^{62} isotope increases void size and decreases void number density[21]. This indicates that the interstitial helium created from transmutation reaction may act to stabilize void embryos, thus greatly affecting the swelling behavior. The addition of carbon impurities (> 4 wppm) decreases the amount of swelling by an order of magnitude, while 600 wppm carbon can totally suppress void formation[13]. This is most likely due to the trapping of point defects which enhances recombination. Cold working provides an incubation period during which there is little swelling. When the incubation dose is reached, swelling begins and increases linearly at a rate of 1% per dpa[22].

Electron irradiation of nickel in the HVEM by Norris[23-26] and Harbottle[27] showed that voids grew only near dislocations and voids could only grow in the presence of a dislocation density of 10^9 cm^{-2}. Since a dislocation has a stronger attraction for interstitials than a void, it acts as a biased sink which facilitates void growth. However, only a very few point defects are produced per incident electron, and so HVEM studies in general are not of great value when attempting to simulate displacement cascade events. It should also be noted that the samples used in HVEM studies are very thin foils which introduces the effect of the surface as a sink for point defects. Therefore, the void parameters obtained might be very different from what would occur in bulk material.

During the past decade, many ion irradiations of pure nickel have been completed. The ion sources used include nickel[3,4,28-33],

proton[34,35], helium[36], selenium[32,37], carbon[3,20], aluminum[3] and copper[3]. The effect of gas atoms on void formation has been studied using simultaneous helium irradiation[33,38], helium pre-injection[4,32,37-39], hydrogen pre-injection[4] and hydrogen introduced during electropolishing[3]. Since practically all the experimental parameters varied greatly between different experiments, it is difficult to draw any definite conclusions from a detailed comparison of all the results. In general, voids were observed in these studies at temperatures ranging from 300 °C under proton irradiation[37] up to 725 °C under intense nickel ion irradiation[31] with the peak swelling temperature ranging from about 550 to 625 °C, depending on the displacement rate. The lowest dose at which voids were observed was 0.06 dpa under 5 MeV nickel ion irradiation[40]. The highest swelling reported is 12% after 5 MeV nickel ion irradiation to 140 dpa at 625 °C[30].

One of the most interesting features of the irradiation of nickel is the development of regular arrays of defects. Kulcinski et al.[32,37] noted that a FCC void lattice structure was formed after irradiation at 525 °C with 6 MeV selenium ions and with 6 MeV nickel ions to doses greater than 100 dpa. The lattice spacing of the void superlattice was found to be several hundred angstroms. At lower temperatures and lower doses, aligned arrays of loops were observed which formed similar superlattices.

The role of gaseous impurities on void formation in nickel is also very interesting.

Brimhall et al.[40] examined the influence of helium on void formation in 5 MeV self-ion irradiated nickel. Helium ions of 200 keV energy were injected either simultaneously with, or prior to, the self-ion irradiation. They found that helium promotes void nucleation with both implantation techniques. Initially, the number density of voids was found to be proportional to the helium deposition rate, and the swelling rate is dominated by the helium driven void nucleation. But the void density rapidly saturates with the increasing helium concentration; after that, swelling continues to increase with increasing dose only due to void growth.

In the early research, it was noted that voids were formed without pre-injected helium in several cases. Lanore et al.[41] in 1975 found that void formation could be completely suppressed in nickel and in copper by thoroughly outgassing the sample prior to bombardment. Later, Whitley[3] also concluded that void nucleation was very difficult in outgassed nickel. So it is believed that when helium is not injected, or is injected in small amount, the controlling influence on void nucleation is probably the residual gaseous impurities in the material such as oxygen and hydrogen. However, in the above mentioned experiments, the amount of residual gases was not specified. It is important to better understand the effect of these residual gases on void formation for both facilitating the comparison of different experiments and judging the desirability of giving a reactor core element a certain type of treatment prior to its use in a reactor system.

Whitley[3] reported that void nucleation could be significantly enhanced by electropolishing prior to irradiation due to the pickup of hydrogen during polishing. Bullen[4] studied the role of hydrogen on void formation in nickel by pre-injection of hydrogen before irradiation with nickel ions and reported an increase in swelling with increasing injected hydrogen concentration.

The cross-section technique for TEM sample preparation first used on ion irradiated nickel by Whitley[3] allows the entire ion damage region to be viewed at once. This is an important advantage since the damage rate and therefore the damage level varies with depth for ion irradiation. Only Farrell et al.[41] and Bullen[4] have investigated the effect of helium on void formation in heavy-ion irradiated nickel utilizing the cross-section technique.

Farrell et al. irradiated the 200-400 keV helium pre-implanted or co-implanted samples to peak damage levels of 1 and 50 dpa with 4 MeV nickel ions at 600 °C. The helium concentrations were 20 and 1000 appm respectively so that the appm helium/dpa ratio was kept constant at 20 at the peak damage region. They found that: (1) all the helium implanted samples showed enhancement of void nucleation and decrease in void size; (2) a greater number density of voids for pre-injected specimens compared with co-implanted specimens occurred; (3) helium pre-injection caused enhanced swelling at low ion dose, and depressed swelling at high dose, while helium co-implantation increased swelling continuously with ion dose. The ion energies used in this study produced

a range of helium and a range of self-interstitial nickel ions which are approximately the same. This may pose problems when attempting to fully understand nucleation of voids with respect to helium concentration and injected interstitial effects.

Bullen[4] pre-injected helium ions of 200-700 keV into nickel samples and irradiated them with 14 MeV nickel ions. With those energies, the helium and injected self-interstitial ranges are separated. In his study, samples uniformly pre-injected with helium to a depth of 1.25 μm at room temperature were irradiated with nickel ions at temperatures of 525 °C and 625 °C to fluences of 1-2.5x10^{20} ions/m^2 (3-7 dpa at 1 μm). All those samples showed some suppression of void formation over the pre-injected area. Irradiations at 625 °C after uniform helium pre-injection produced almost complete suppression of visible voids (where appm helium/dpa > 30). Suppression of void formation was also noted after irradiation at 525 °C for a relatively low damage level (where appm helium/dpa also > 30) with visible void formation observed at high damage level (where appm helium/dpa < 15). The suppression of void formation by helium pre-injection was attributed to the over-enhanced nucleation of small cavities which are below the resolution limit of the electron microscope.

From the above results, it is obvious that more experimental work on nickel, especially irradiation of samples with specified amounts of residual gases and helium pre-injection with appm helium/dpa ratio

lower than 15 should be performed to allow more accurate study of the effect of gases on void formation.

B. Void Formation in Irradiated Pure Copper

There have been many irradiations using neutrons, electrons and ions conducted on copper. Knoll[42] surveyed the copper radiation damage literature in 1980 and summarized the void and loop formation results obtained up to that time. That survey has been extended to include the recent reports by Zinkle[43]. Most of the results of void swelling studies of irradiated copper are tabulated in detail in the latter. Only a brief summary including some more recent results is given below.

Non-outgassed copper has been found to be susceptible to void formation when irradiated to doses on the order of only a fraction of a dpa at temperatures between 200 and 550 °C (0.35-0.61 T_m)[43].

Voids were observed in copper irradiated with neutrons to a dose of $5x10^{24}$ n/m^2 (0.14 dpa) at temperatures of 220 °C to 500 °C with peak swelling of about 0.40% occurring at 340 °C [44-46]. In this range, the average diameter of voids increases from 5 nm to more than 150 nm with increasing temperature, while the void density decreases rapidly, showing that higher temperature inhibits nucleation but favors growth. The lowest neutron dose at which void swelling has been found is less than 10^{21} n/m^2 (10^{-4} dpa)[47]. Studies also indicate that the number density of voids increases with increasing neutron dose, and the peak

swelling temperature decreases with decreasing dose rate[46]. The highest void swelling in copper after neutron irradiation is 55.8%[48], this occurred following irradiation to 98 dpa with neutrons in FFTF-MOTA at 450 °C.

Under electron irradiation in the HVEM, voids have been observed without any appreciable incubation dose in the temperature range of 250-550 °C [43,49]. The peak swelling temperature is around 450-500 °C depending on the dose rate. The swelling rate has been found to be 0.5-0.8%/dpa[50]. A swelling level as high as 17% and a swelling saturation was observed for doses greater than 75 dpa[51]. As in electron irradiated nickel, it appeared that voids can only form in the presence of a minimum dislocation density. In foils thin enough for most dislocations to escape (< 300 nm), no voids formed. That is in agreement with the theory[52]. The amount of void swelling depends critically on the dislocation density[50] and it seems that maximum swelling occurs for a cold-work level of 50%. Barlow[53] reported that the void density at a given temperature was roughly constant with respect to dose, whereas it decreased by a factor of five with the irradiation temperature increasing from 250 °C to 500 °C. This is very similar to the results obtained from neutron irradiation.

There have been several studies of the effect of gases on void formation in electron irradiated copper. Makin[51] observed that copper injected with argon displayed enhanced void nucleation. Barlow[53] reported that pre-injected helium enhances void formation for

concentration levels up to 50 appm. Too much helium (2000 appm) apparently over-stimulates void nucleation and suppresses observable void swelling[53]. Glowinski[54] found that ordinary high purity copper swelled very easily, while copper that had been degassed in high vacuum prior to irradiation showed reduced swelling and a shift of the swelling peak to lower temperatures. No voids formed in degassed copper specimens irradiated above 440 °C. That indicated the important role which the residual gas content in the sample may play.

Glowinski et al.[55-57] also carried out a comprehensive investigation of the effect of ion irradiation on void swelling in copper. After irradiation with 500 keV copper ions at a dose rate of $1x10^{-4}$ dpa/s void swelling occurred in non-degassed pure copper within the temperature range of 400-500 °C. Void size increased with the increasing temperature, while the void density remained the same. Increasing the ion damage rate by an order of magnitude caused the swelling curve to shift upward in temperature by 50 °C. The maximum void swelling occurred at 500 °C with a value of 9% after irradiation to 15 dpa at a dose rate of $1x10^{-3}$ dpa/s. The swelling peak region of the high dose rate case consisted of a lower density of larger voids as compared to the low dose rate case. The peak swelling temperature for ion irradiated copper at a damage rate of $1x10^{-4}$ dpa/s was increased by 115 °C compared with neutron irradiations, with a dose rate of $8x10^{-8}$ dpa/s[43]. As seen in electron irradiated copper, a minimum dislocation density is also found to be necessary for void formation under ion irradiation.

The gas effect on void formation in ion irradiated copper was also extensively investigated in Glowinski's studies[55-57]. High purity copper which had not been outgassed formed voids readily with an ion dose of 1.5 dpa. Copper specimens which were completely outgassed did not show any voids even when irradiated to 15 dpa at what previously had been the peak swelling temperature. Partially outgassed samples exhibited a bimodal void size distribution (mean void diameters of 75 nm and 130 nm) along with a reduction in the amount of swelling. Pre-injection of outgassed copper specimens with helium or oxygen resulted in void formation during irradiation. Helium has been observed to be more efficient than oxygen in nucleating voids for implanted concentrations of less 30 appm. No void formation occurred in specimens that had been implanted with hydrogen prior to irradiation. Specimens implanted with oxygen or helium in conjunction with carbon exhibited less swelling than if the carbon was absent.

Following Glowinski's work on the effect of specimen gas content, Knoll[58] irradiated both non-outgassed and outgassed high-purity copper with 14 MeV copper ions and examined them in cross section. No voids were observed in either case following irradiations at 400-500 °C to a peak damage level of 3-10 dpa. The absence of voids was attributed to the high purity of the copper (lack of gaseous impurities), in support of the Glowinski et al.'s results. Later, it was argued that Knoll may have been at too high an irradiation temperature range to observe void formation in copper that did not contain any gas[43]. This was because a void

nucleation calculation[59] indicated that the swelling regime for ion-irradiated pure copper in the absence of gas should be 100-250 °C. Again, the oxygen level was not specified for the outgassed specimens in the above mentioned studies.

Zinkle[50] irradiated high purity copper without further outgassing treatment using 14 MeV copper ions to peak damage levels of 40 dpa over the temperature range of 100-400 °C (0.28-0.50 T_m). Only a sparse distribution of voids was observed in the sample irradiated at 400 °C. The average void diameter for this condition was < 100 nm, with an estimated density of only 10^{17} m^{-3} ($\Delta V/V < 5x10^{-5}$). No voids were observed in pure copper for any of the other irradiation conditions. Instead, "black spot" defect clusters occurred in those samples. Detailed analysis indicated these "black spots" might be small interstitial loops and stacking fault tetrahedra. The defect cluster density was roughly constant for irradiation temperature of 100 and 200 °C. Irradiation at temperatures above 300 °C resulted in a very low defect cluster density. A room temperature injection of 45 appm helium into copper followed by a 40 dpa peak damage ion irradiation at 300 °C resulted in small voids in the helium implanted region. The average diameter of the voids was only 2.6 nm with a high density of $6x10^{21}$ m^{-3}. Conversely, pre-implantation of 45 appm hydrogen did not produce any observable cavity formation following irradiation to a peak damage of 40 dpa at 300 °C.

Recently, a vacancy cluster stability model has been developed[45,62] to predict the most stable vacancy cluster morphology in copper and

other metals as has been mentioned in Chapter 2. By this model, stacking fault tetrahedra are predicted to be the most stable configuration of vacancy clusters in copper when gas is absent. This is in agreement with the experimental findings of Zinkle. Small amounts (0.01-10 appm) of helium and oxygen are predicted to reduce the energies of voids so as to cause void formation to preferentially occur over stacking fault tetrahedra formation. A more accurate experimental investigation has just been completed by Zinkle (Sept. 1988)[61] to show the small amount of oxygen required for void stability in high purity copper foils (the detailed results have not been published yet).

C. Related Studies on Nickel-Copper Alloys

C.1. The Cu-Ni System

The Cu-Ni system is one of the few alloy systems which shows complete miscibility in the solid state at temperatures where thermal diffusion is sufficiently high for an observable mass transport. The early phase diagram published by Hansen[62] indicates that the system is single phase at all compositions, even at very low temperatures. However, from thermodynamic analysis, the existence of a miscibility gap at temperatures below 600 K is predicted by several authors[63-65]. In the recent edition of the Metals Handbook[66], a miscibility gap is indicated in the Cu-Ni phase diagram based on the calculation of Elford[67]. The phase diagram has been shown in Chapter 1 as Figure

1.1. The miscibility gap was calculated to be a maximum at 595 K for the Cu-80Ni (at.%) alloy. This prediction could not be verified for thermally treated samples since the thermally activated mass transport becomes too small around 620 K.

C.2. Solute Segregation and Phase Stability in Irradiated Ni-Cu Alloys

There have been several investigations of radiation enhanced diffusion and radiation induced segregation in Ni-Cu alloys. Following low energy (2-3 keV) neon and argon ion bombardment, the near-surface region of a Cu-Ni alloy was found to be nickel rich compared to the bulk when the dose rate is high[68]; while at low dose rates, a Cu-rich near-surface region, with a large Cu-depleted zone present underneath it, was reported[69]. The segregation of nickel toward the surface of initially homogeneous Ni-Cu alloys was also observed after a 2.2 MeV argon ion irradiation[70]. A post-irradiation anneal significantly reduced the amount of the segregation, indicating that it was radiation-induced as opposed to radiation-enhanced. Takahashi et al.[71] observed nickel segregation to grain boundaries and voids following a 650 keV electron irradiation. Similar results were later obtained by Takeyama[72] who observed a Cu-depleted zone at grain boundaries following electron irradiation. The radiation-induced segregation of nickel to sinks can be explained by the size effect as mentioned in Chapter 2. In addition, measurements of radiation-enhanced diffusion coefficients led to a conclusion that diffusion of nickel in copper under irradiation was by an

interstitialcy mechanism, which is in agreement with the previous proposal for alloys with similar solute/solvent sizes[73]. Recently, Lam et al.[74] have measured changes in the surface compositions induced by heating and by ion sputtering (3 keV neon) of Ni-40Cu in the temperature range of 25-700 °C, and found that copper atoms segregated to the alloy surface during sputtering upon heating, and diffusion in the altered surface region is significantly enhanced by ion bombardment below ~ 550 °C.

Clustering or precipitation on a very small scale is believed to occur in Cu-Ni alloys following certain irradiations based on electrical resistance changes. Schule et al.[75] studied the decreased resistivity during neutron irradiation in twelve different Cu-Ni alloys with nickel contents from 35 to 85 wt.%. The alloy with 70% nickel had the largest decrease in electrical resistivity at low temperatures although the change was already detectable below 700 °C. A great resistivity decrease was also observed in the alloy containing 55% nickel during neutron irradiation at temperatures between 100-150 °C. The resistivity decrease was also reported in neutron irradiated Cu-50Ni at irradiation temperatures of 100-300 °C by Chountas[76] and in Cu-5Ni during a room temperature 14 MeV neutron irradiation by Zinkle and Kulcinski[77]. Those observations were attributed to precipitation[77] or the creation of nickel-rich domains due to radiation enhanced-diffusion[76].

Poerschke and Wollenberger[78,79] have carried out extensive studies of the behavior of irradiated Cu-Ni alloys utilizing resistivity,

neutron diffraction and positron annihilation techniques. They found that irradiation of Cu-Ni with 3 MeV electrons at temperatures above 100 K caused a decrease in resistivity which was attributed to decomposition of the solid solution by nickel clustering. Arguments were given to show that the clustering is due to an irradiation-induced interstitialcy diffusion mechanism. Isochronal annealing and positron annihilation measurements following low temperature electron irradiation indicated atomic clustering between 110 K and 250 K due to interstitial migration. They and Wagner[80] together performed diffuse and small-angle neutron diffraction studies of Ni-41Cu after irradiation with 3 MeV electrons at temperatures between 373 K and 640 K. Besides an increase in the short range clustering, a periodic decomposition with a wavelength around 4.5 nm was observed after irradiation at temperatures below 480 K. The authors concluded that the process consists of an ordering of the short range order (SRO) clusters with a resulting SRO cluster "lattice" with a lattice constant 4.5 nm. The decomposition structure was found to be stable against thermal annealing and irradiation at least up to 510 K. Upon thermal treatment above 600 K dissolution of the long-range decomposition took place. The observation is in very good agreement with the predictions derived from thermodynamic calculations by Elford, where the critical temperature of the miscibility gap for the alloy is about 560 K (see Figure 1.1). Wagner et al. interpreted their results in terms of radiation-enhanced diffusion, but also considered the possibility of an irradiation induced-transformation.

The low damage level (< $5x10^{-3}$ dpa) is unlikely to give an irradiation-induced transformation but could certainly increase the atomic mobility by orders of magnitude over the thermal values. The short-range order parameter α_1[81] has been measured for Cu-Ni system by several authors[65,82,83], their results indicating not only that local clustering does occur in the Ni-Cu alloys but also that the tendency for clustering is higher in a more concentrated Ni-Cu solid solution than in a dilute solution, and is higher at lower temperatures. Some of those results will be shown in Chapter 6 with the discussion of the results from the present study.

Barlow[53] had proposed that G.P. zones may occur during HVEM irradiation of Cu-Ni at elevated temperatures based on a dislocation loop analysis, but no direct evidence was obtained. Because the atomic scattering factors and atomic diameters of the copper and nickel atoms are very similar, it would be almost impossible to detect G.P. zones in Ni-Cu alloys by electron diffraction. In another paper, Singh, Leffers and Barlow[84] noted that the density of "black dots" observed in copper based Cu-Ni alloys under HVEM increased with nickel concentration. They assumed those "black dots" to be nickel clusters surrounded by small interstitial loops.

In summary, there seems to be strong evidences to suggest that clustering takes place in Cu-Ni alloys during irradiation, although the evidence may not be direct.

C.3. Void Formation Study on Neutron Irradiated Ni-Cu Alloys

The first experimental study on void formation in Ni-Cu alloys was performed by Brimhall and Kissinger[8] in 1972 using fast neutron irradiation. The irradiation conditions and the results of their study are summarized in Table 3.1. In the study, copper, nickel and Cu-Ni alloys containing 2, 20, 50, 80 and 98 at.% nickel were irradiated to a constant dose of 2.4×10^{19} fast neutrons/cm^2 (0.01 dpa) at 285 °C. Voids were only observed in copper, nickel and Cu-2Ni. In the Cu-2Ni alloy, the void size increased to approximately 30 nm compared to 18 nm in pure copper. The void density, however, decreased by approximately 20 times resulting in a net swelling of about 0.01% as compared to 0.074% for pure copper. The void distribution was also very nonuniform compared to pure copper. A low density of very small black spots ($d < 5$ nm) were also present.

In the Cu-20Ni alloy, no voids were detected. The only manifestation of damage was the low density of small black spots ($d < 5$ nm).

In the high nickel alloys ranging from 50% nickel to 98% nickel, the damage structure was basically the same. No voids were observed but a number of small prismatic dislocation loops of interstitial type were found. That kind of loop was also found in pure nickel together with voids. The loops tended to increase in size and decrease in number density on decreasing the nickel content of the alloy. This corresponds to the effect of an increase in the temperature on the nucleation of

Table 3.1 Results of fast neutron irradiations† of Cu, Ni and Cu-Ni alloys reported by Brimhall and Kissinger[8]

Material	Defect*	$\bar{d}$* (nm)	N_v* (10^{20} m^{-3})	$\Delta V/V$* (%)
Cu	V	18.7	2.2	0.074
Cu-2Ni	V	30	0.1	0.01
Cu-20Ni	—	—	—	—
Cu-50Ni	L	—	—	—
Ni-20Cu	L	—	—	—
Ni-2Cu	L	—	—	—
Ni	V, L	10.5	3.6	0.2

† Irradiation conditions: 285 °C, 2.4×10^{23} n/m^3 (0.01 dpa), dpa rate: $< 9 \times 10^{16}$ n/m^2s

* V — Void, L — Dislocation loop (interstitial type),

$\bar{d}$ — Mean void density, N_v — Void density, $\Delta V/V$ — Swelling

interstitial loops[53]. Although no voids were observed in these alloys, the presence of interstitial loops suggests that a considerable vacancy concentration must have been generated. Precision lattice parameter measurements showed that irradiation produces a lattice parameter decrease in these high nickel alloys, indicating an excess vacancy concentration[63]. The fraction of excess vacancies generated was estimated from the size and the density of the interstitial loops, and the result gave quite good agreement with the unit cell volume change calculated from the lattice parameter measurement. It also agreed with the value of void volume fraction observed in pure nickel irradiated under the same conditions. It was therefore implied that vacancies or

small vacancy clusters were present, but these evidently were trapped and prevented from forming observable voids in these Ni-Cu alloys.

Brimhall and Kissinger interpreted these results in terms of the trapping of point defects by single atoms of the alloy constituents. Based on the simple reasoning of atom size, the small nickel atom in the matrix of larger copper atoms would have a greater affinity for the interstitial in the copper-rich alloys. In this case, trapping of the interstitials by nickel atoms prevented them from forming loops and, hence, making them more available for recombination with vacancies. In fact, high copper alloys showed a notable lack of general radiation damage of any type except some unidentified small black spots. This argument was also supported by the lattice parameter measurements which showed no change produced by the irradiation of high copper alloys. In the nickel based alloys, excess vacancies or small vacancy clusters are present but are trapped by the larger copper atoms. Therefore, the void suppression mechanism is not the same in high nickel alloys as for high copper alloys, although both of them have been related to the trapping of point defects by alloying constituents.

The other mechanism, which could occur simultaneously, mentioned by Brimhall and Kissinger is the combining of the gas atoms with the alloying elements and thereby removing these atoms as potential nucleating sites. This was supported by the observation of a reduction in void density in the Cu-2Ni alloy.

When considering an alloy of Cu-50Ni, explanations based on trapping by alloying elements break down. Also, the effect of single atoms of solute on the point defect mobilities is unlikely to be significant in the case of Ni-Cu alloys where the nickel and the copper atoms are of similar size. So, better explanations for the void suppression in Ni-Cu alloys are needed.

Based on the mechanism of point defect trapping by alloying elements, Brimhall and Kissinger further predicted that at the composition around 50%, the onset of void formation had just essentially been delayed to a higher fluence, and the potential for void formation is much greater in the nickel-rich alloys than in the copper-rich alloys.

Recently, Brager and Garner[48] have reported a large amount of swelling in fast neutron irradiated Cu-5 wt.% Ni. The samples were irradiated at 450 °C in FFTF to the fluences which for pure copper correspond to 16, 63 and 98 dpa. The swelling at 16 dpa (2.15%) is about one third of the swelling observed in pure copper irradiated at the same condition (6.5%). However, at higher doses the amount of swelling in Cu-5Ni is very large (31.8% at 63 dpa, 52.9% at 98 dpa), and is comparable with that observed in pure copper (33.2 at 63 dpa, 55.8 at 98 dpa). Unfortunately, no other Cu-Ni alloys with higher nickel contents were irradiated in that study for comparison.

C.4. Void Formation Study on Ion Irradiated Ni-Cu alloys

In order to extend the investigation of Cu-Ni alloys to higher damage levels, Mazey and Menzinger[85] irradiated pure nickel, pure copper and five Cu-Ni alloys at various temperatures between 300 °C and 600 °C with Ni^+, Cu^+ and C^+ ions at 0.1 MeV, or Ni^{6+} ions at 46.5 MeV. The compositions of the five irradiated alloys were the same as those which had been irradiated with neutrons by Brimhall and Kissinger[8], i.e. Cu-Ni alloys containing 2, 20, 50, 80, and 98 at.% nickel. The experimental conditions and results are shown in Table 3.2. Before irradiation with the ions, the samples were injected with helium to a uniform concentration of 10 appm. The high energy (46.5 MeV) nickel ion irradiations were performed using the Variable Energy Cyclotron (VEC) at AERE Harwell, and the peak damage level for the irradiations was determined to be 30 dpa. The samples of the VEC irradiated material were examined at different depth along the ion range by a back-thinning technique. Actually only three alloy samples were irradiated in the VEC by high energy nickel ions. Most experiments in their study were carried out using the combined heavy-ion accelerator/200 kV electron microscope ("Link") facility. In these experiments the ion beam of 0.1 MeV was inclined at 45 degrees with respect to the sample surface, the evolution of damage being observed in-situ in the 200 kV electron microscope during irradiation. Obviously, in this case the samples must be very thin, and therefore the surface effects and injected interstitial effects would exert a large influence on void formation. This makes attempts at extracting any

Table 3.2 Characteristics of ion irradiated Ni-Cu alloys reported by Mazey and Menzinger[85]

Material (% of Ni)	Temp. (°C)	Ion	Energy (MeV)	Dose (10^{16} ions/m^2)	Void Presence	$\bar{d}$* (nm)	ΔV/V (%)
Ni	450-710	Ni^+ or Cu^+	0.1	4	Yes	16.1	6 (600 °C)
98	500	Cu^+	0.1	4	No		
98	500	C^+	0.1	13	Yes		
98	600	Ni^+	0.1	10	Yes	20.7	6
80	500	C^+	0.1	4	No		
80	500	Ni^{6+}	46.5	2.5 (30 dpa)	No		
80	600	C^+	0.1	10	No		
50	300-400	Cu^+	0.1	8	No		
50	450	Cu^+	0.1	4	No		
50	530	Cu^+	0.1	20	No		
20	450	C^+	0.1	4	No		
20	500	Ni^{6+}	46.5	2.5 (30 dpa)	No		
2	400	Ni^{6+}	46.5	2.5 (30 dpa)	Yes	30	0.9
2	420	Cu^+	0.1	3	No		
2	450	C^+	0.1	7	No		
Cu	275-350	Cu^+	0.1	12	No		
Cu	400	Ni^{6+}	46.5	2.5 (30 dpa)	Yes	30	1.0
Cu	350-450	C^+ or Cu^+	0.1	12	Yes		

* $\bar{d}$ — Average diameter of voids, ΔV/V — Swelling

quantitative information from those experiments of dubious value. A calculation which did not take the surface effect into consideration gave 80 dpa for $1x10^{16}$ ions/cm^2 of 0.1 MeV copper or nickel, and about 6 dpa for $1x10^{16}$ ions/cm^2 of 0.1 MeV carbon.

As shown in Table 3.2, after irradiation, only the pure metals and the alloys containing 2% nickel or copper showed voids, while those containing 20, 50, 80% nickel were found to be completely free from voids. At the copper end, the void diameter in both 46.5 MeV nickel ion irradiated pure copper and Cu-2Ni was found to be always close to 30 nm and swelling was slightly higher in pure copper. An increase in swelling with depth was observed in those two samples, but as a consequence of some inhomogeneity in void distribution and insufficiency of data, Mazey et al. were not able to establish a swelling versus depth relation for the high energy irradiation. No data were obtained for comparison of void formation in Ni-2Cu and pure nickel at high energy irradiations, but it was found that after bombardment with 0.1 MeV nickel ions at 600 °C similar swelling (6%) was attained in both materials at a dose which was 2.5 times higher in the alloy than in the pure metal. The average diameter of voids in this instance was 20.7 nm in the alloy and 16.1 nm in pure nickel.

The high-concentration alloys had no observable voids after high- or low-energy ion irradiation, but a well-developed damage structure consisting of clusters, dislocation loops and tangled dislocations was observed. The loops were larger at higher doses. A higher density of

loops was observed in the 80% nickel alloy where dislocation tangles were the characteristic feature. At 50% nickel, only low energy irradiations were carried out, and in these conditions the damage had a very fine structure consisting of dislocation loops and a high density of small black spot defects with a diameter of about 5 nm.

It was proposed that fine-scale clusters having a different composition from the solid solution matrix might be present in the alloys and those clusters would act as traps for displaced interstitials and vacancies, so inhibiting vacancy agglomeration into voids. The fact that clusters of nickel atoms were present, at least in copper-rich alloys, was indicated by some weak ferromagnetism in the samples at room temperature.

Leister[86] has carried out an investigation of the effect of nickel solute concentration on void swelling in Cu-Ni alloys. Cu-Ni alloys containing 0.1, 1, 10, 20 and 50% nickel were irradiated with 200 keV copper ions to damage levels up to 120 dpa. The alloy containing 0.1% nickel exhibited enhanced swelling as compared to pure copper, while the 1% nickel and 10% nickel alloys showed reduced swelling as compared to pure copper. This can be seen in Figure 3.1. No swelling was observed in the alloys containing 20 and 50% nickel. Increasing the nickel content from 0.1 to 1% caused a delay in the incubation dose and a lower void density. Swelling in Cu-0.1Ni began to saturate at a dose of 60 dpa with a value of 10-20%. The Cu-1Ni alloy showed swelling saturation at a dose of 40 dpa with a value of 3-4%. A possible problem for Leister's

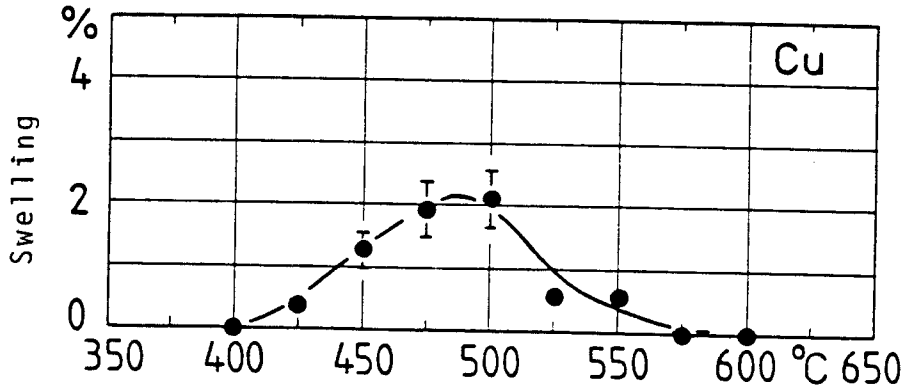

(a)

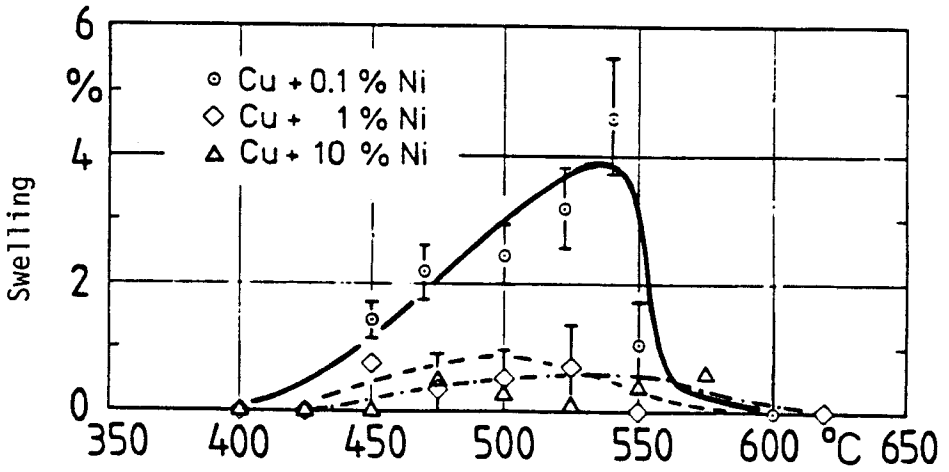

(b)

Figure 3.1 Swelling versus temperature for (a) pure Cu and (b) Cu-Ni alloys containing 0.1, 1 and 10 at.% Ni after irradiation of 200 keV Cu ions to 60 dpa by Leister[86].

experiments is that the damage region for 200 keV copper ions only extends to about 50 nm from the surface. In this case, as mentioned before, the surface effects on void formation can not be neglected. Therefore, it is probably not appropriate to attempt to extract quantitative data out of the Leister study. However, the observed qualitative trends may still be applicable.

Another series of heavy-ion irradiations of Cu-Ni alloys was performed by Dauben and Wahi[87]. In their study, specimens of pure copper and Cu-Ni alloys with 1 to 58.6% nickel were irradiated at 700 K with 300 keV copper ions at displacement rates of $3x10^{-4}$ dpa/s to $7x10^{-3}$ dpa/s. The total fluence varied from 0.2 dpa to 14.7 dpa. After irradiation, no voids but many dislocation loops were found. The dislocation loops were uniformly distributed and grouped into two distinct size classes- large loops of mean diameter of about 13 nm having a number density of $5x10^{15}$ cm^{-3}, and smaller loops (d < 4 nm) having a number density of one order of magnitude higher. By applying the 2 1/2-D method the small loops were identified as perfect vacancy loops with a Burgers vector of a/2<110>. The larger loops were identified as 70% faulted (Frank) loops ($\bar{b}$ = a/3 <111>) and 30% perfect loops. The vacancy/interstitial nature of the larger loops was not determined by experimental measurements, but on the basis of growth kinetics, calculations for dislocation loops under the irradiation conditions concluded that the large loops were of interstitial nature. All measured parameters such as loop density, diameter, Burgers vector and loop nature did not change, within the

experimental uncertainty, with the irradiation conditions. These results show that the density and size of the loop saturate very early in the course of irradiation so that within the range of fluences employed in the study these parameters remain approximately constant.

Summarizing this section, most heavy-ion irradiations of Ni-Cu alloys were conducted using low energy ions (0.1-0.3 MeV) where the surface effect would have a big influence on void formation. Only three alloy samples (Cu-2Ni, Cu-20Ni and Cu-80Ni) were irradiated by high energy ions (46.5 MeV) and no cross-section analysis has been done. After heavy-ion irradiation, no voids were reported for copper-rich Cu-Ni alloys with nickel concentration greater than 10% and for nickel-rich Ni-Cu alloys with copper concentration greater than 2%.

C.5. Void Formation Study of Ni-Cu Alloys by HVEM

Barlow[53] and co-workers[84] have studied Cu-Ni alloys in detail under 1 MeV electron irradiation, in the temperature range of 250-600 °C in the high voltage electron microscope (HVEM). The alloys irradiated are those containing 1, 2, 5, 10, 80, 90, 95, 98 and 99% nickel by weight. The thickness of the irradiated area was of the order of 1000-2000 nm. Generally, they found that voids were more difficult to form with increasing solute concentration.

For the Cu-based alloys, the void swelling versus nickel content curves were determined for several irradiation conditions, i.e. 250 °C, 90 dpa; 350 °C, 45 dpa and 450 °C, 30 dpa. The curves are shown in Figure

3.2 (a). The figure clearly shows that, at all the three conditions, the swelling decreases with increasing nickel content and becomes practically zero at a nickel content of 10%. Also, they found that the mean diameter of voids decreased dramatically as the nickel content increased from 1% to 5%, as shown in Figure 3.2 (b), whereas the void densities changed only slightly. From those observations they determined that the decrease in swelling in Cu-based Cu-Ni alloys comes mainly via reduced void growth or growth rate. They attributed this suppression of void growth to the formation of radiation-induced submicroscopic nickel clusters which act as vacancy or interstitial traps, thereby increasing point defect recombination.

In the case of the Ni-based alloys, voids were increasingly more difficult to form with increasing copper content. Although no swelling data was shown, it was stated that, in Ni-1Cu and Ni-2Cu, voids were formed during almost every irradiation at 450 °C 550 °C and 600 °C. In Ni-5Cu voids were formed readily at 550 °C and 600 °C but no voids were observed in three out four irradiations at 450 °C although a dislocation network was produced in each case. In Ni-10Cu voids were often formed at 600 °C but no voids were seen at 450 and 550 °C despite repeated attempts; a dislocation network is also formed in each irradiation. In Ni-20Cu, no voids were observed in irradiations at all the three temperatures, even with a dose of about 100 dpa. But in contract to the copper-based alloys, the observed average diameter of voids seemed to be independent of alloy composition in the range of Ni-1Cu to Ni-10Cu (see

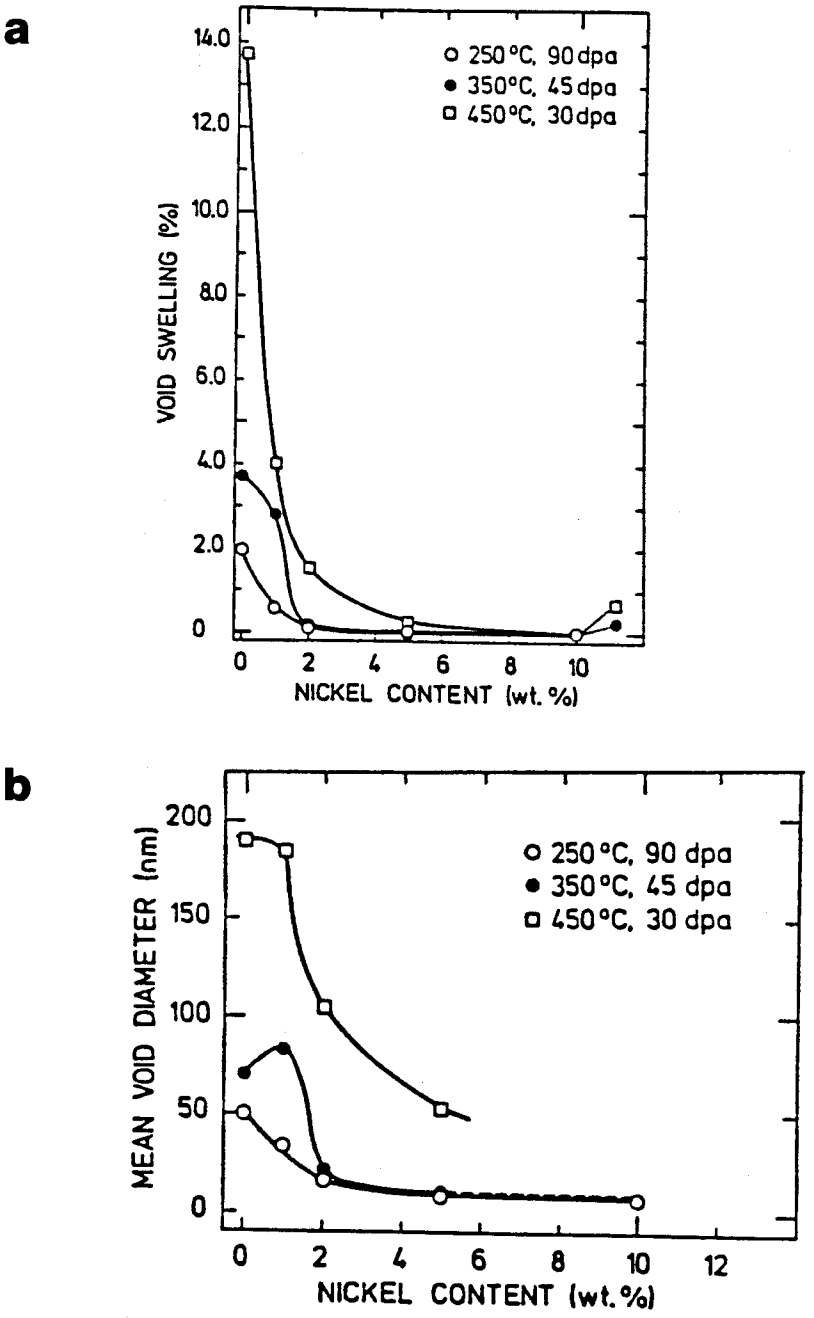

Figure 3.2 Swelling(a) and mean void diameter(b) as functions of Ni content for Cu-based Cu-Ni alloys after electron irradiation in HVEM at three different conditions by Barlow[53].

Figure 3.3), whereas the number density of voids decreased with increasing copper content. From that fact, it was concluded that nickel-based Ni-Cu alloys have little effect on void growth but tend to suppress void nucleation. The mechanism of the void nucleation suppression in this case was not discussed.

The result of the HVEM study seems to be in good agreement with neutron and ion irradiations reviewed previously.

C.6. Helium Bubble Formation in Ni-Cu Alloys

In order to investigate some of the properties of the Cu-Ni system which may be related to its void resistant nature, Zinkle et al.[88] have undertaken a study of helium bubble formation. In this study, copper, nickel and three Cu-Ni alloys containing 20, 50 and 80% nickel were irradiated with 200-400 keV helium ions at a constant homologous temperature of 0.65 T_m. A helium concentration of 200 appm was obtained at a depth of approximately 0.7 μm by the implantation. All samples were held at the implantation temperature for one hour following the irradiation to ensure there was no survival of displacement damage structure from the helium irradiation. The implanted region of the samples was been analyzed by TEM using the back-thinning technique. A low density of helium bubbles was observed in the pure copper, pure nickel and in all the three alloys. The helium bubbles for all samples investigated were found to be at, or in the vicinity of a strain field such as a dislocation or grain boundary. The variation of bubble

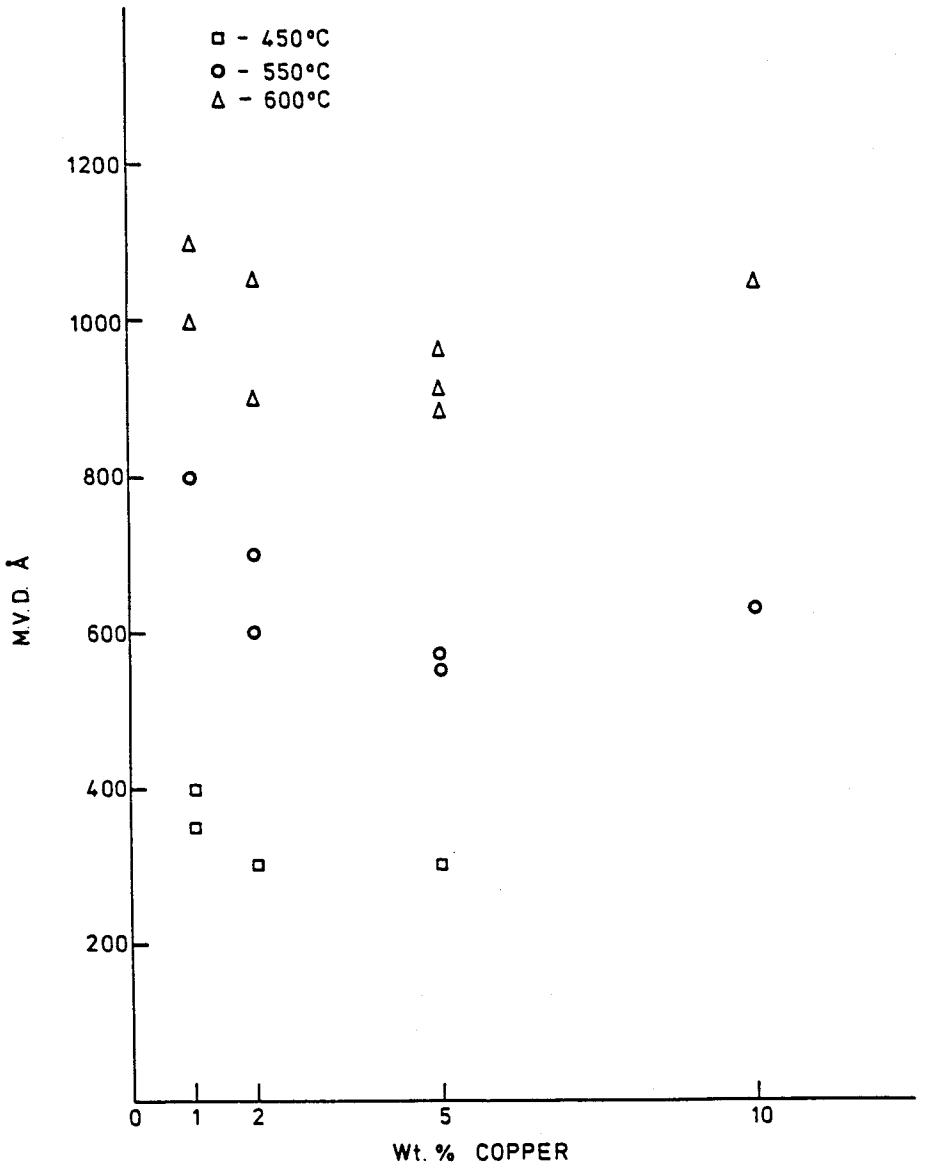

Figure 3.3 Mean void diameter as a function of Cu content for Ni-based Ni-Cu alloys after electron irradiation in HVEM to 50 dpa by Barlow[53].

density and size as a function of alloy composition is shown in Figure 3.4. The observed bubble parameters of the alloys are similar to those in pure copper, no significant differences having been found. The helium bubble formation is not unexpected as there are theoretical and experimental indications that helium tends to undergo spontaneous precipitation when implanted in metals. The fact that nothing special was observed in the bubble parameters for the Cu-Ni alloys was considered as an indication of nothing anomalous about the vacancy formation energy for the Cu-Ni alloys. As can be seen in Figure 3.4, the addition of copper to nickel causes a decrease in the bubble number density and an increase in the bubble size. The cause of that was not determined. In any event, nothing concerning helium bubble growth in the Cu-Ni system which would explain the void resistance of the alloys was found.

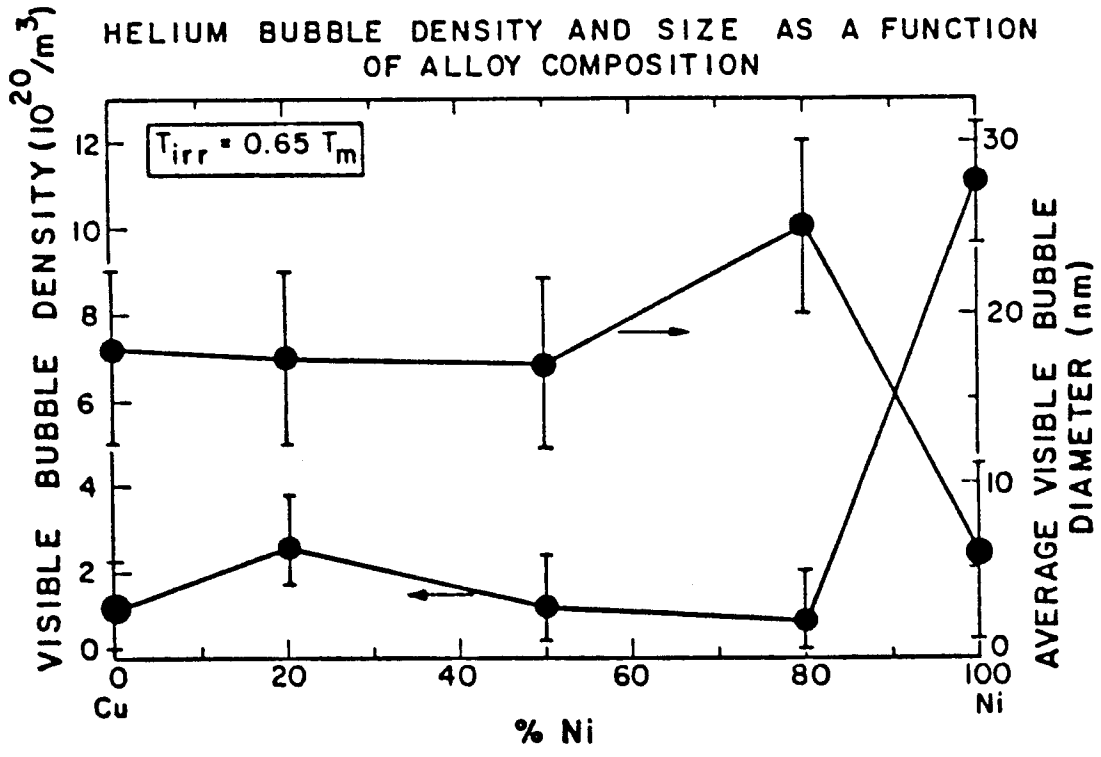

Figure 3.4 Variation in the He bubble density and average bubble size with alloy composition measured by Zinkle et al[88] after injection of He at 0.65 T_m.

References for Chapter 3

1. C. Cawthorne and E.J. Fulton, Nature 216 (1967) 575-576.
2. J.L. Brimhall and B. Mastel, J. Nucl. Mater. 28 (1968) 115.
3. J.B. Whitley, Ph.D. Thesis, University of Wisconsin-Madison (1978).
4. D.B. Bullen, Ph.D. Thesis, University of Wisconsin-Madison (1984).
5. J.L. Brimhall and B. Mastel, J. Nucl. Mater. 33 (1969) 186.
6. J.L. Brimhall and B. Mastel, J. Nucl. Mater. 29 (1969) 123.
7. J.L. Brimhall and B. Mastel, Scripta Met. 4 (1970) 51.
8. J.L. Brimhall and H.E. Kissinger, Rad. Effects 15 (1972) 259-272.
9. J.L. Brimhall, H.E. Kissinger and G.L. Kulcinski, Radiation Induced Voids in Metals, ed. Corbett and Ianniello, Albany, NY, 1971.
10. J.O. Steigler and E.E. Bloom, Rad. Effects 8 (1971) 33.
11. Y. Adda, Radiation Induced Voids in Metals, ed. Corbett and Ianniello Albany, NY, 1971.
12. N.H. Packan, K. Farrell and J.O. Steigler, J. Nucl. Mater. 78 (1978) 143-155.
13. S.M. Sorenson and C.W. Chen, Fundamental Aspects of Radiation Damage in Metals, Gatlinburg, TN, (1975) P.1213-1220.
14. J.E. Harbottle and S.M. Dickerson, J. Nucl. Mater. 44 (1972) 313-317.
15. E.E. Bloom and J.O. Steiger, Am. Nucl. Soc. Trans. 12 (1969) 116.
16. J.J. Holmes, Am. Nucl. Soc. Trans, 12 (1969) 117.
17. F.A. Smidt, J.A. Reed and J.A. Sprague, NRL Memorandum Report No. 3588, Sept. 1977.

18. C. Brown, Proceedings of Symposium on Physics of Irradiation Produced Voids, Harwell, England, Sept. 9-11, 1974, AERE-R-7934, 1975, p. 90.

19. C.W. Chen and R.W. Buttry, Rad. Effects 56 (1981) 210-228.

20. T.D. Ryan, Ph.D. Thesis, University of Michigan (1975).

21. V. Levy, Consultant Symposium on The Physics of Irradiation Produced Voids, ed. Nelson, Harwell, U.K., 1974, AERE-R7934, 1975, p. 50.

22. F.A. Garner, J. Nucl. Mater. 117 (1983) 177-197.

23. D.I.R. Norris, Phil. Mag. 22 (1970) 1273.

24. D.I.R. Norris, Nature 227 (1970) 830.

25. D.I.R. Norris, Phil. Mag. 23 (1971) 135.

26. D.I.R. Norris, J. Nucl. Mater. 40 (1971) 66.

27. J.E. Harbottle, Phil.Mag. 27 (1973) 147.

28. J.L. Brimhall, L.A. Charlot and E.P. Simonen, J. Nucl. Mater. 103 & 104 (1981) 1147-1150.

29. J.A. Sprague, J.E. Westmoreland, F.A. Smidt, Jr. and P.R. Malmberg, J. Nucl. Mater. 54 (1974) 286-298.

30. W.G. Johnston, J.H. Rosolowski, A.M. Turkalo and L. Lauritzen, J. Nucl. Mater. 54 (1974) 24-40.

31. N.H. Packan, K. Farrell and J.O. Steigler, J. Nucl. Mater. 78 (1978) 143-155.

32. G.L. Kulcinski, J. Brimhall and H. Kissinger, Int. Conf. on Radiation Induced Voids in Metals, ed. Corbett and Ianniello, Albany, NY, 1971, CONF-710601, p. 449 (1972).

33. F. Menzinger and F. Sacchetti, J. Nucl. Mater. 57 (1975) 193-197.

34. D.J. Mazey and J.A. Hudson, J. Nucl. Mater. 37 (1970) 13-17.

35. H.H. Neely and K. Herschbach, Rad. Effects 7 (1971) 187-194.

36. G. Fenske, S.K. Das, M. Kaminsky, and G.H. Miley, J. Nucl. Mater. 85 & 86, (1979) 707-711.

37. G.L. Kulcinski, J.L. Brimhall and H.E. Kissinger, J. Nucl. Mater. 40 (1971) 166-174.

38. J.L. Brimhall and E.P. Simonen, J. Nucl. Mater. 68 (1977) 235-243.

39. K. Farrell, N.H. Packan and J.T. Houston, Rad. Effects 62 (1982) 39-52.

40. J. L. Brimhall and E.P. Simonen, BNWL-01939, UC-20 (April 1976), p.24.

41. J.M. Lanore, L. Glowinski, A. Risbet, P. Regnier, J. Flament and Y. Choi, Int. Conf. on Fund. Aspects of Radiation Damage in Metals, Gatlinburg, Tenn., 1975, CONF-751006, p. 1169 (1976).

42. R.W. Knoll, UWFDM-384, University of Wisconsin (Oct, 1980).

43. S.J. Zinkle and R.W. Knoll, UWFDM-578, University of Wisconsin (June 1984).

44. V. Levy, J. Mathie, A. Risbet, R. Levy and J.P. Poirier, in: Voids Formed by Irradiation of Reactor Materials, S.F. Pugh (Ed.), British Nuclear Energy Society (1971) 64-68.

45. Y. Adda, in: Radiation-Induced Voids in Metals, J.W. Corbet and L.C. Ianniello (Eds.), AEC Symposium Series No. 26 (1972) pp. 31-81.

46. M. Labbe, G. Brebec and J.P. Pairier, J. Nucl. Mater. 49 (1973/74) 232-234.

47. C.A. English, J. Nucl. Mater. 108 & 109 (1982) 104-123.

48. H.R. Brager and F.A. Garner, Fusion Reactor Materials, DOE/ER-0313/3 (Sept. 1987), pp. 254-259.

49. T. Takeyama, S. Ohnuki and H. Takahashi, J. Nucl. Mater. 89 (1980) 253-262.

50. S.J. Zinkle, Ph.D. Thesis, University of Wisconsin-Madison (1985).

51. M.J. Makin, in: Voids Formed by Irradiation of Reactor Materials, S.F. Pugh (Ed.), British Nuclear Engineering Society (1971), pp. 269-274.

52. W.G. Wolfer, J. Nucl. Mater. 122 & 123 (1984) 367-378.

53. P. Barlow, Ph.D. Thesis, University of Sussex, England (1977).

54. L.D. Glowinski, J. Nucl. Mater. 61 (1976) 8-21.

55. L.D. Glowinski, C. Fiche and M. Lott, J. Nucl. Mater. 47 (1973) 295-310.

56. L.D. Glowinski and C. Fiche, J. Nucl. Mater. 61 (1976) 22-28.

57. L.D. Glowinski and P. Regnier, Scripta Met. 11 (1977) 133-136.

58. R.W. Knoll, Ph.D. thesis, University of Wisconsin-Madison (1981).

59. B. Badger, Jr., D.L. Plumton, S.J. Zinkle, R.L. Sindelar, G.L. Kulcinski, R.A. Dodd and W.G. Wolfer, ASTM STP 870 (1985) 297-316.

60. S.J. Zinkle, L.E. Seitzman and W.G. Wolfer, Phil. Mag. A 55 (1987) 111-125.

61. S.J. Zinkle, presented at the Symposium on Irradiation Enhanced Materials Science and Engineering, 1988 TMS Fall Meeting, September 26-29, 1988, Chicago, Illinois, to be published in Metallurgical Transactions.

62. M. Hansen, Constitution of Binary Alloys, 2nd edition, McGraw-Hill Book Company, Inc., 1958.

63. B. Mozer, D.T. Keating and S.C. Moss, Phys. Rev. 175 (1968) 868.

64. J. Vrijen, ECN Petten Report, ECN-31, 1977.

65. J. Vrijen and S. Radelaar, Physical Review B 17 (1978) 409-421.

66. Metals Handbook, 8th edition, American Society for Metals, Vol.8 (1973), p. 294.

67. L. Elford, F. Muller and O. Kubaschewski, Ber Bunsenges Physik Chem. 73 (1969) 601-605.

68. H. Shimizu et al., J. Japan Inst. of Metals 45 (1981) 210.

69. H. Shimizu, N. Koyama and Y.Ishida, J. Japan Inst. of Metals 45 (1981) 768.

70. L.E. Rehn, W. Wagner and H. Wiedersich, Scripta Met. 15 (1981) 683-687.

71. H. Takahashi, S. Ohnuki and T. Takeyama, J. Nucl. Mater. 103 & 104 (1981) 1415-1420.

72. T. Takeyama, Bull. Japan Inst. Met. 22 No. 2 (1983) 135-137.

73. H. Wiedersich, P.R. Okamoto and N.Q. Lam, J. Nucl. Mater. 83 (1979) 98-108.

74. N.Q. Lam, H.A. Hoff, H. Wiedersich and L.E. Rehn, Surface Science 149 (1985) 517-536).

75. W. Schule, P. Spindler and E. Lang, Z. Metallk 66 (1975) 50.

76. K. Chountas et al., Rad. Effects Letters 43 (1979) 249-251.

77. S.J. Zinkle and G.L. Kulcinski, J. Nucl. Mater. 122 & 123 (1984) 449.

78. R. Poerschke and H. Wollenberger, Thin Solid Films 25 (1975) 50.

79. R. Poerschke and H. Wollenberger, Rad. Effects 49 (1980) 225-232.

80. W. Wagner, R. Poerschke and H. Wollenberger, J. Phys, F: Met. Phys. 12 (1982) 405.

81. R.A. Swalin, Thermodynamics of Solids, John Wiley & Sons, New York, NY, 1972, p. 149.

82. A.T. Aldred, B.D. Rainford, T.J. Hicks and J.S. Kouvel, Physical Review B 7 (1973) 218-229.

83. R.A. Medina and J.W. Cable, Physical Review B 15 (1977) 1539-1551.

84. B.N. Sigh, T. Leffers and P. Barlow, Fifth International Conference on HVEM, Kyoto, Japan, Aug. 29-Sept. 1, 1977, p.581-584.

85. D.J. Mazey and F. Menzinger, J. Nucl. Mater. 48 (1973) 15-20.

86. K-H. Leister, Ph.D. Thesis, Kernforschungszentrum Karlsruhe (May 1983).

87. P. Dauben and R.P. Wahi, Progress Report No.2 (1981-1984), Reports of the Hahn-Meitner-Institute.

88. S.J. Zinkle, R.A. Dodd, G.L. Kulcinski and K. Farrell, J. Nucl. Mater. 117 (1983) 213-217.

CHAPTER 4

EXPERIMENTAL PROCEDURES

Twenty two specimens, twelve pure nickel with various pretreatment procedures, four Ni-10Cu (at.%), two Ni-25Cu and four Ni-50Cu, have been irradiated and analyzed by cross-sectional TEM in this study. The residual gas content, the amount of helium or oxygen pre-injected into the sample and the condition under which heavy-ion irradiations were performed have been listed in Table 4.1. The details are described in the following sections.

A. Pre-Irradiation Specimen Preparation

The pure nickel foil (0.25 mm thick after polishing) used in this study is the Marz grade (99.995 wt.% pure) from the Materials Research Corporation. The nominal impurity contents[1] are listed in Table 4.2. Since the oxygen content is not analyzed for every batch of the material by the manufacturer and yet is important for this study, a segment of the material was sent to Los Alamos National Laboratory for the accurate analysis of oxygen content by the vacuum fusion technique. The result shows that the as-received nickel foil contains 180 appm oxygen, which is much higher than the nominal value listed in Table 4.2 (55 appm). Only two nickel samples were irradiated in the as-received condition. In order to study the effect of helium or oxygen concentration on void formation more accurately, it was necessary to reduce the residual gas content in

Table 4.1 Samples and irradiation conditions used in the present study

No.	Material* (at.% Cu)	Residual Oxygen (appm)	Pre-injection (appm gas)	Irradiation Temp.(°C)	Fluence (10^{19} ions/m^2)	Dose at 1 μm (dpa)
01	Ni (AR)	180	none	500	8 (14 MeV Ni)	~ 3
02	Ni (AR)	180	none	500	30 (14 MeV Ni)	~ 10
03	Ni (VA)	180	none	500	8 (14 MeV Ni)	~ 3
04	Ni (VA)	180	10 helium	500	8 (14 MeV Ni)	~ 3
05	Ni (VA)	180	30 helium	500	8 (14 MeV Ni)	~ 3
06	Ni (HR)	75	none	500	8 (14 MeV Ni)	~ 3
07	Ni (HR)	75	10 helium	500	8 (14 MeV Ni)	~ 3
08	Ni (HR)	75	50 helium	500	8 (14 MeV Ni)	~ 3
09	Ni (HR)	75	none	500	30 (14 MeV Ni)	~ 10
10	Ni (HR)	75	75 oxygen	500	15 (14 MeV Ni)	~ 5
11	Ni (HR)	75	none	500	65 (14 MeV Ni)	~ 25
12	Ni (HR)	75	none	500	60 (14 MeV Cu)	~ 25

* Denotation for pre-irradiation heat treatment of Ni:

AR — as-received; VA — vacuum annealing; HR — hydrogen reduction + vacuum annealing

(This table is continued on the next page)

Table 4.1 Samples and irradiation conditions used in the present study (continued)

No.	Material* (at.% Cu)	Residual Oxygen (appm)	Pre-injection (appm gas)	Irradiation Temp.(°C)	Fluence (10^{19} ions/m^2)	Dose at 1 μm (dpa)
13	Ni-10	100	100 oxygen	485	14 (14 MeV Ni)	~ 5
14	Ni-10	100	100 oxygen	485	28 (14 MeV Ni)	~ 10
15	Ni-10	100	50 helium	485	14 (14 MeV Ni)	~ 5
16	Ni-10	100	none	485	70 (14 MeV Ni)	~ 25
17	Ni-25	—	100 oxygen	465	14 (14 MeV Ni)	~ 5
18	Ni-25	—	none	465	70 (14 MeV Ni)	~ 25
19	Ni-50	100	100 oxygen	425	10 (14 MeV Ni)	~ 5
20	Ni-50	100	100 oxygen	425	21 (14 MeV Ni)	~ 10
21	Ni-50	100	50 helium	425	10 (14 MeV Ni)	~ 5
22	Ni-50	100	none	425	52 (14 MeV Ni)	~ 25

Table 4.2 Nominal impurity contents* in Marz grade nickel (99.995 wt.% pure)

Impurity	wppm (appm)	Impurity	wppm (appm)
C	20 (100)	Li	< 0.1
H	< 1.0 (60)	Mg	1.5
O	15.0 (55)	Mn	0.12
N	< 5.0 (20)	Mo	< 0.18
Ag	< 0.10	Na	0.27
Al	1.6	Nb	0.04
As	0.27	Pb	< 0.1
Bi	< 0.1	Ph	< 0.1
Ca	0.39	S	0.35
Cd	0.10	Sb	0.30
Cl	1.5	Si	14.0
Co	1.2	Sn	0.8
Cr	1.3	Ta	< 0.16
Cu	0.09	Ti	0.14
Fe	22.0	V	< 0.10
Ga	< 0.10	W	< 1.10
Ge	0.26	Zn	0.07
Hf	< 0.28	Zr	0.40
K	0.10		

* Analysis methods: Mass Spectrographic, Vacuum Fusion for gases, Conductometric for Carbon

the material as much as possible. Three of the nickel samples had been annealed at 800 °C for 1 hour at a vacuum of $4x10^{-5}$ Pa ($3x10^{-7}$ Torr) for outgassing before irradiation. According to Sievert's law[2] and the published solubility data for oxygen in nickel[3], it was estimated that after the treatment, oxygen content in the nickel foil would drop to below 1 appm. However, analysis performed by Los Alamos National Laboratory revealed that the oxygen level in the nickel foil was not changed after such a treatment. It is believed that the oxide layer originally present on the surface of the foil worked as a diffusion barrier which prevented oxygen in the matrix leaving the foil during vacuum annealing. To remove the surface oxide, the remaining seven nickel samples were first heated at 1000 °C in flowing dry hydrogen for 120 hours. During that period oxygen is expected to react with hydrogen to form water at the surface of the foil, and this is then removed. After that, the samples were annealed at 150 °C in a vacuum of $6.6x10^{-7}$ Pa ($5x10^{-9}$ Torr) for a half hour to remove hydrogen in the foil. Analysis performed by Los Alamos National Laboratory indicated that the oxygen content in the nickel foil treated this way was reduced to ~ 75 appm (more than 50% reduction).

Three Ni-Cu alloys, namely, Ni-10Cu, Ni-25Cu and Ni-50 Cu, have been fabricated from Marz nickel and Marz copper (99.999 wt.% pure) by using an arc melter. Before melting the raw materials, the chamber of the melter was evacuated to 20 mTorr and then filled with argon gas five times. A titanium getter was used to absorb active gases in the chamber

during melting. The ingots were inverted and remelted several times to assure homogeneity. The ingots of the alloys were cold rolled to 0.5 mm thick foils with intermittent annealing in flowing argon at 800 °C. Specimens of Ni-10Cu and Ni-50Cu were also sent to Los Alamos National Laboratory for the determination of the oxygen content, and they were both found to contain ~ 100 appm oxygen. Although the oxygen content of the Ni-25Cu foil has not been analyzed, a similar level is expected because of the similar preparation process.

All the samples are in the shape of a 1 cm x 0.5 cm x 0.25 cm foil. It is extremely important that the surfaces of each samples be clean to allow metal to be plated on to them after irradiation for the cross-section TEM sample preparation. To assure good plating adherence, prior to irradiation each specimen was mechanically polished on a polishing wheel using 0.3 μm and/or 0.05 μm alumina slurry. It should be noted that the samples were not electropolished prior to irradiation as has been done in some previous studies. The reason for that is to prevent the possible introduction of gas atoms[4-6] other than those implanted during the pre-injection irradiation.

B. Helium Pre-injection

To investigate the effect of helium concentration on void formation in both pure nickel and Ni-Cu alloys, six samples in this study were pre-injected with various fluences of helium ions before irradiation with heavy ions. The helium pre-injection of nickel samples (No. 4, 5, 7 and 8

in Table 4.1) was performed using the UW 700 kV light ion irradiation facility. This facility, which consists of a 700 kV electrostatic accelerator, beam focussing and analyzing equipment, vacuum system and a specimen chamber, is shown schematically in Figure 4.1 and is described in detail by Bullen et al.[6,7]. The helium is contained in a small gas tank inside the dome of the accelerator. A thermo-mechanical leak is used to regulate the flow of helium to the r.f. source in the dome. Helium ions are accelerated through the dome and directed to the target section of the facility. There are three major beam handling components situated along the beam line. They are up-down, left-right steerers, a magnetic quadrupole doublet and a 90 degree analyzing magnet. The sample holder is capable of accommodating three 0.5 cm x 1.0 cm foils and maintains electrical isolation with the sample while it masks the irradiated area to allow for accurate measurement of the current density. The accelerator operates at an accelerating potential ranging from 200 to 700 kilovolts. With a helium beam of varied energy (200-700 keV, 100 keV as a step), a relatively uniform concentration of helium is injected into the depth range of 0.5-1.3 μm as shown in Figure 4.2 (a). Helium pre-injection of the two Ni-Cu samples (No. 15 and 21 in Table 4.1) was performed at Oak Ridge National Laboratory with the energy of helium ions varying continuously between 200 and 400 keV. The distribution of the 200-400 keV helium in Ni-50Cu is in the depth range of 0.5-1.0 μm as shown in Figure 4.2 (b).

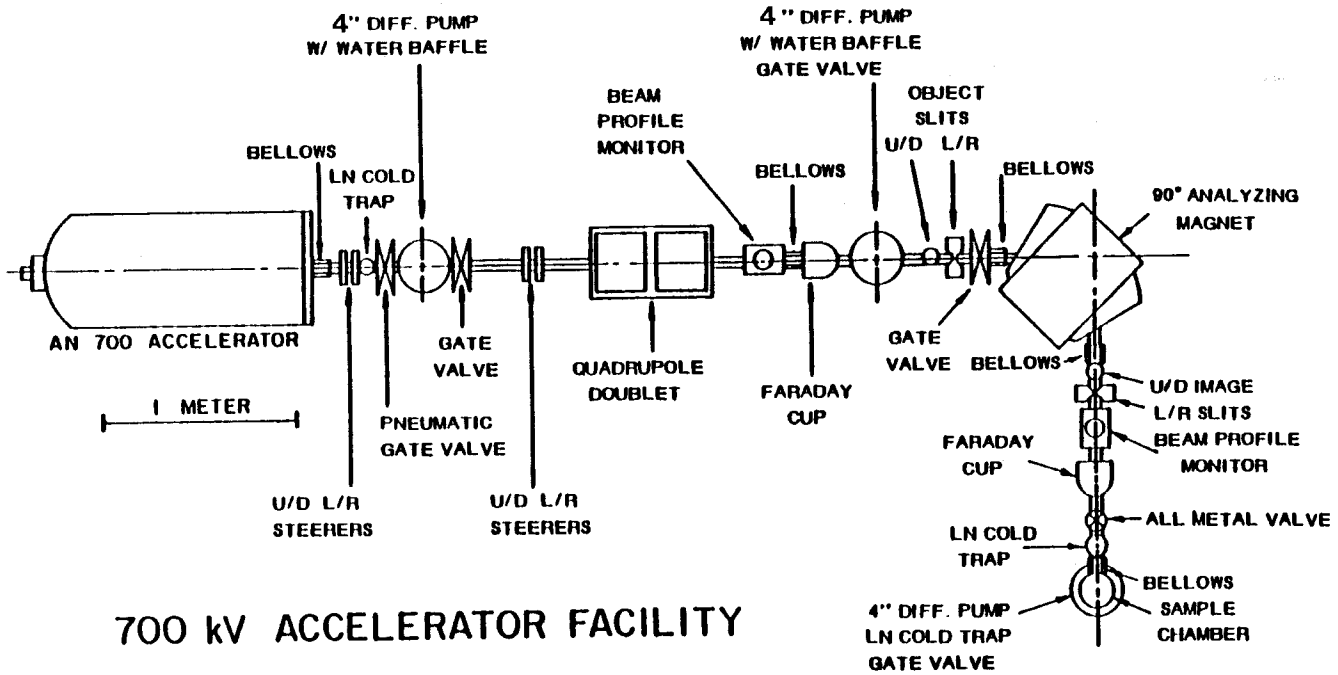

Figure 4.1 Schematic of the University of Wisconsin 700 kV Accelerator Facility showing beam handling and vacuum components.

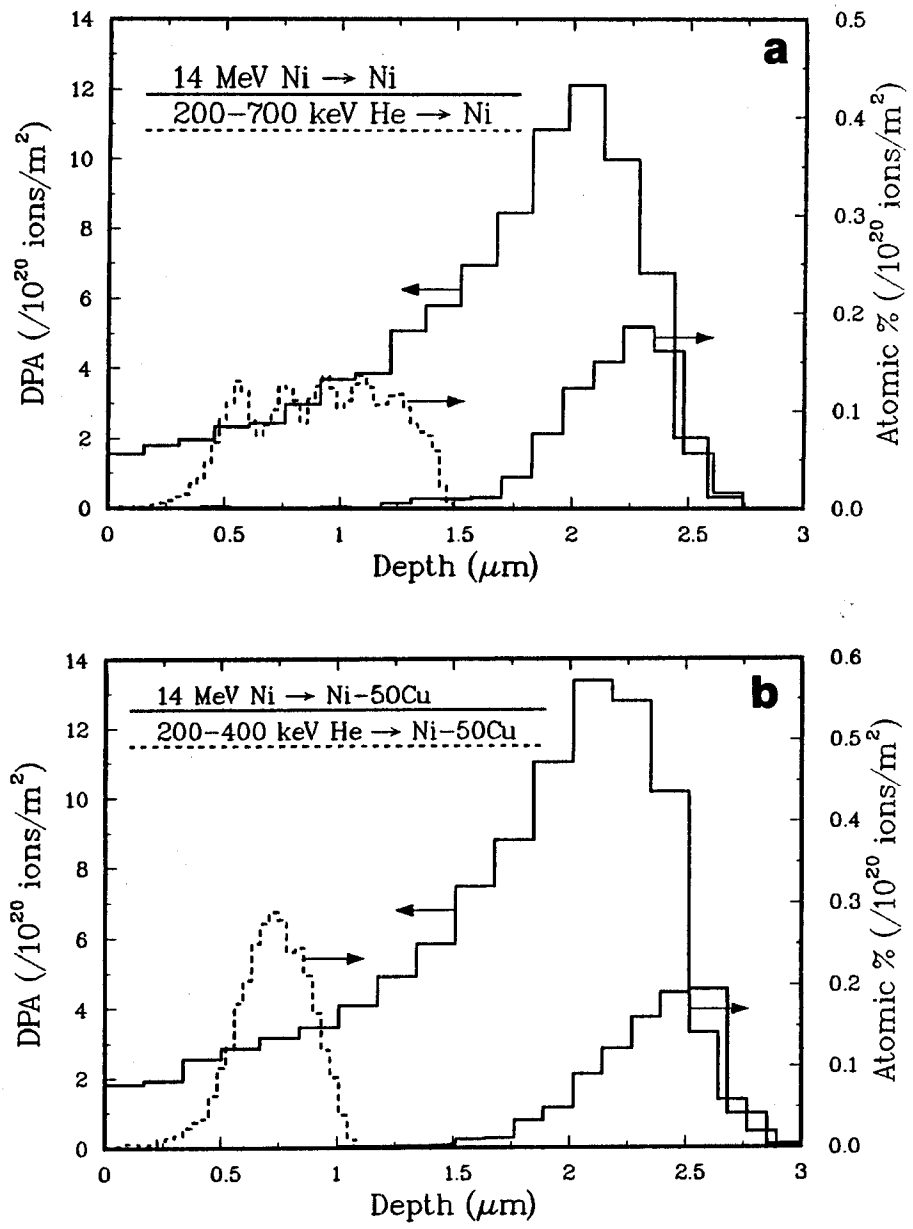

Figure 4.2 Displacement damage (by 14 MeV Ni ions) and injected ion distributions in (a) pure Ni (14 MeV Ni ions and 200-700 keV He ions) and (b) Ni-50Cu (14 MeV Ni ions and 200-400 keV He ions) calculated by using the Monte Carlo code, TAMIX (1000 ion histories).

From Figure 4.2, one can see that the pre-injected helium range and the injected nickel ion range (1.5-2.8 μm below surface) in this study are separated because of the proper energy selection, and this allows their effects to be separated. The injected-appm-helium/dpa ratio used in this study is much lower than that used by Bullen[6], because it has been shown that a higher ratio would cause overnucleation of copious small voids which are probably under the resolution limit of the microscope available for this study. All the helium pre-injections were conducted at room temperature.

C. Oxygen Pre-injection

Six samples (No. 10, 13, 14, 17, 19 and 20) were pre-injected with 5-6 MeV O^{2+} ions before nickel ion irradiation to an average concentration which equals the residual oxygen level in the sample. Therefore, the injected region contains twice as much as the oxygen in the other regions of the specimen. The oxygen pre-injections were conducted in the University of Wisconsin Heavy-Ion Irradiation Facility[4-9] (see next section for brief introduction of the facility) utilizing the oxygen beam generated during the first few hours of sputtering of the nickel ion source (during that period, the nickel oxide layer on the source surface is sputtered off). All the oxygen pre-injections are also conducted at ambient temperature.

The calculated range of injected 5 MeV oxygen in pure nickel, Ni-10Cu and Ni-50Cu have been shown in Figures 2.1 and 2.2 in Chapter 2.

It should be mentioned that after the oxygen pre-injection of a pure nickel sample (sample No. 10 in Table 4.1), the sample was removed from the target chamber of the accelerator and then sputtered with 3.5 kV Ar^+ ions to remove the first micrometer of the surface before being returned to the accelerator again for the 14 MeV nickel ion irradiation. As a result of this process, the oxygen range in the sample is about one micrometer closer to the surface compared to the calculated range shown in Figure 2.1 (b). In other words, the range of the injected oxygen is therefore completely separated from that of the injected 14 MeV nickel ions.

D. Heavy-Ion Irradiation

Most samples in this study have been irradiated with 14 MeV nickel ions while only one nickel sample has been irradiated with copper ions of the same energy to study the effect of a small amount of injected copper. All the heavy-ion irradiations were carried out in the University of Wisconsin Heavy-Ion Irradiation Facility. The schematic of the facility is shown as Figure 4.3. The facility includes a SNICS negative ion source[10], a 7 MV tandem Van de Graaf electrostatic accelerator, various beam handling and monitoring equipment and a target chamber.

In the SNICS source, negative nickel ions, Ni^- or Cu^- are created through the sputtering of a nickel or copper cathode by energetic cesium ions. The negative ions exit the source with an energy of 2-4 kV which

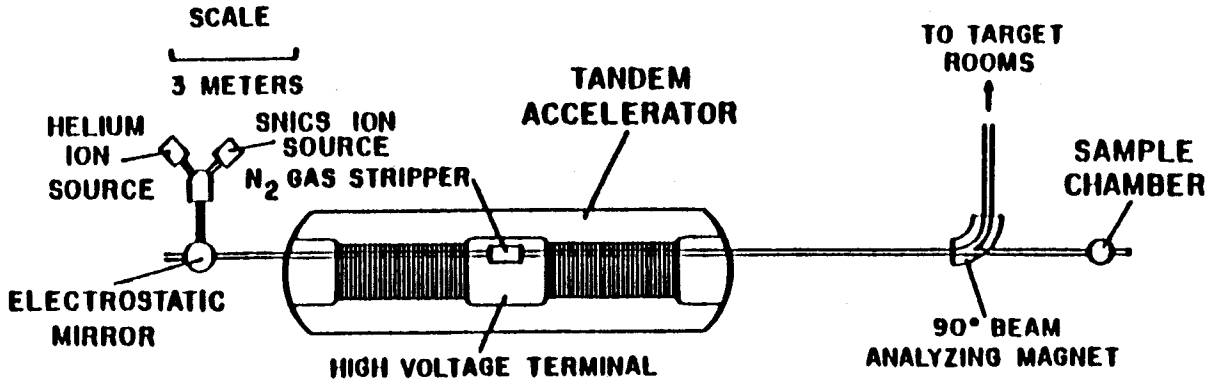

Figure 4.3 Schematic of the University of Wisconsin Tandem Accelerator Facility.

equals the sputter cathode potential. Then they are injected into the tandem accelerator (built by High Voltage Engineering Corporation, Model EN) at ground potential and are accelerated into the high-voltage terminal which operates with a positive potential V. A N_2 gas stripper is used to strip electrons from the negative ions via a collision process converting them into positive ions. With varying degrees of stripping, a distribution of charge states of the ions are created with charge nq, n being an integer. These positive ions are further accelerated through the potential V and exit the high energy end of the accelerator with the energy

$$E = qV(1+n) \tag{4.1}$$

A given charge state can be selected by use of an electromagnetic quadrupole lens on the high energy beam tube. For this study, a charge state of n = 3 is selected in conjunction with a terminal potential of 3.5 MV to give 14 MeV ions to irradiate the specimen.

The 14 MeV Ni^{3+} or Cu^{3+} ions are then directed towards the target chamber of the facility. The target chamber is pumped by a titanium sublimation pump and an orbitron pump, with which a vacuum of low 10^{-4} Pa (10^{-6} Torr) or better can be maintained during irradiations even at the elevated temperatures (500-700°C).

The specimen holder assembly consists of a carousel with eight individual sample holders. Samples are individually heated during irradiation by thermal radiation from ohmic-heated tantalum sheets.

Individual chromel-alumel thermocouple leads allow continuous monitoring of the temperature of all eight samples during an irradiation run. Specimens adjacent to the sample being irradiated are thermally shielded from the heater to prevent post-irradiation annealing effects. The range of operating temperatures for the heater is roughly 100-700 °C. The beam current is measured by three Faraday cups, the entrance cup, the mask cup and the exit cup, at different locations along the beam axis. The entrance cup is located at the entrance to the target section, the removable mask cup can be put just in front of the sample while the exit cup is directly behind the specimen. When the mask cup is not used to check the beam current, a tantalum mask containing a 3 mm aperture is inserted to define the irradiation spot on the specimen. The beam intensity profile is essentially constant over the 3 mm beam spot diameter[11].

The dose rate used in this study varied from $1x10^{16}$ ions/m^2s to $3x10^{16}$ ions/m^2s, depending upon the beam current available on the target during a particular irradiation run. That gives a damage rate of ~ $4x10^{-4}$ to $1x10^{-3}$ dpa/s at 1 μm depth for 14 MeV nickel ion irradiated pure nickel.

As mentioned in Chapter 1, all the heavy-ion irradiations in this study were conducted with the specimen temperature controlled at 0.45 T_m (i.e. 45% of the melting temperature in Kelvin) of the target material, i.e. 500°C, 485°C, 465 °C and 425°C for pure nickel, Ni-10Cu, Ni-25Cu and Ni-50Cu respectively.

E. Post-Irradiation Specimen Preparation and Analysis

After irradiation, the specimens were all prepared in cross-section for TEM observation, so that the complete damage profile along the depth could be studied in one foil. This technique was first applied to an ion-irradiated material by Spuring and Phodes[12]. It has been well developed and successfully applied on pure nickel, pure copper and several alloys here by the radiation damage group at the University of Wisconsin. The details of this technique have been described previously by Zinkle and Sindelar[13]. Figure 4.4 shows the schematic of the preparation steps of a nickel foil cross-sectioned for TEM analysis. During preparation of the cross-section TEM specimens, the original surface of irradiation has been electroplated with nickel, so it becomes an interface in the TEM micrograph. A few modifications have been made in the process of electroplating of nickel for the preparation of cross-sectional Ni-Cu alloys, details of which have been shown elsewhere[14]. To obtain electron transparent thin area which covers the entire ion damage range, some samples were ion milled repeatedly with intermittent TEM examination after the double-jet electropolishing. It should also be mentioned that a surface layer of up to 0.3 μm thick was removed from the original surface before electroplating to ensure good bonding at the interface. Therefore, the actual depth from the irradiated surface is about 0.3 μm more than the depth marked in the cross-sectional TEM micrographs.

The specimens were analyzed using JEOL-100B and JEOL-200CX

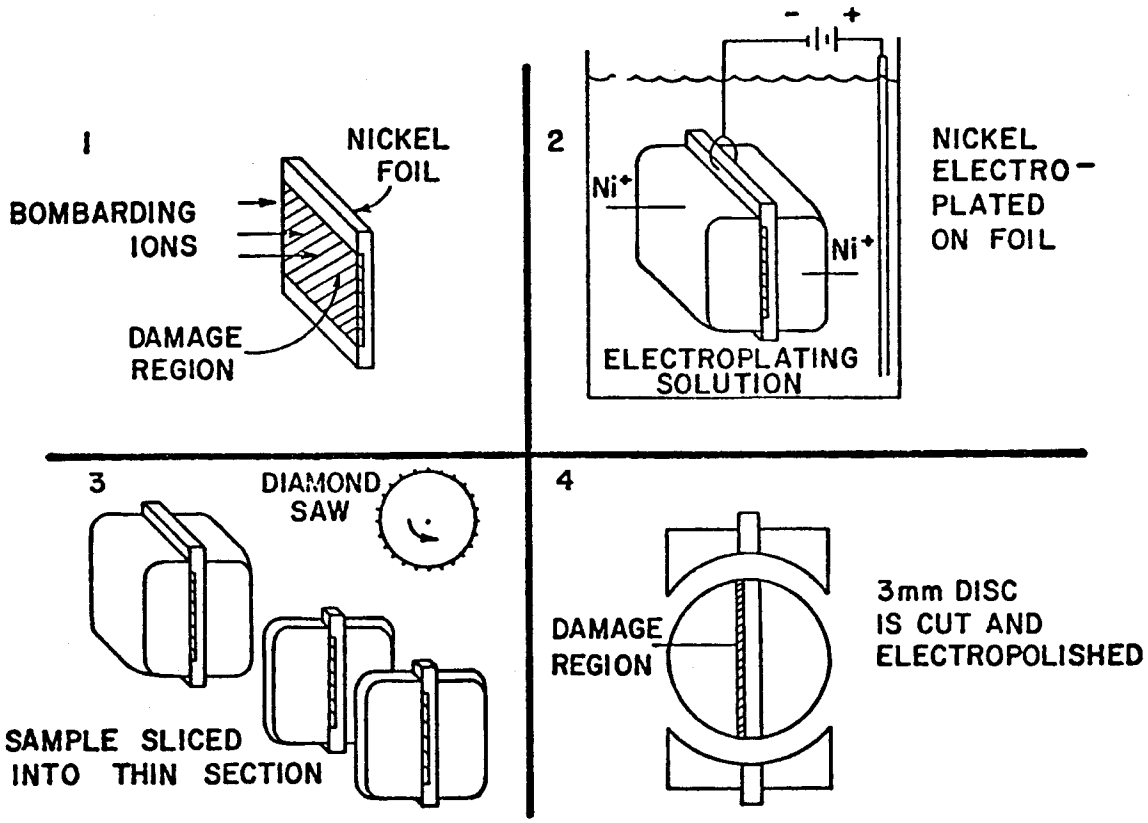

Figure 4.4 Schematic of the preparation steps of a foil cross-sectioned for TEM analysis.

transmission electron microscopes. The depth distribution of voids was determined by division of the micrographs into regions of uniform thickness parallel to the irradiated surface. To analyze the number density of voids and dislocation loops, the foil thickness must be known. The thickness measurements were performed by using a stereo pair technique when a reasonable density of defect clusters was available, or by counting the thickness fringes when the edge of the perforation hole in the TEM sample cut across the irradiated region, or by putting a contamination spot onto the sample and then taking micrographs corresponding to foil orientations tilted at ~ 15° from one another. In the stereo pair measurement, the image parallax was measured with a Hilger-Watts stereoviewer. The foil thickness t (in angstroms) is determined using the equation

$$t = \frac{P \times 10^7}{2M \sin\frac{\theta}{2}} \tag{4.2}$$

where P is the image parallax in mm determined by using features on opposite surfaces, M is the magnification of the analyzed print and θ is the total angle of tilt between the stereo pair prints. The accuracy of the sample thickness measurements is estimated to be ± 20%. The size distributions of voids and dislocations were determined using a Zeiss particle counter. To reduce the uncertainties in the swelling calculation, the morphology of the voids was studied by viewing them with the electron beam close to several main zone axes, an example of which is

shown in Figure 4.5. Then the appropriate truncation parameter[15] and volume factor[15] along with the measured void dimension in the <110> direction are taken to determine the volume of the void using a method provided by Gelles et al[15]. The average diameter of voids reported in Chapter 5 is the diameter of the sphere which has the same equivalent volume as the average void volume.

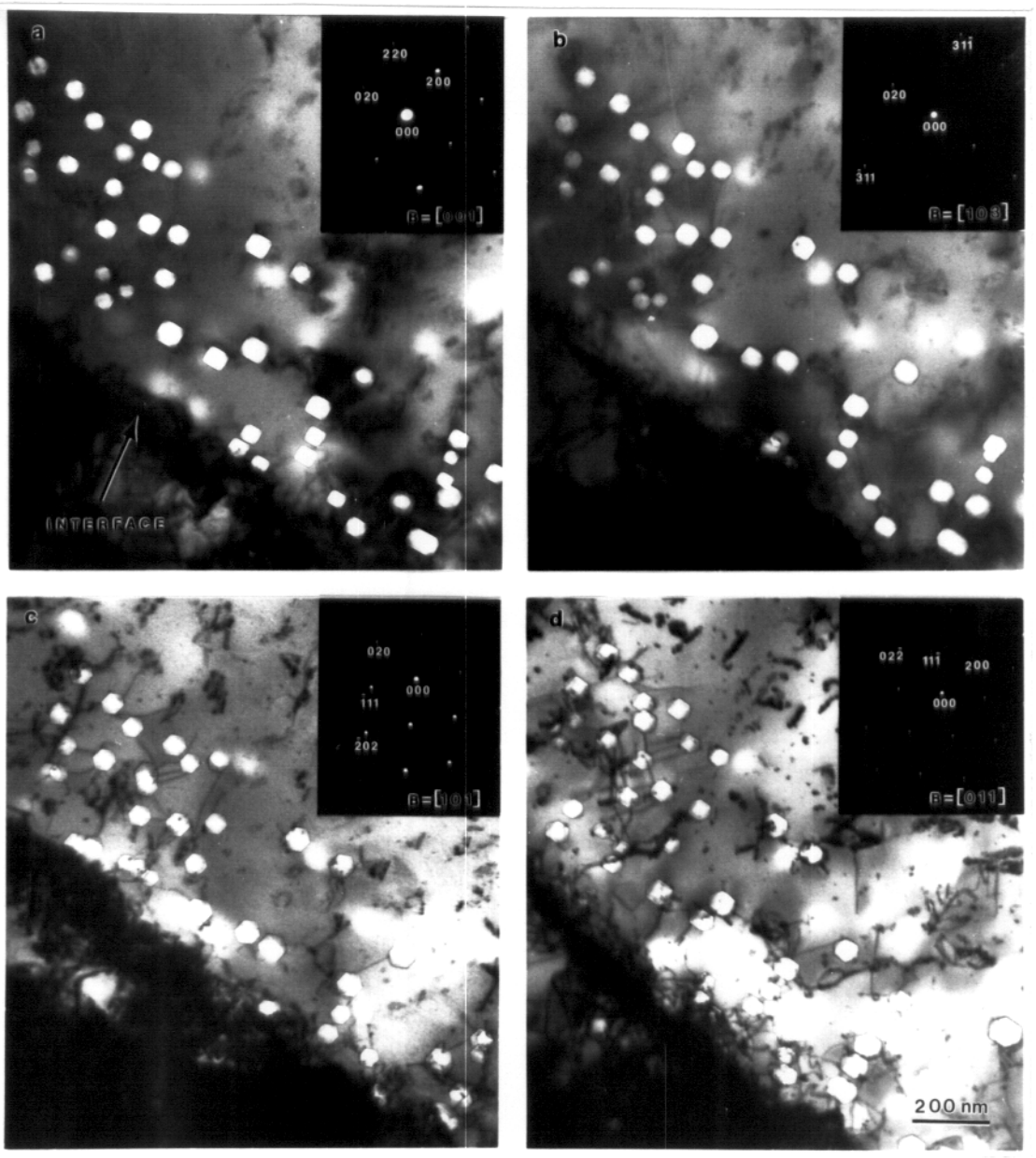

Figure 4.5 Morphology of voids in 14 MeV Cu ion irradiated Ni. (a) B = [001], (b) B = [103], (c) B = [101] and (d) B = [011]. The voids are determined to be bounded by {100} and {111} faces (cubic truncated by octahedron) with truncation parameters between 0.5 and 0.6.

References for Chapter 4

1. MRC Standard Products Catalog, Materials Research Corporation, 1980.

2. R.A. Swalin, Thermodynamics of Solids, John Wiley & Sons, New York, NY, 1972, p. 177.

3. M. Hansen, Constitution of Binary Alloys, 2nd Ed., McGraw-Hill Book Company, New York, 1958.

4. J.B. Whitley, Ph.D. Thesis, University of Wisconsin-Madison (1978).

5. R.W. Knoll, Ph.D. Thesis, University of Wisconsin-Madison (1981).

6. D.B. Bullen, Ph.D. Thesis, University of Wisconsin-Madison (1984).

7. D.B. Bullen, J.H. Billen and G.L. Kulcinski, in: Proc. of the 7th Conf. on the Application of Accelerators in Research and Industry, Denton, Texas, November 1982.

8. R.G. Lott, Ph.D. Thesis, University of Wisconsin-Madison (1979).

9. W.J. Weber, Ph.D. Thesis, University of Wisconsin-Madison (1977).

10. G.T. Caskey, R.A. Douglas, H.T. Richard and H. V. Smith, Jr., Nucl. Instr. and Meth. 157 (1978) 1-7.

11. S.J. Zinkle, Ph.D. Thesis, University of Wisconsin-Madison (1985).

12. R.A. Spuring and C.G. Phodes, J. Nucl. Mater. 44 (1972) 341.

13. S.J. Zinkle and R.L. Sindelar, Nucl. Instr. and Meth. B16 (1986) 154-162.

14. L.E. Seitzman, L.M. Wang, R.D. Griffin, A.P. Komissarov, G.L. Kulcinski and R.A. Dodd, to be published in Ultramicroscopy.

15. D.S. Gelles, R.M. Claudson and L.E. Thomas, Fusion Reactor Materials, DOE/ER-0313/3 (Sept. 1987), pp. 131-136.

CHAPTER 5

EXPERIMENTAL RESULTS

In this chapter, the results from TEM observations of all the twenty two irradiated samples are organized into several sections to show the effects of oxygen, helium and copper content on damage structure evolutions in a comparative manner. Section A shows the effects of residual oxygen, pre-injected helium and pre-injected oxygen on void formation in 14 MeV nickel ion irradiated pure nickel. Section B gives the results on damage structure observations in the three irradiated Ni-Cu alloys (with and without oxygen pre-injection). By comparing them with each other and with the result obtained from irradiated pure nickel, the role of copper content on damage structure evolution can be revealed. Further information on the latter is provided by the following two sections. In section C, the effects of pre-injected helium in irradiated pure nickel, Ni-10Cu and Ni-50Cu are compared, while section D compares the damage structures of 14 MeV copper ion irradiated nickel with that of 14 MeV nickel ion irradiated nickel.

The numbers assigned to the samples in Table 4.1, which tabulates the pre-irradiation and irradiation conditions of each sample, are used during the description of the results in this chapter. As far as the peak damage level (dpa) is concerned, a rough estimation which equals four times the dpa number at 1 μm depth listed in Table 4.1 is used in the description of this chapter. It is worth mentioning again that

a surface layer of ~ 0.3 μm thick was removed from all samples during the process of cross-section specimen preparation to assure good bonding at the interface, so the actual depth from the irradiated surface is 0.3 μm more than the depth from the interface indicated in the cross-section micrographs to be shown in this chapter.

A. Gas Effects on Void Formation in Irradiated Nickel

A.1. Heterogeneous Void Formation in Irradiated As-received Nickel

Sample No. 01 was irradiated with 14 MeV nickel ions at 500 °C in the as-received state (20% cold-worked, 180 appm oxygen). While the unirradiated material contains only a line dislocation structure with a density of ~ $2x10^{14}$ m^{-2}, a substantial number of voids were observed after irradiation to a fluence of $8x10^{19}$ Ni^{3+}/m^2 (3 dpa at 1 μm). Figure 5.1 is a cross-section micrograph showing the entire ion damage depth range of that sample. Although most voids in the sample are located in the depth range of 1-2.5 μm below the irradiated surface, the fine distribution of voids is rather heterogeneous. While high densities of voids are found at some areas to form void clusters (one of those clusters is shown in Figure 5.2 (A)), some other areas (even at the peak damage depth) are almost void free. Voids are also found to form preferentially on dislocation lines and around a very occasional impurity particle as shown in Figure 5.2 (B) and (C). As shown in Figure 5.2 (D), an Energy Dispersive X-ray Spectroscopy (EDXS) analysis from the particle showed only the presence

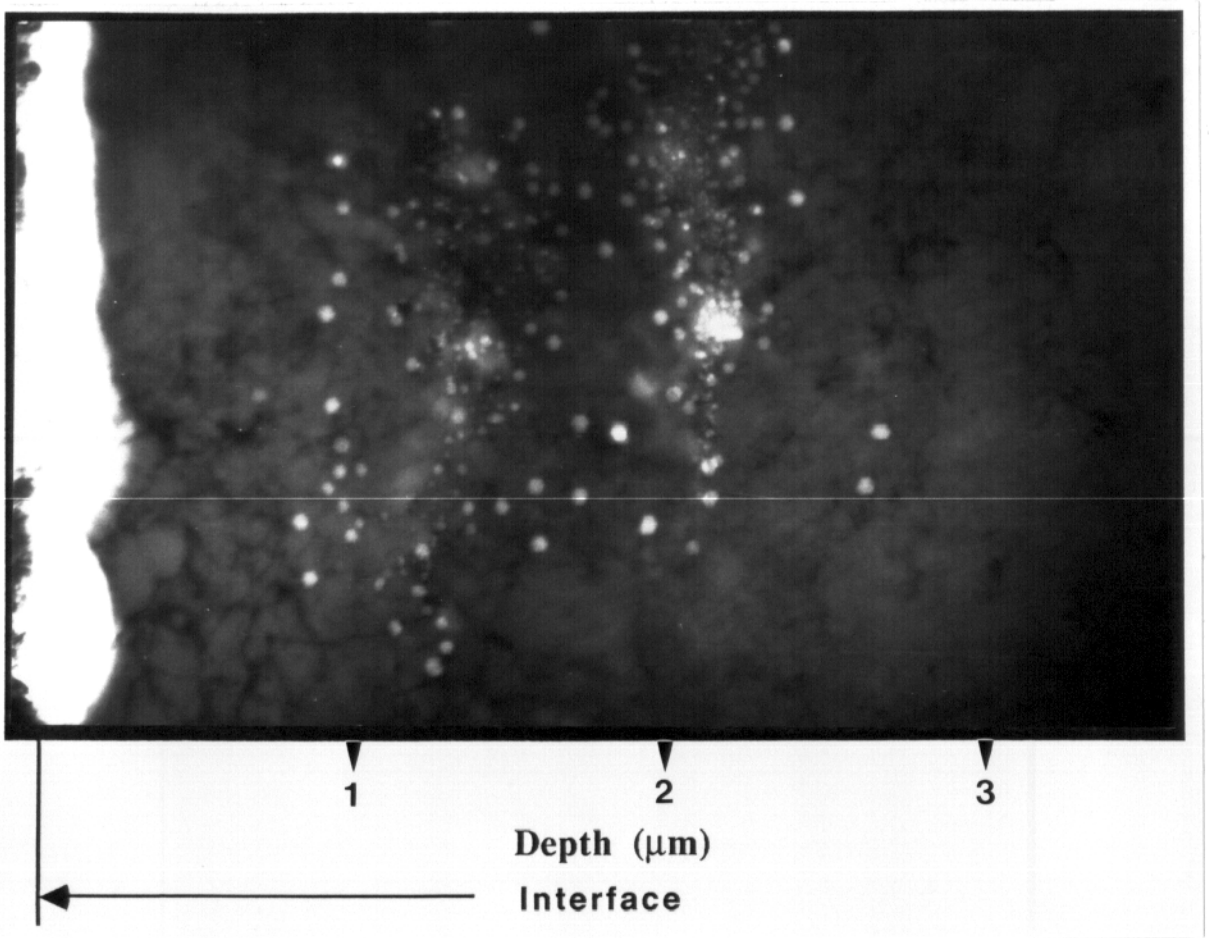

Figure 5.1 Cross-section TEM micrograph of 14 MeV Ni ion irradiated as-received pure Ni (No. 01, 180 appm oxygen, 3 dpa at 1 μm, 500 °C).

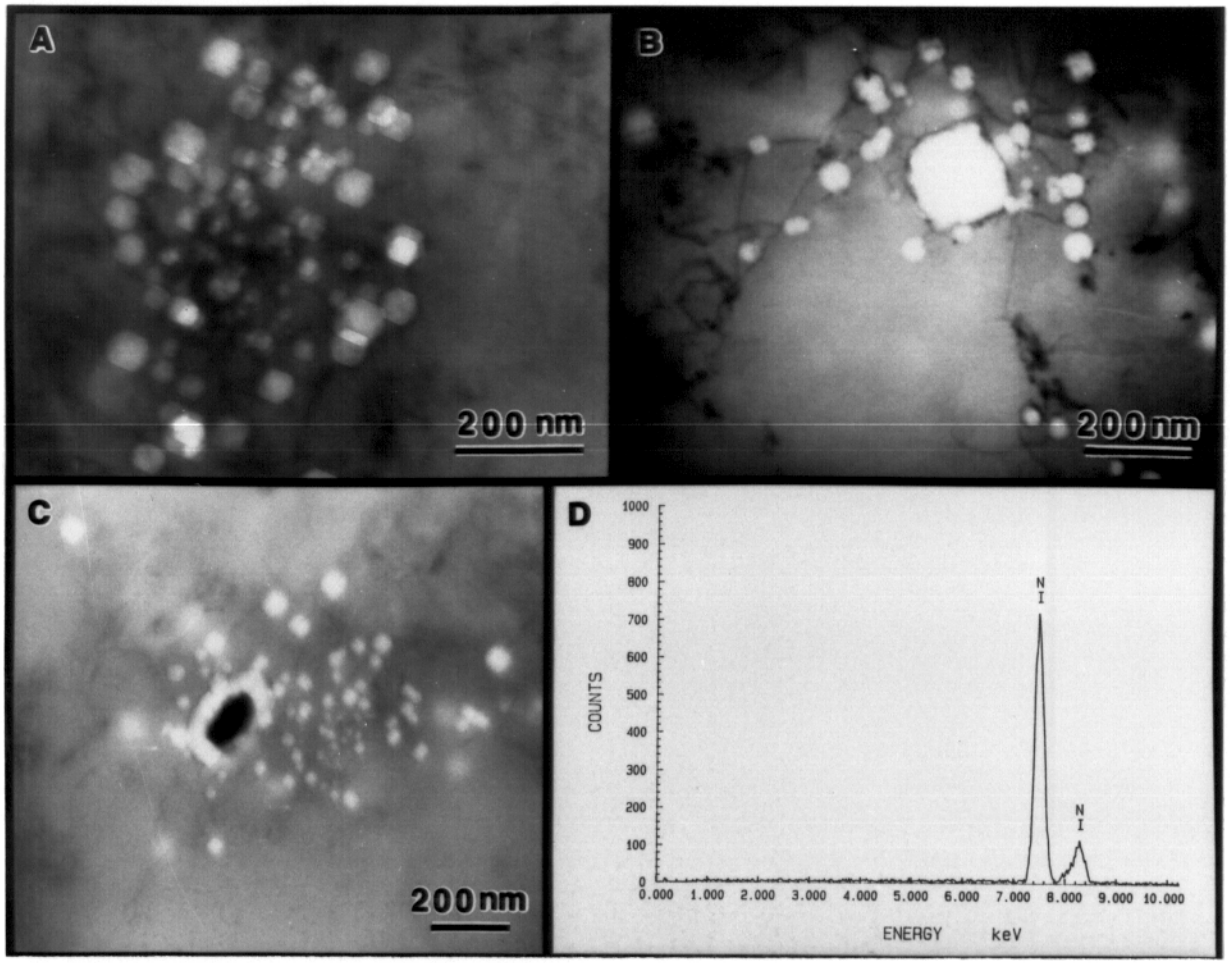

Figure 5.2 Heterogeneous void formation in 14 MeV Ni ion irradiated as-received Ni (10 dpa, 500 °C). (A) a cluster of voids; (B) voids in association with dislocations; (C) high density of voids around an impurity particle; (D) EDX spectrum recorded from the impurity particle shown in (C).

of the nickel signal. Since the EDXS system used is unable to detect the low z elements ($z \leq 10$) and no diffraction pattern was obtained (the particle was lost during ion milling in a attempt to remove the surface contamination on it), the exact identity of the particle remains uncertain. However, it is quite reasonable to assume that particle is nickel oxide. If that is the case, then the high void density around the particle might be attributed to the higher local free oxygen content because of the re-solution of nickel oxide during ion irradiation. The higher void density observed at other locations may also be attributed to the heterogeneous distribution of the oxygen in that sample. Despite the heterogeneous nature of the void distribution, the average void density was determined to be 6×10^{19} m^{-3} at the depth of 1 μm and 2×10^{20} m^{-3} at the damage peak; the corresponding average void diameter was 35 nm at the 1 μm depth and 30 nm at the damage peak. The heterogeneous distribution of voids was also observed in another nickel specimen (No. 02), which was irradiated also in the as-received state but to a higher damage level.

A.2 Void Formation in Vacuum Annealed Nickel (180 appm Oxygen) with or without Helium Pre-injection

As mentioned in Chapter 4, three specimens were irradiated in the vacuum annealed state. The annealing reduced the density of line dislocations from 2×10^{14} m^{-2} in the as-received state by almost an order of magnitude, but did not reduce the residual oxygen content. Figure 5.3 shows the entire ion damage region of the three vacuum annealed nickel

specimens (Nos. 03, 04 and 05) which contain 180 appm oxygen and varying levels of pre-injected helium in the first ~ 1μm region, and received same dose of 14 MeV nickel ions as sample No. 01. Figure 5.4 shows the void distribution in the ~ 1 μm deep region of the three samples at a higher magnification, and the variation of void density and average diameter with depth is shown in Figure 5.5. It is clear from Figure 5.3 (a) that the heterogeneous void distribution of the irradiated, as-received nickel (No. 01) is not a feature in the irradiated, vacuum annealed nickel (No. 02). Also, compared to sample No. 01, the void density is much higher, and the void size is much smaller in sample No. 02. This change might be explained by homogeneous distribution of oxygen atoms due to thermal diffusion during annealing.

The effect of pre-injected helium on void formation in the vacuum annealed, high oxygen content (180 appm) nickel is depicted by comparing the micrographs and curves presented in Figures 5.3 - 5.5. Pre-injection of 10 appm helium enhanced void nucleation remarkably, while pre-injection of 30 appm helium reduced the void density. Compared to the sample without helium pre-injection, pre-injection of 10 appm helium increased the void density at 1 μm depth (3 dpa) by a factor of 3, but pre-injection of 30 appm helium reduced the void density by a factor of 2.6. The suppression of void formation by pre-injected helium was previously reported for higher helium levels than used in this study[1], and was considered to be the result of copious nucleation of sub-microscopic cavities in the implanted region. To verify this explanation,

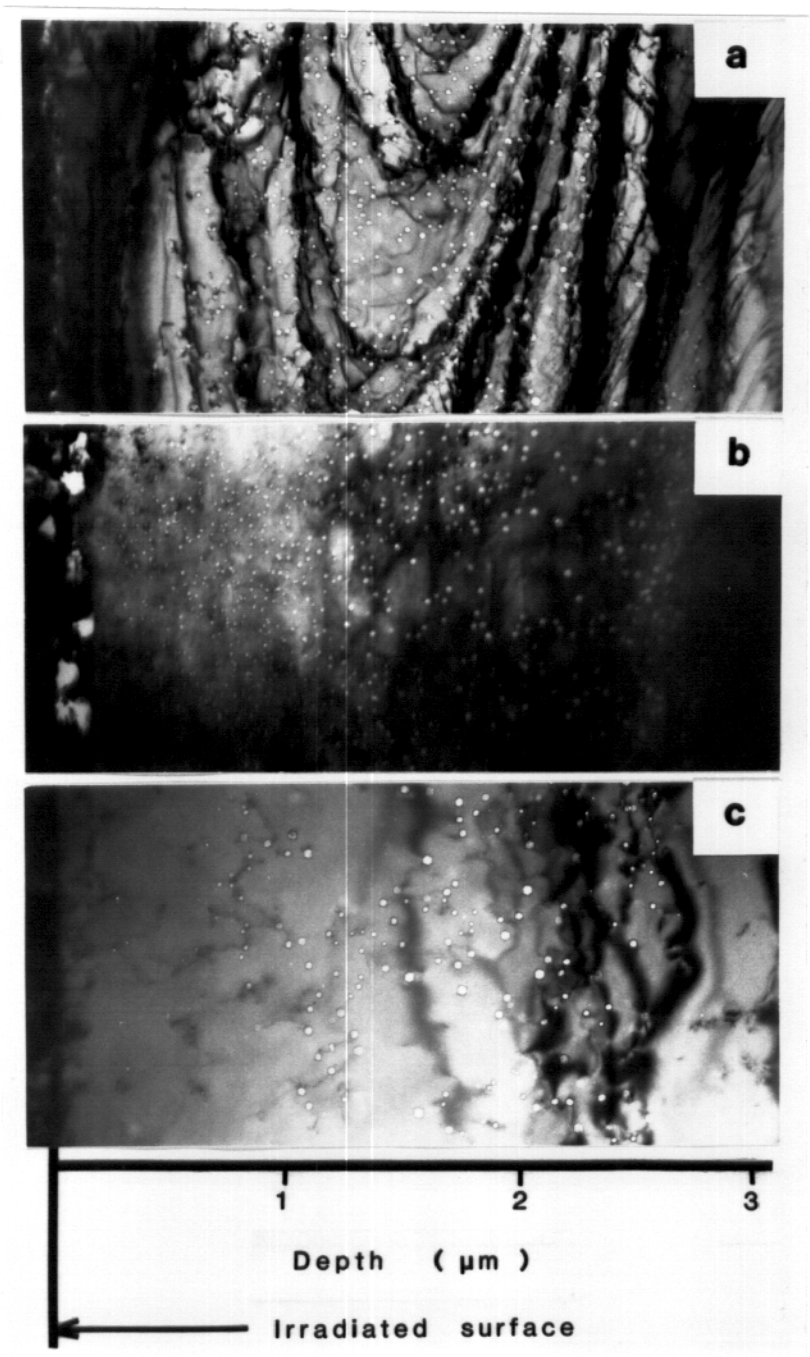

Figure 5.3 Cross-section TEM micrographs of 14 MeV Ni ion irradiated Ni samples (annealed) containing 180 appm oxygen (3 dpa at 1 μm, 500 °C). (a) without helium pre-injection (No. 03); (b) with 10 appm helium pre-injection (No. 04); (c) with 30 appm helium pre-injection (No. 05).

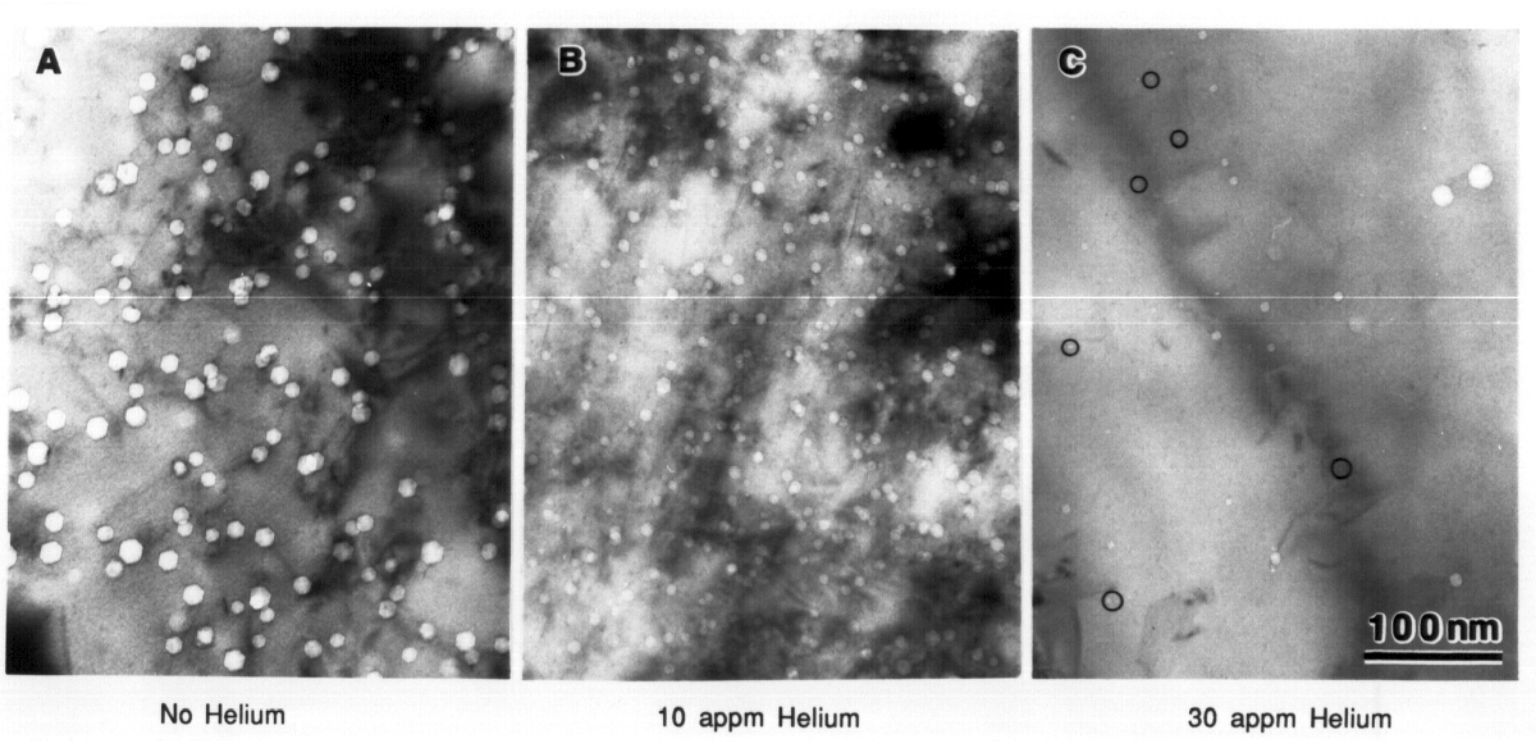

Figure 5.4 Effect of pre-injected helium on void formation in 14 MeV Ni ion irradiated pure Ni (180 appm oxygen, 3 dpa 500 °C). (A) No helium; (B) 10 appm helium; (C) 30 appm helium.

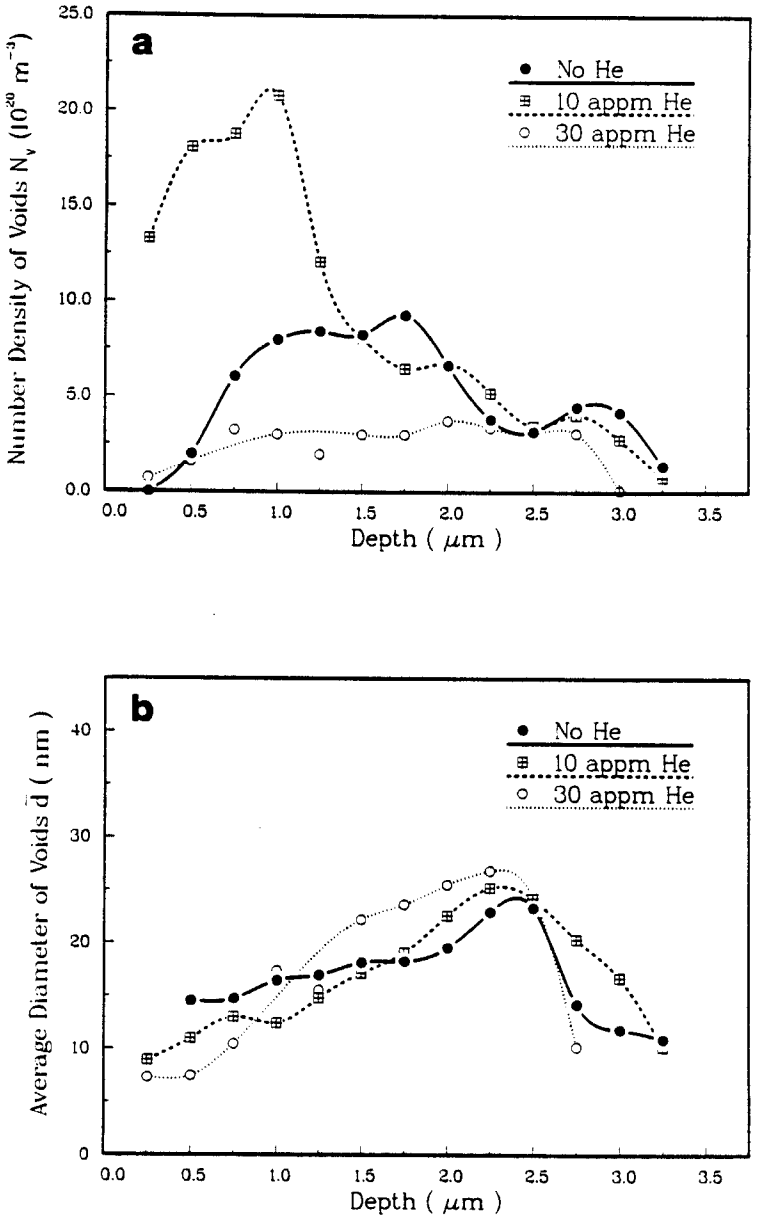

Figure 5.5 Number density (a) and average diameter (b) of voids versus depth for the Ni ion irradiated high oxygen (180 appm) Ni samples (No. 03, 04 and 05, 3 dpa at 1 μm, 500 °C) containing various amount of pre-injected helium.

the region pre-injected with 30 appm helium was examined very carefully at a magnification of 200,000x, and some very small cavities with diameter as small as ~ 2 nm (already close to the resolving power limit of the microscope used) were resolved, examples being encircled in Figure 5.4 (C).

A.3 Void Formation in Degassed Nickel (75 appm Oxygen) with or without Helium Pre-injection

The variation of void distribution and the dependence of the void parameters with depth in two irradiated low-oxygen content (75 appm) nickel specimens (Nos. 06 and 07) are shown in Figures 5.6 and 5.7. These samples received the same ion dose as samples mentioned in sections A.1 and A.2 (3 dpa at 1 μm). Sample No. 07 shown in Figure 5.6 (b) had 10 appm helium injected in the first ~ 1 μm region. For the purpose of comparison, the void parameter curves for sample No. 03 (vacuum annealed, 180 appm oxygen, no helium) is also included in Figure 5.7. Void density in Figure 5.7 is drawn on a logarithmic scale because the void density in the low oxygen content samples is at least one order of magnitude lower than that in the high oxygen content sample except in the helium pre-injected region. On the other hand, the average void size in the low oxygen content samples is much larger. Figure 5.8 shows the effect of residual oxygen content on void density and void size by comparing the near damage peak region of samples No. 03 and 06.

In the helium pre-injected region of sample No. 07 (75 appm oxygen) there is a high density of small voids as shown in Figure 5.6 (b),

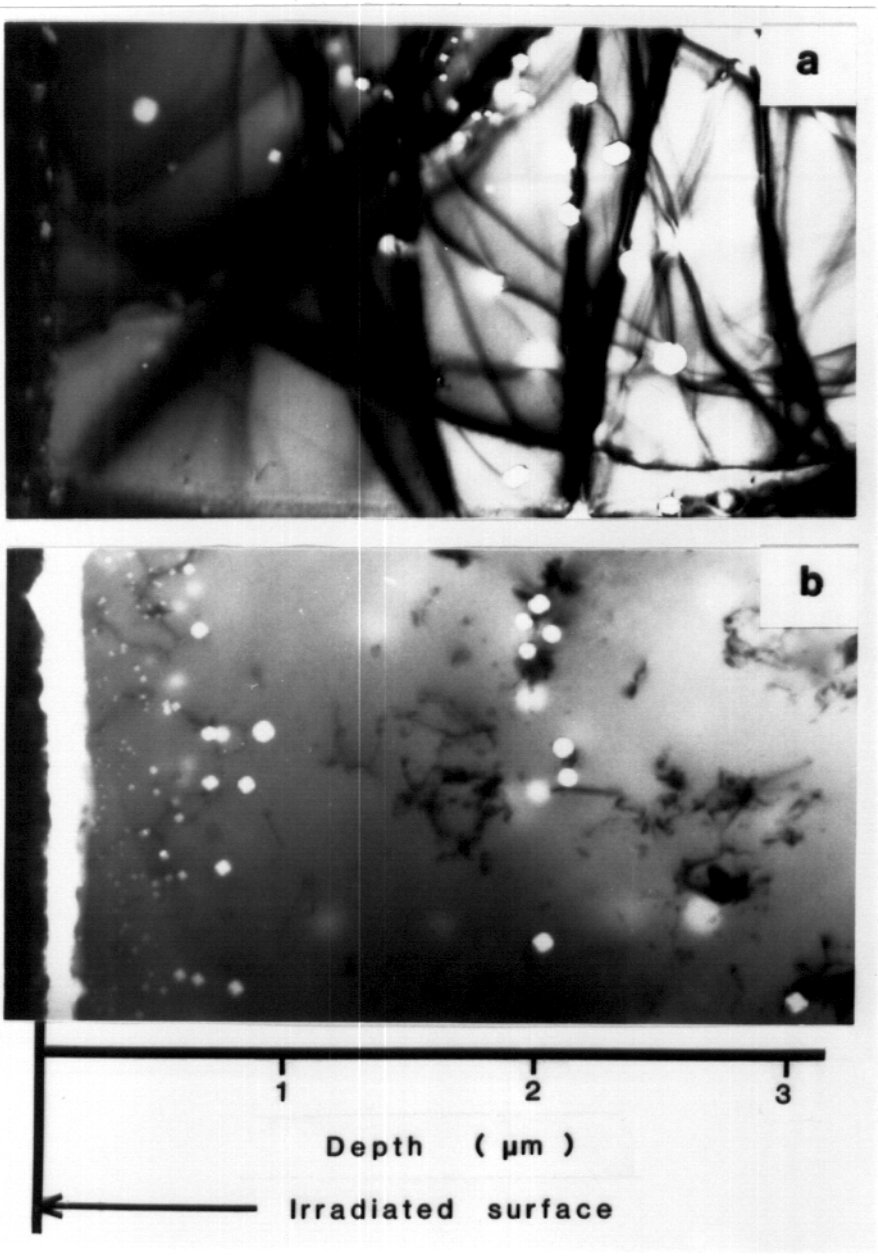

Figure 5.6 Cross-section micrographs of Ni ion irradiated low oxygen (75 appm) Ni samples (No. 06 and 07, 3 dpa at 1 μm, 500 °C) without (a) or with (b) 10 appm helium pre-injection.

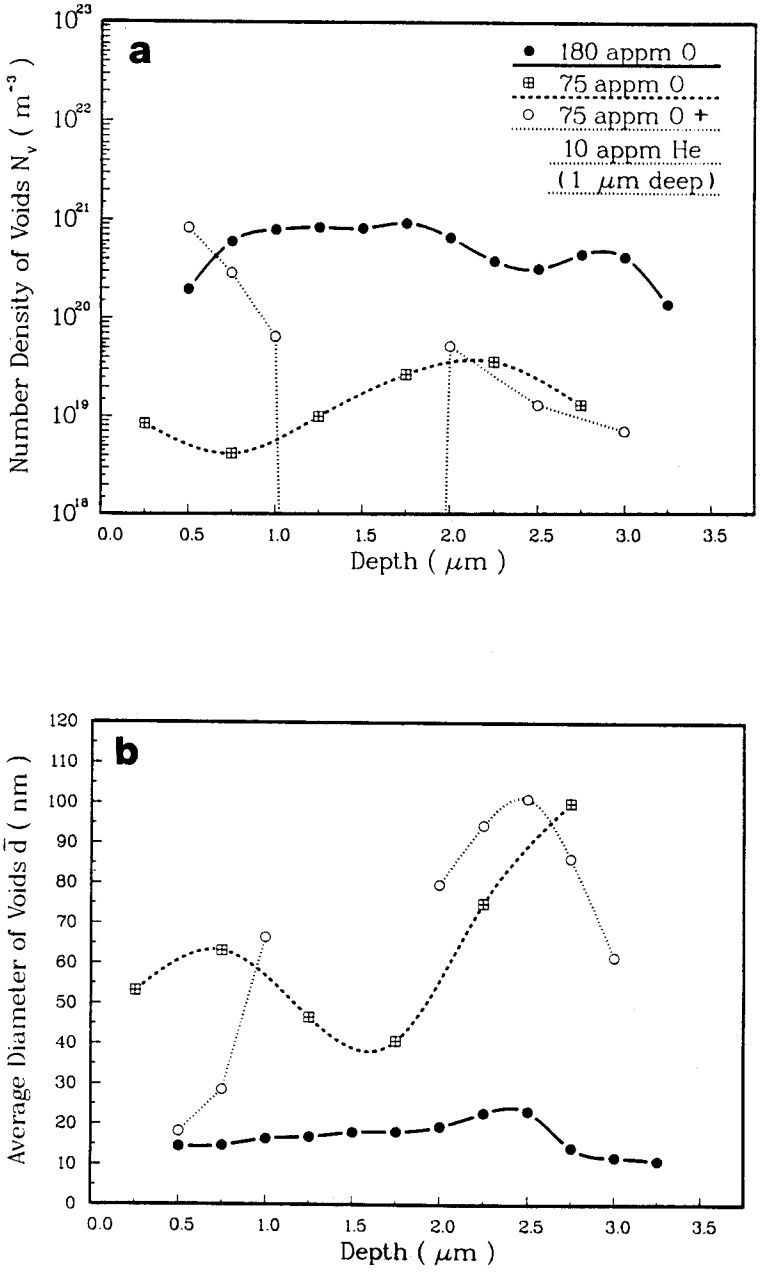

Figure 5.7 Number density (a) and average diameter (b) of voids versus depth for the irradiated low oxygen (75 appm) Ni samples without or with 10 appm helium pre-injection (samples No. 06 and 07, 3 dpa at 1 μm, 500 °C). The curves for the high oxygen (180 appm) zero helium sample (No. 03) shown in Fig. 5.5 are repeated here for comparison.

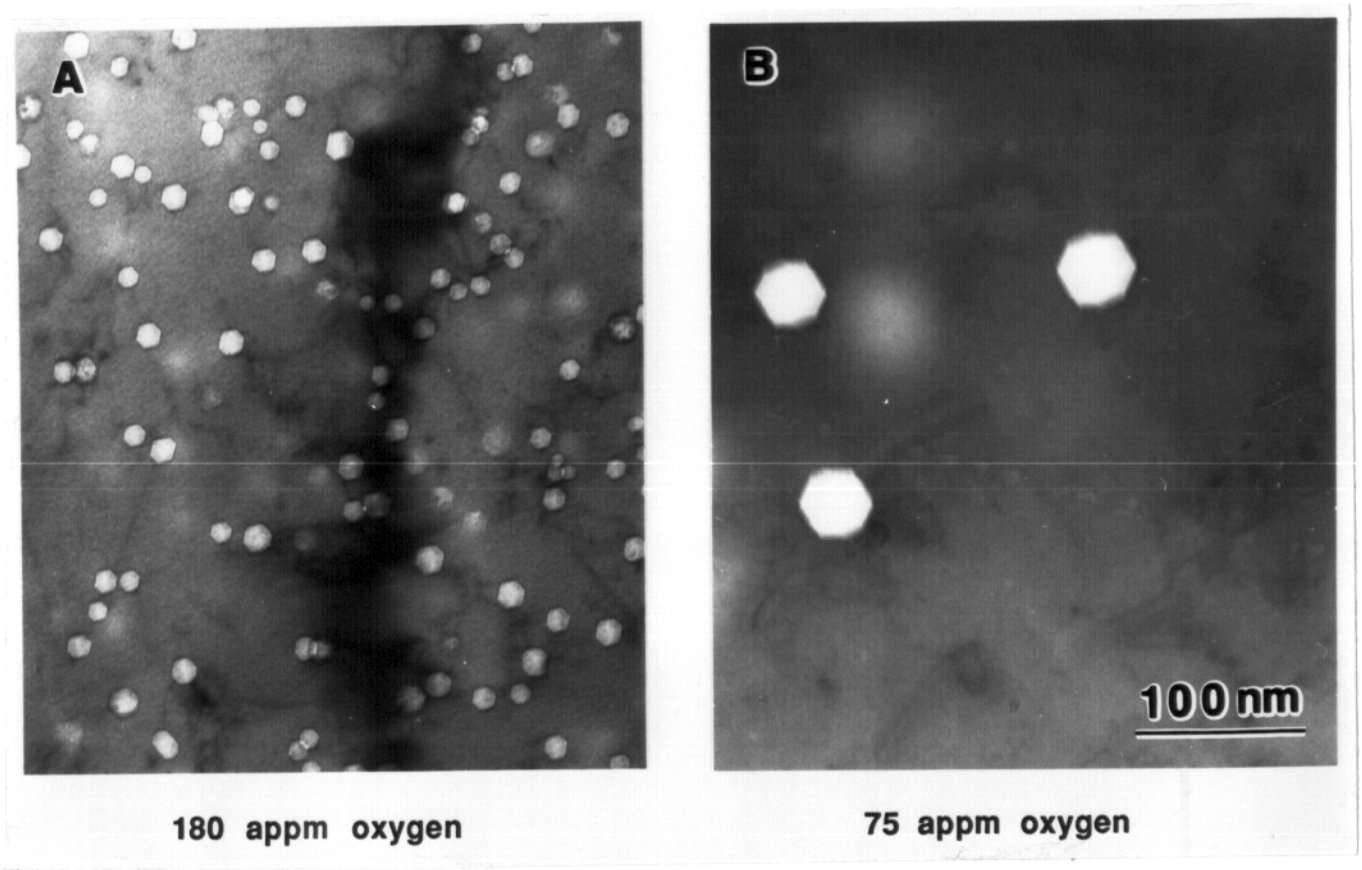

Figure 5.8 Effect of residual oxygen on void formation in 14 MeV Ni ion irradiated Ni (10 dpa, 500 °C). (A) 180 appm oxygen; (B) 75 appm oxygen.

but, compared to the 10 appm helium region of sample No. 04 (180 appm oxygen), the void density in the same region of sample No. 07 is much lower and the average void size is larger. Another notable difference is that toward the end of the helium range (1 μm) in sample No. 07, the void size gets progressively larger and the void density becomes progressively lower. There is a void denuded zone in the sample between the end of the helium zone and the peak damage depth, because not enough gas atoms are available for void nucleation at that damage level (5-10 dpa) in this region. This phenomenon was not seen in the high oxygen content sample that was pre-injected with the same amount of helium because there were enough oxygen atoms available to stabilize the void embryos.

A.4 Effect of Oxygen on Void Formation in Irradiated Nickel

In addition to the results shown above, results obtained from the three other nickel samples with different residual oxygen content and with pre-injected oxygen (Nos. 02, 09 and 10) and with higher irradiation doses are compared in Figure 5.9 and Table 5.1 to further clarify the effect of oxygen on void formation in heavy-ion irradiated nickel. Sample No. 02 is irradiated in the as-received state which contained 180 appm residual oxygen. While samples No. 09 and 10 contain the same amount of residual oxygen (75 appm), sample No. 10 has an additional 75 appm implanted oxygen in the first ~ 1.2 μm region.

Although in all the three cases the swelling at the damage peak resulted from a relatively low density of voids with diameter of 40-60 nm,

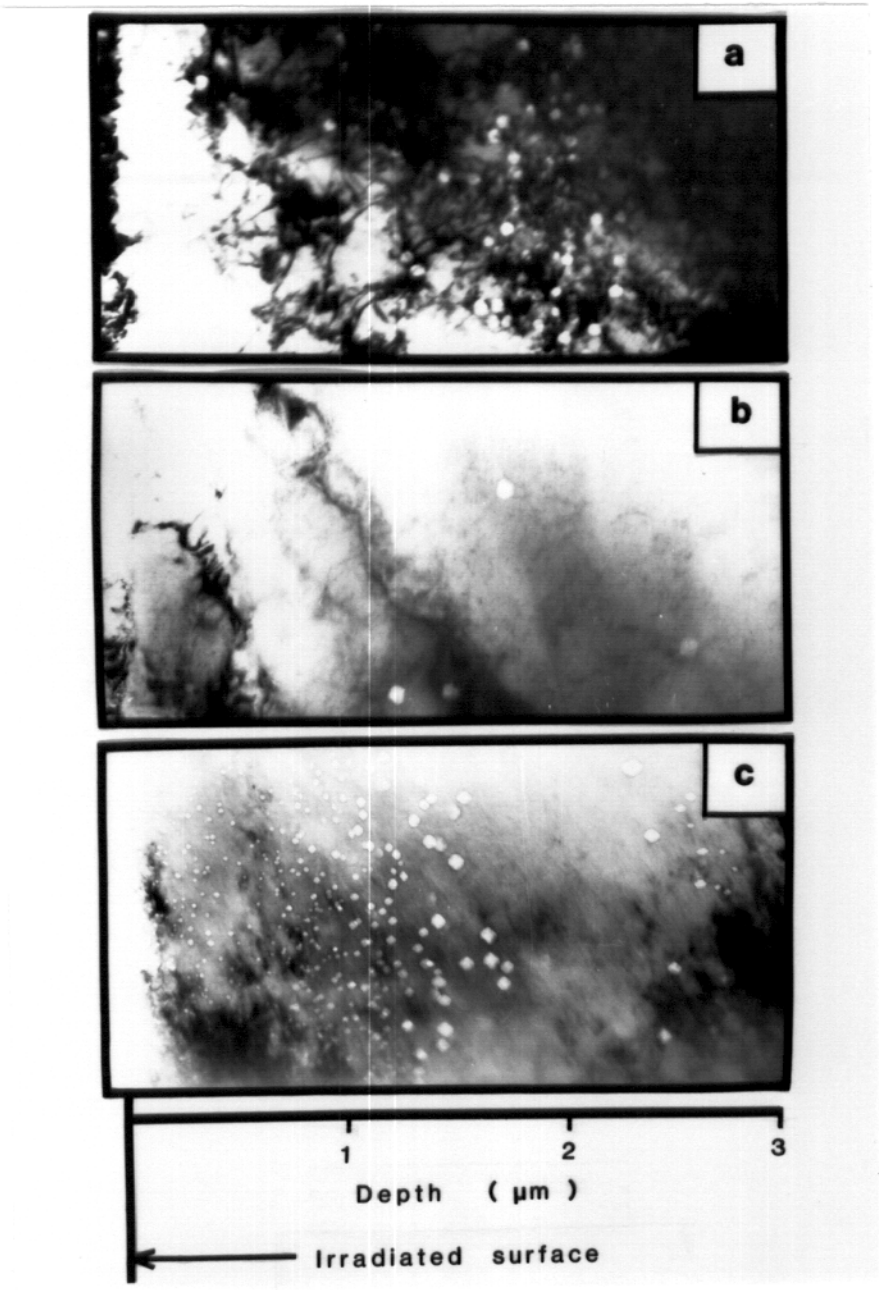

Figure 5.9 Cross-section TEM micrographs showing the effect of oxygen on void formation in 14 MeV Ni ion irradiated Ni. (a) 180 appm oxygen, 10 dpa at 1 μm (No. 02); (b) 75 appm oxygen, 10 dpa at 1 μm (No. 09); (c) 75 appm oxygen plus 75 appm pre-injected oxygen at first ~ 1.2 μm, 5 dpa at 1 μm (No. 10).

the void density at the peak damage depth in the as-received nickel is approximately an order of magnitude greater than in the degassed or oxygen-implanted foils. In the first micrometer of the as-received and degassed nickel, a sparse, heterogeneous population of large voids exists. However, at the 1 μm depth in the oxygen implanted sample, the void size is remarkably smaller and the void density is about two orders of magnitude higher in comparison to the as-received or degassed nickel foils. It is very clear that both residual and pre-injected oxygen atoms promote void nucleation in nickel-ion-irradiated pure nickel, and the effect of the injected oxygen seems to be more significant.

Table 5.1 Comparison of void parameters in 14 MeV Ni-ion-irradiated Ni samples with various oxygen contents

Sample No.*	Irradiation Temp.	Location	Oxygen (appm)	Dose (dpa)	Void Density ($10^{20}/m^3$)	Average Void Diameter
02	500 °C	1 μm	180	10	0.3	50 nm
		peak	180	40	1.0	50 nm
09	500 °C	1 μm	75	10	0.1	50 nm
		peak	75	40	0.07	60 nm
10	500 °C	1 μm	150†	5	20.0	14 nm
		peak	75	20	0.2	40 nm

* See Table 4.1 for the pre-irradiation and irradiation conditions of the samples

† 75 appm residual oxygen plus 75 appm pre-injected oxygen.

B. Defect Cluster Formation in Irradiated Ni-Cu Alloys with or without Oxygen Pre-injection

B.1 Results from Irradiation of Ni-10Cu

Figure 5.10 shows the entire ion damage range of the Ni-10Cu alloy, sample (No. 13), which has been pre-injected with 100 appm oxygen and then irradiated with 14 MeV nickel ions to a peak damage level of 20 dpa. In contrast with the microstructures of irradiated pure nickel, most defect clusters observed in this alloy are dislocation loops (Figure 5.10 (A)), although some voids are also found by tilting the loops out of contrast (Figure 5.10 (B)). These voids are mainly located in the oxygen implanted region, and they have an average diameter of 12 nm and a local density of 7×10^{19} m^{-3}. Only a few voids with an average diameter of 8 nm occur at the peak damage depth.

Figure 5.11 is a cross-section micrograph showing the distribution of radiation-induced dislocation structure in the Ni-10Cu sample (No. 14) which also contains 100 appm pre-injected oxygen but received a 14 MeV nickel ion dose twice as much as that received by sample No. 13. Again, the dislocation loop constitutes the major defect cluster. Some voids are found in the oxygen implanted region of this sample too, but their distribution is relatively heterogeneous. Several larger voids of ~ 50 nm in diameter were found to be surrounded by many smaller voids of only ~ 5 nm in diameter (as shown in Figure 5.14 (C)), which implies the agglomeration of smaller voids during the continuous irradiation. Only

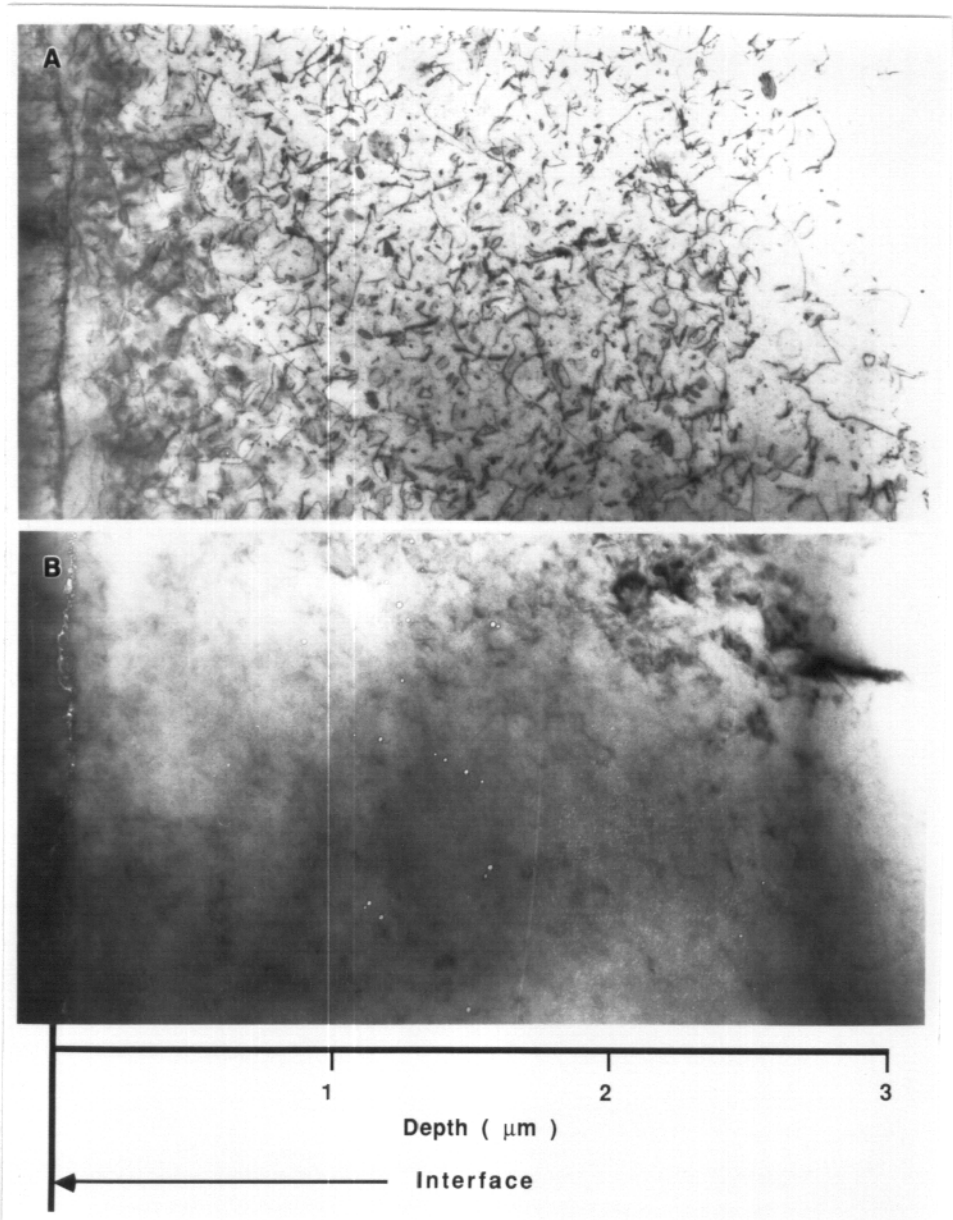

Figure 5.10 Cross-section TEM micrographs taken from a Ni-10Cu sample (No. 13) with 100 appm oxygen pre-injection and a damage level of 5 dpa at 1 μm (irradiated by 14 MeV Ni ions at 485 °C). (A) distribution of dislocation loops (g = [220]); (B) loops tilted out of contrast showing presence of voids in the oxygen injected region.

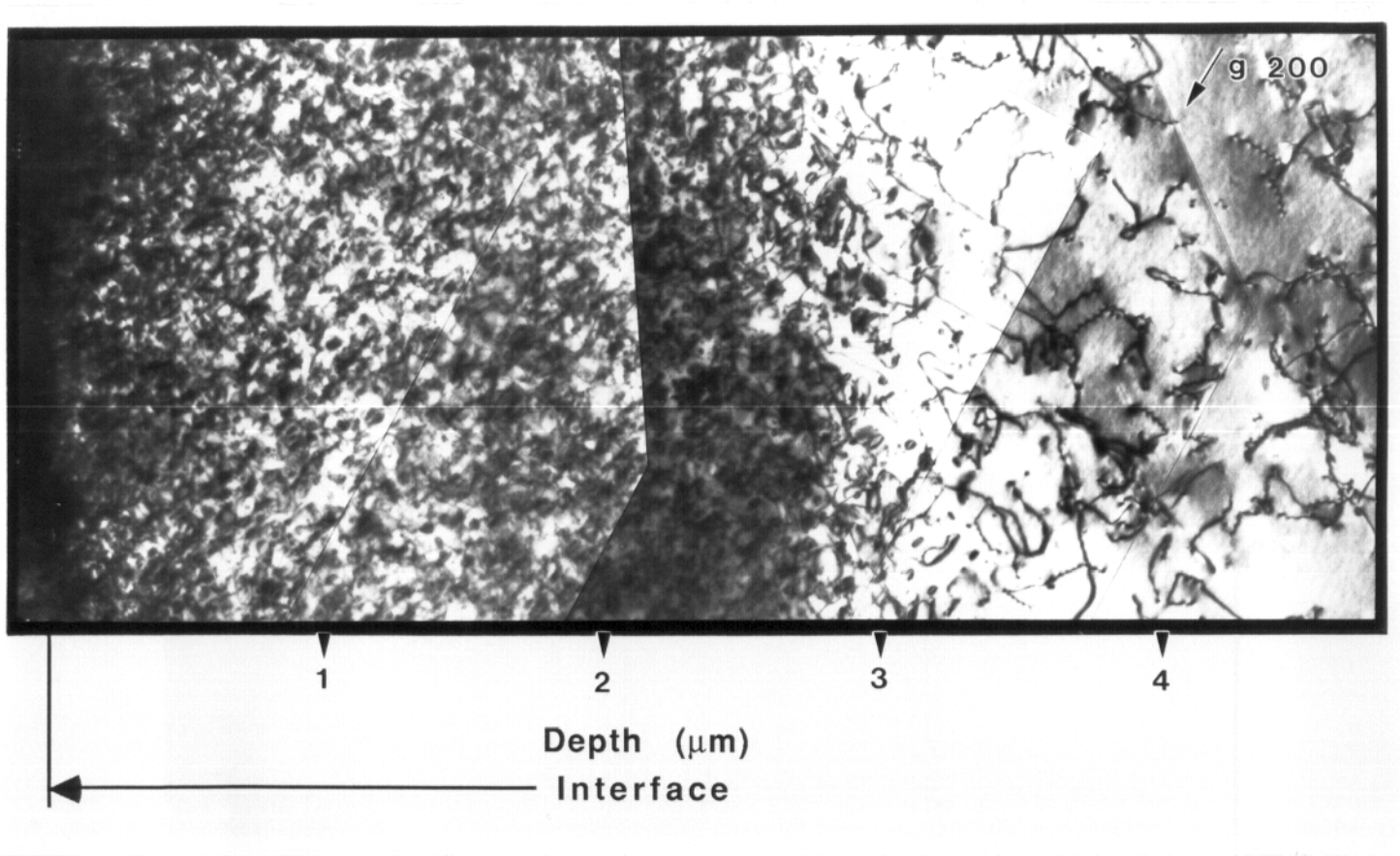

Figure 5.11 Cross-section micrograph of 14 MeV Ni ion irradiated Ni-10Cu (No. 14, 100 appm oxygen pre-injection, 10 dpa at 1 μm, 485 °C).

one larger void (125 nm in diameter) was found at the damage peak region of this sample.

Figures 5.12 and 5.13 are the cross-section micrographs taken from the Ni-10Cu sample (No. 16) which received the highest nickel ion dose (100 dpa at the peak) but without oxygen pre-injection. While Figure 5.12 clearly depicts the distribution of dislocation loops in the sample using g = [200], Figure 5.13 was taken in a low contrast diffracting condition to show the distribution of voids. The voids found in this sample are all located in the peak damage region (~ 2.5 μm from the original surface). The local void density in that region is about $9x10^{19}$ m^{-3}, and the average void diameter is ~ 14 nm.

In Figure 5.14, void structures in the irradiated Ni-10Cu samples are compared with each other and with that obtained from the oxygen implanted region of an irradiated nickel specimen. It is much harder for voids to form in Ni-10Cu than in pure nickel when a similar amount of pre-injected oxygen is present. Without the help of pre-injected oxygen, voids formed in Ni-10Cu only when the damage level reached ~ 100 dpa, even though the Ni-10Cu foil used in this study contained about 100 appm residual oxygen.

Figure 5.15 gives a comparison of the dislocation structures in the Ni-10Cu alloy with various irradiation conditions. The unirradiated area contains only line dislocations with a density of ~ $3x10^{13}$ m^{-2} as shown in Figure 5.15 (A), but in the all the irradiated areas dislocation loops with an average density of $1x10^{21}$ m^{-3} are found. When comparing the density

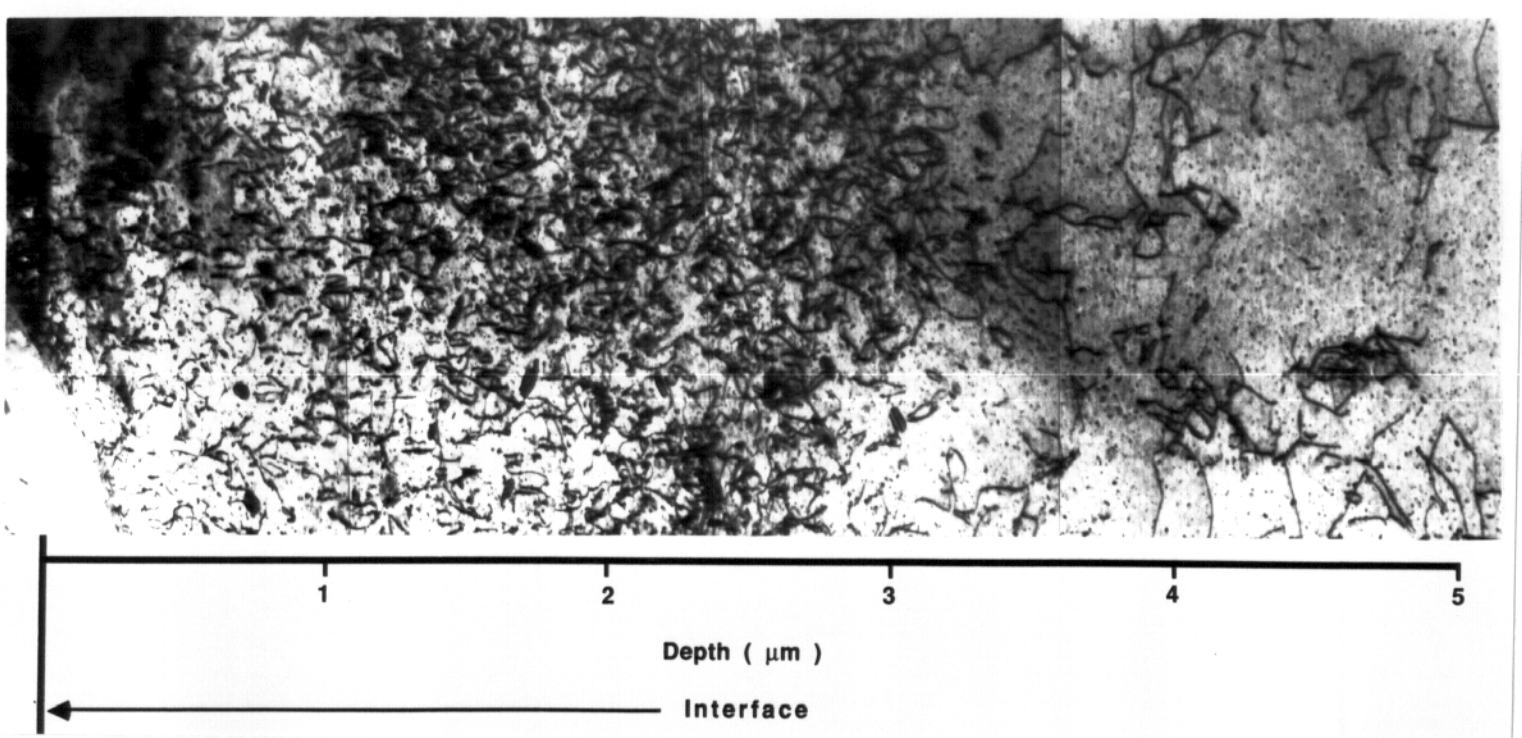

Figure 5.12 Cross-section micrograph of 14 MeV Ni ion irradiated Ni-10Cu (No. 16, 25 dpa at 1 μm, 485 °C) showing the distribution of dislocation loops.

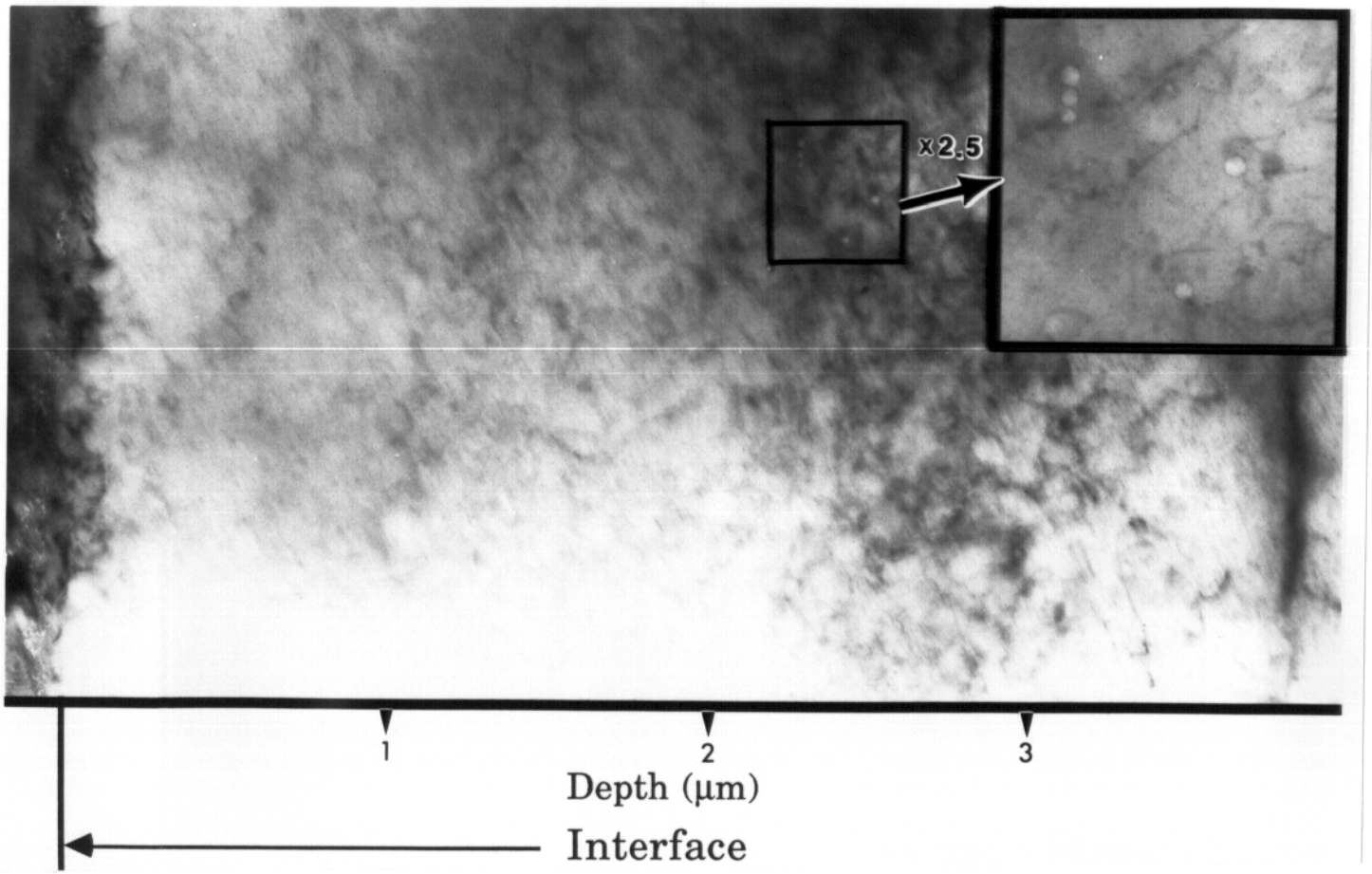

Figure 5.13 Cross-section micrograph of 14 MeV Ni ion irradiated Ni-10Cu (No. 16, 25 dpa at 1 μm, 485 °C) showing the distribution of voids.

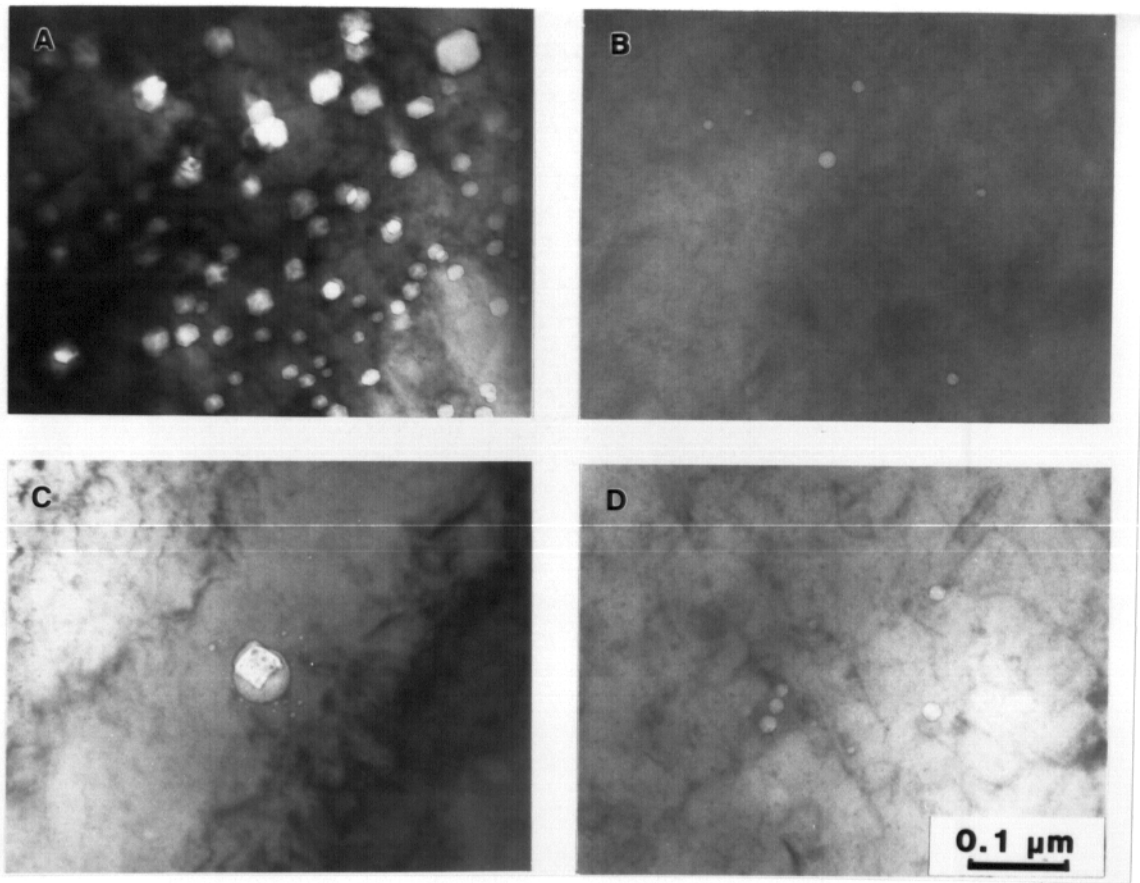

Figure 5.14 Comparison of void structures in irradiated Ni and Ni-10Cu samples. (A) Ni, 10 dpa, 75 appm pre-injected oxygen; (B) Ni-10Cu, 10 dpa, 100 appm pre-injected oxygen; (C) Ni-10Cu, 20 dpa, 100 appm pre-injected oxygen; (D) Ni-10Cu, 100 dpa. (A), (B) and (C) were taken from a 1.3-1.8 μm depth of samples No. 09, 13 and 14 respectively, and (D) was taken from the peak damage region of sample No. 16.

of line dislocations in the unirradiated region with the loop density in the irradiated regions it should be noted that Figure 5.15 (A) has a much lower magnification than that of the other three micrographs in Figure 5.15. The dislocation loops are identified as either perfect loops on {111} planes with $\vec{b}$ = a/2 <110> or Frank loops (faulted loops) enclosing a stacking fault with $\vec{b}$ = a/3 <111>. The size of the dislocation loops in the irradiated Ni-10Cu varies from ~ 5 nm to 85 nm in diameter, with the average diameter around 25 nm. The analysis of the interstitial/vacancy nature of the dislocation loops has only been performed on some of the larger loops with diameter ≥ 50 nm in Ni-10Cu using the method outlined by Edington[2], but both vacancy and interstitial loops have been identified. The presence of pre-injected oxygen does not seem to have any effect on altering the loop parameters in Ni-10Cu.

B.2 Results from Irradiation of Ni-50Cu

The damage structure throughout the entire damage range in the Ni-50Cu sample (No. 19), which has been pre-injected with 100 appm oxygen and then irradiated with 14 MeV nickel ions to a peak damage level of 20 dpa, is shown in the cross-section micrographs in Figure 5.16. Dislocation loops with much smaller size and much higher density compared to those in irradiated Ni-10Cu are observed (Figure 5.16 (A)), and no voids were found when the loops were tilted out of contrast even in the oxygen implanted region (Figure 5.16 (B)). Figures 5.17 and 5.18 are cross-section micrographs of the other two irradiated Ni-50Cu samples

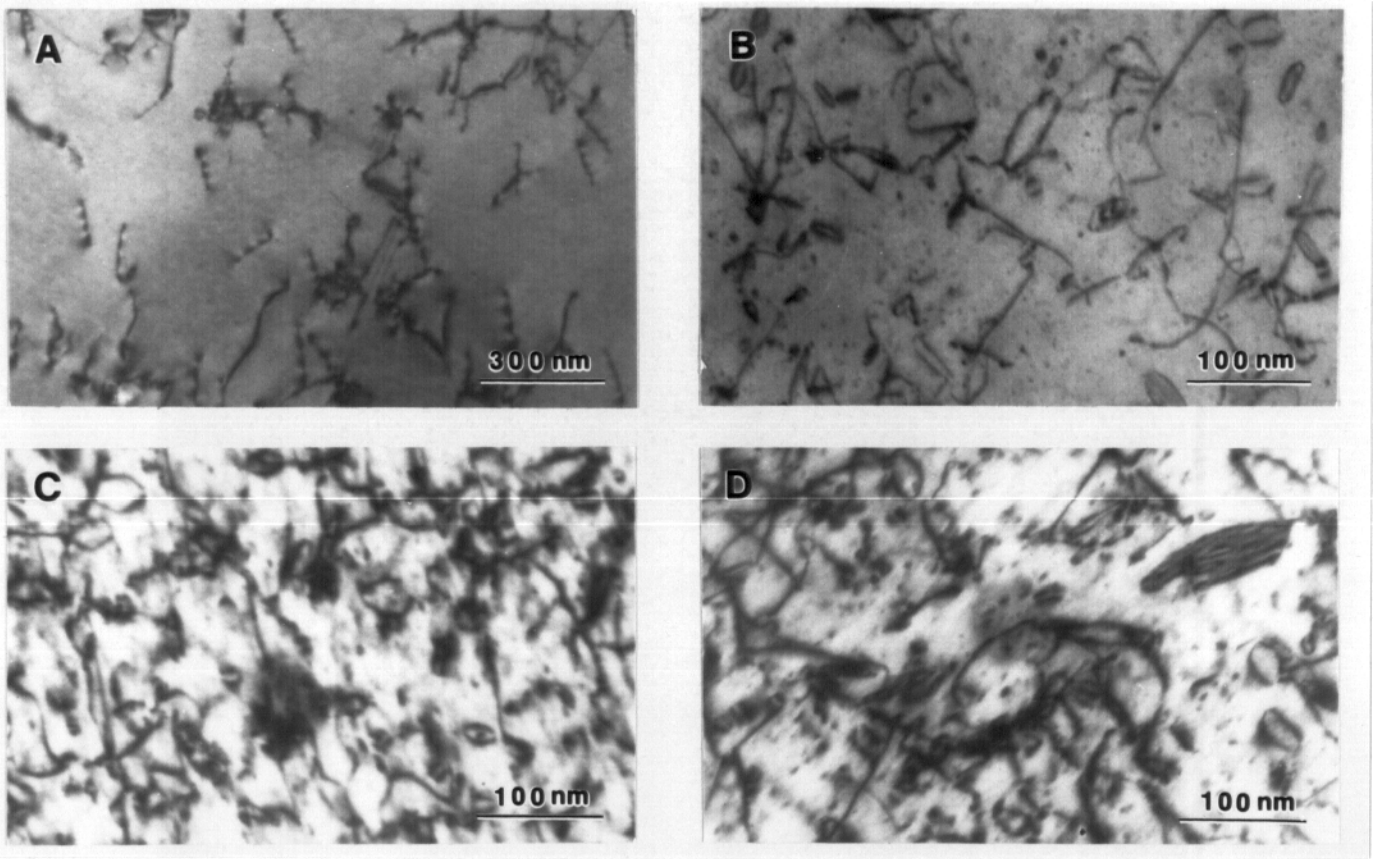

Figure 5.15 Comparison of the dislocation structures in Ni-10Cu with various irradiation conditions at 485 °C. (A) control region (unirradiated); (B) 10 dpa, 100 appm pre-injected oxygen; (C) 20 dpa, 100 appm pre-injected oxygen; (D) 50 dpa. (B), (C) and (D) were taken from a 1.3-1.8 μm depth of samples No. 13, 14 and 16 respectively.

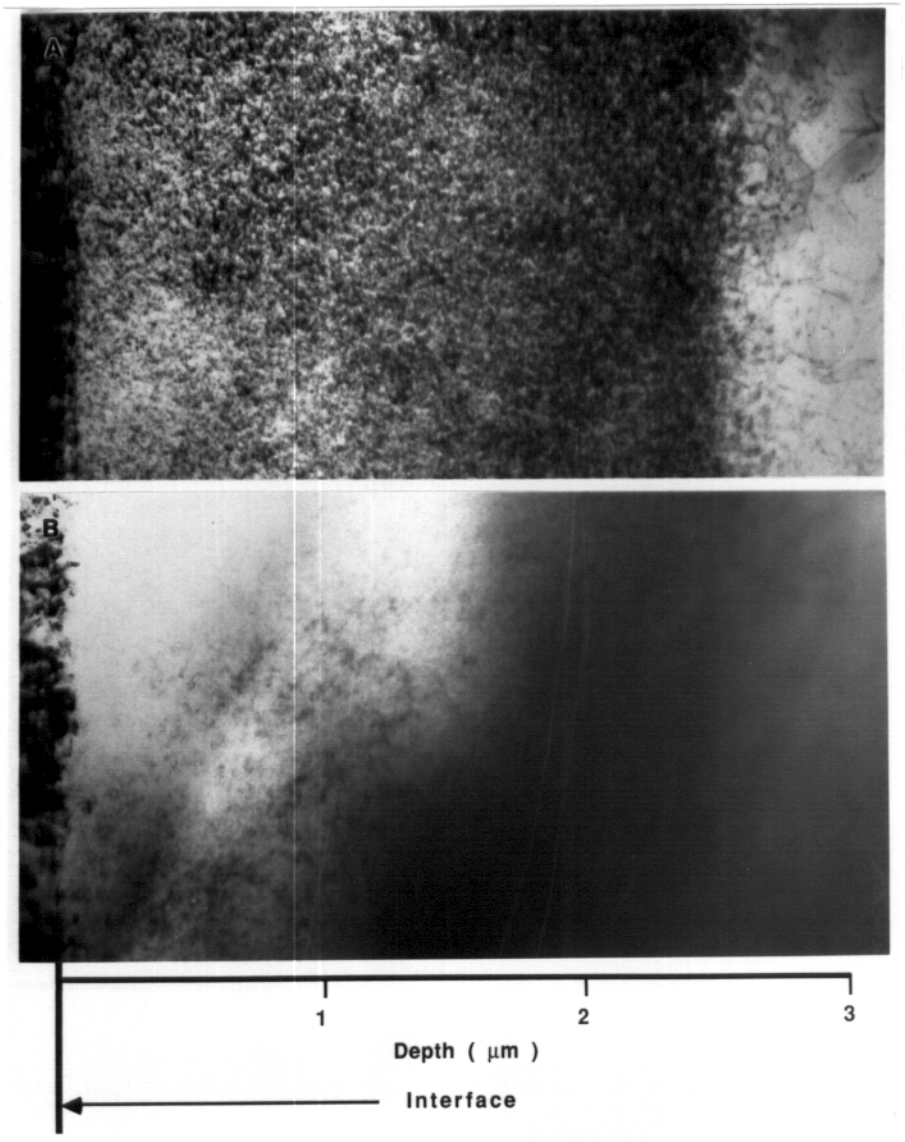

Figure 5.16 Cross-section TEM micrographs taken from a Ni-50Cu sample (No. 19) with 100 appm oxygen pre-injection and a damage level of 5 dpa at 1 μm (irradiated by 14 MeV Ni ions at 425 °C). (A) distribution of dislocation loops (g = $[1\bar{1}1]$); (B) loops tilted out of contrast showing absence of voids.

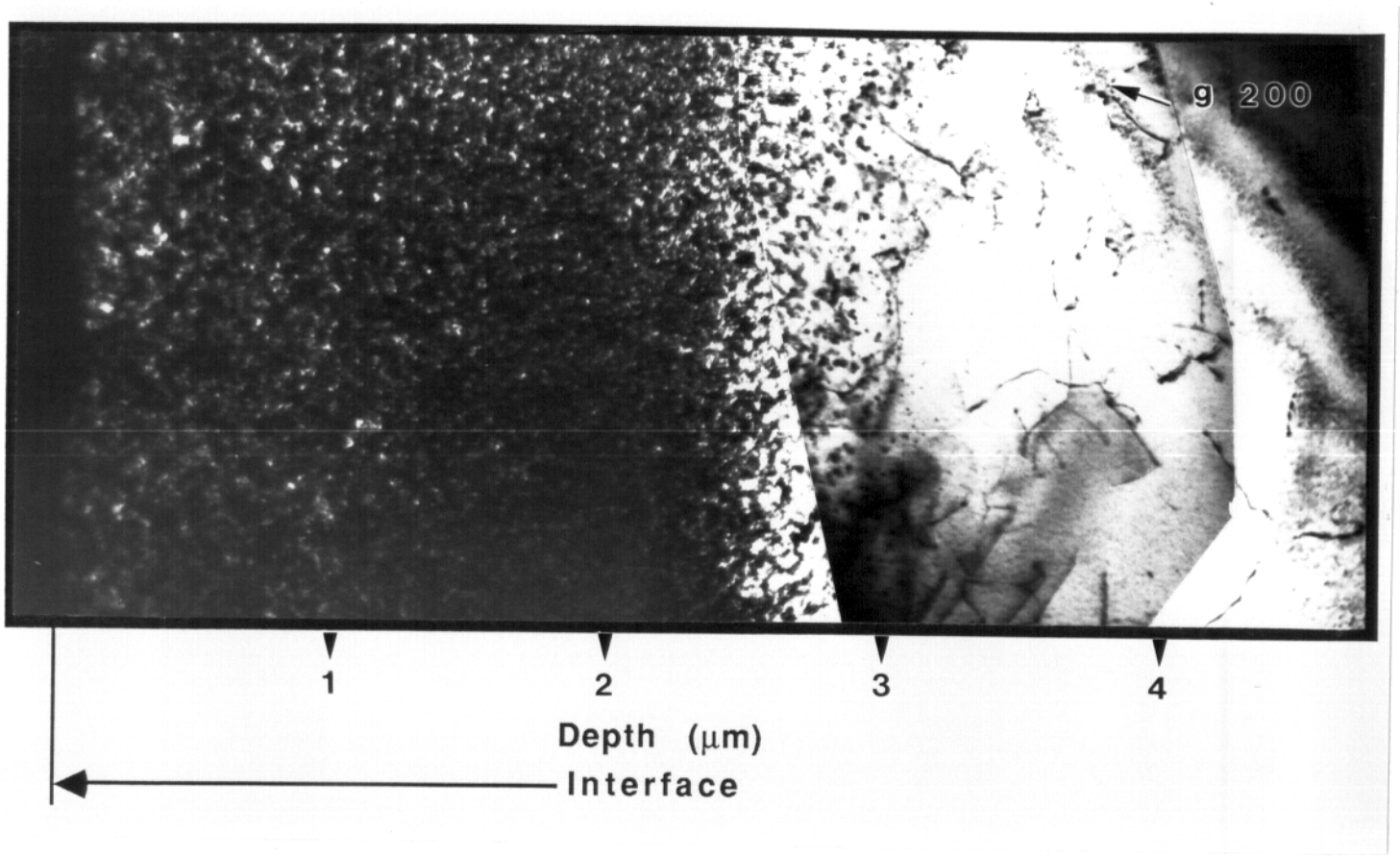

Figure 5.17 Cross-section TEM micrograph of 14 MeV Ni ion irradiated Ni-50Cu (No. 20, 100 appm oxygen pre-injection, 10 dpa at 1 μm, 425 °C).

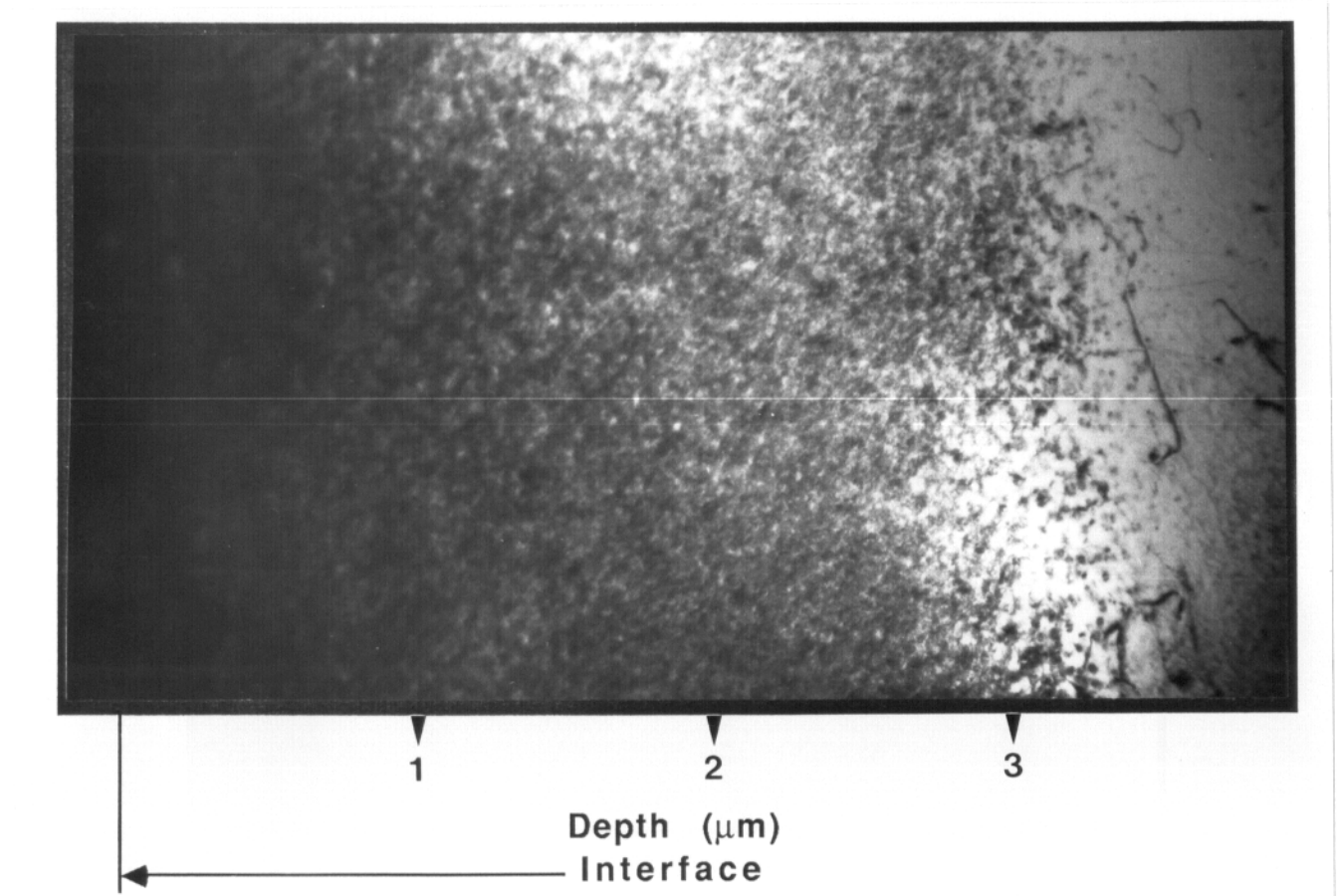

Figure 5.18 Cross-section TEM micrograph of 14 MeV Ni ion irradiated Ni-50Cu (No. 22, 25 dpa at 1 μm, 425 °C).

(Nos. 20 and 22). Sample No. 20 had 100 appm pre-injected oxygen and was then irradiated with 14 MeV nickel ions to 40 dpa at the damage peak. Sample No. 22 does not contain any pre-injected oxygen, but has received a nickel ion dose which would provide 100 dpa at the peak damage depth. Both samples contain similar dislocation loop distribution in the damage region as that seen in sample No. 19, and neither of them contain any observable voids. A comparison of the dislocation structures in the Ni-50Cu alloy with various irradiation conditions is given in Figure 5.19. Because the size of the loops in the irradiated Ni-50Cu alloy is so small (average diameter is only 6-10 nm), and the density is so high ($5\text{-}7\times10^{21}$ m^{-3}), loop analysis is difficult. Only perfect loops on {111} planes with $\vec{b} = a/2 \langle 110 \rangle$ have been identified, and the interstitial/vacancy nature of the loop has not been determined experimentally. However, it seems reasonable to assume that at least most of the small loops are vacancy type by comparing with Leister's results[3]. In Figure 5.20, the size distributions of dislocation loops in irradiated Ni-10Cu and Ni-50Cu are compared, and it is clear from the figure that the loop size in Ni-50Cu is much smaller than in Ni-10Cu, and that higher doses generally produce more larger loops in both alloys.

B.3 Results from Irradiation of Ni-25Cu

Two Ni-25Cu samples have been irradiated with 14 MeV nickel ions (Nos. 17 and 18). Sample No. 17 had been pre-injected with 100 appm oxygen before nickel ion irradiation to a peak damage level of 20 dpa and

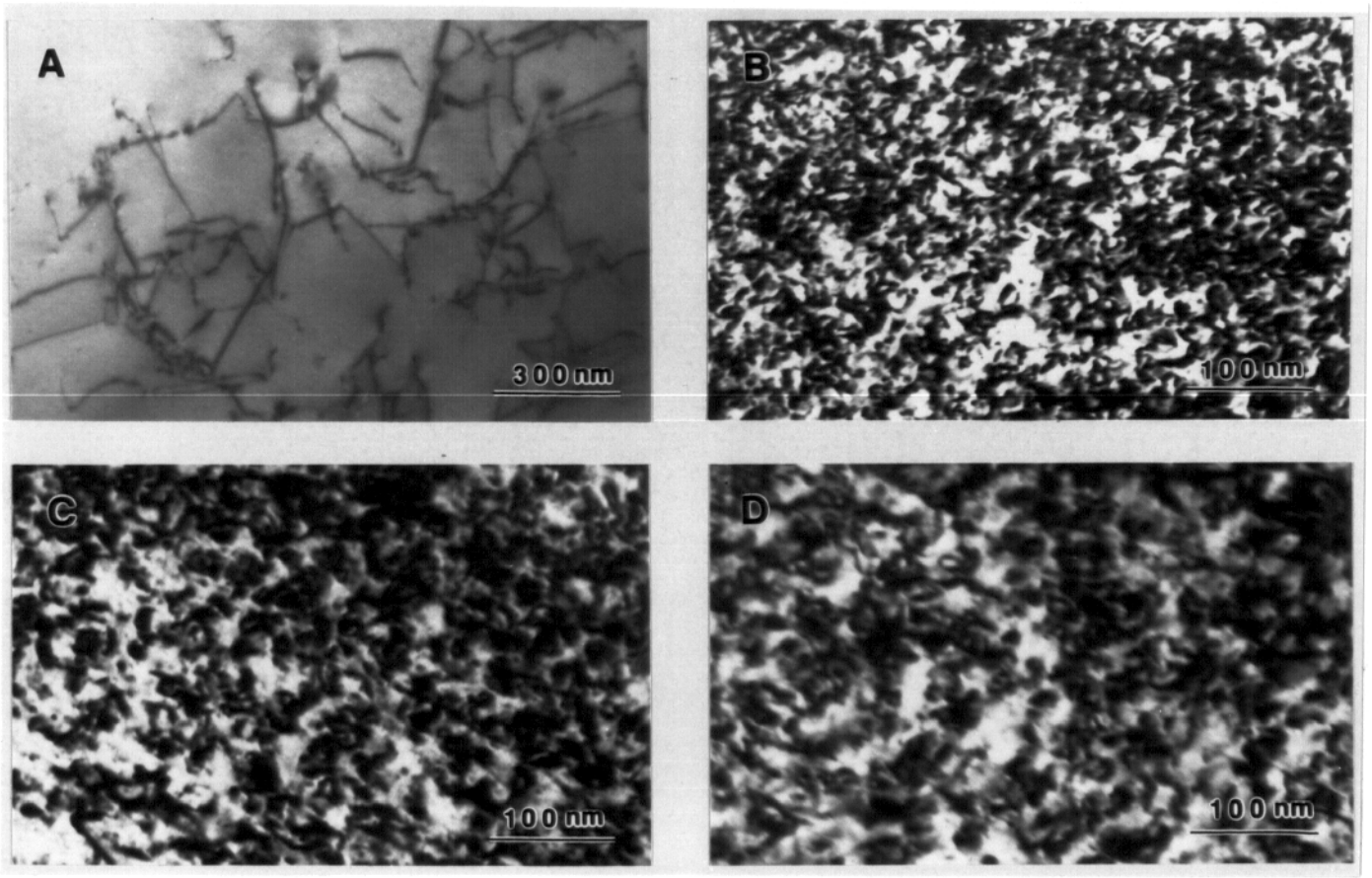

Figure 5.19 Comparison of the dislocation structures in Ni-50Cu with various irradiation conditions at 425 °C. (A) control region (unirradiated); (B) 10 dpa, 100 appm pre-injected oxygen; (C) 20 dpa, 100 appm pre-injected oxygen; (D) 50 dpa. (B), (C) and (D) were taken from a 1.3-1.8 μm depth of samples No. 19, 20 and 22 respectively.

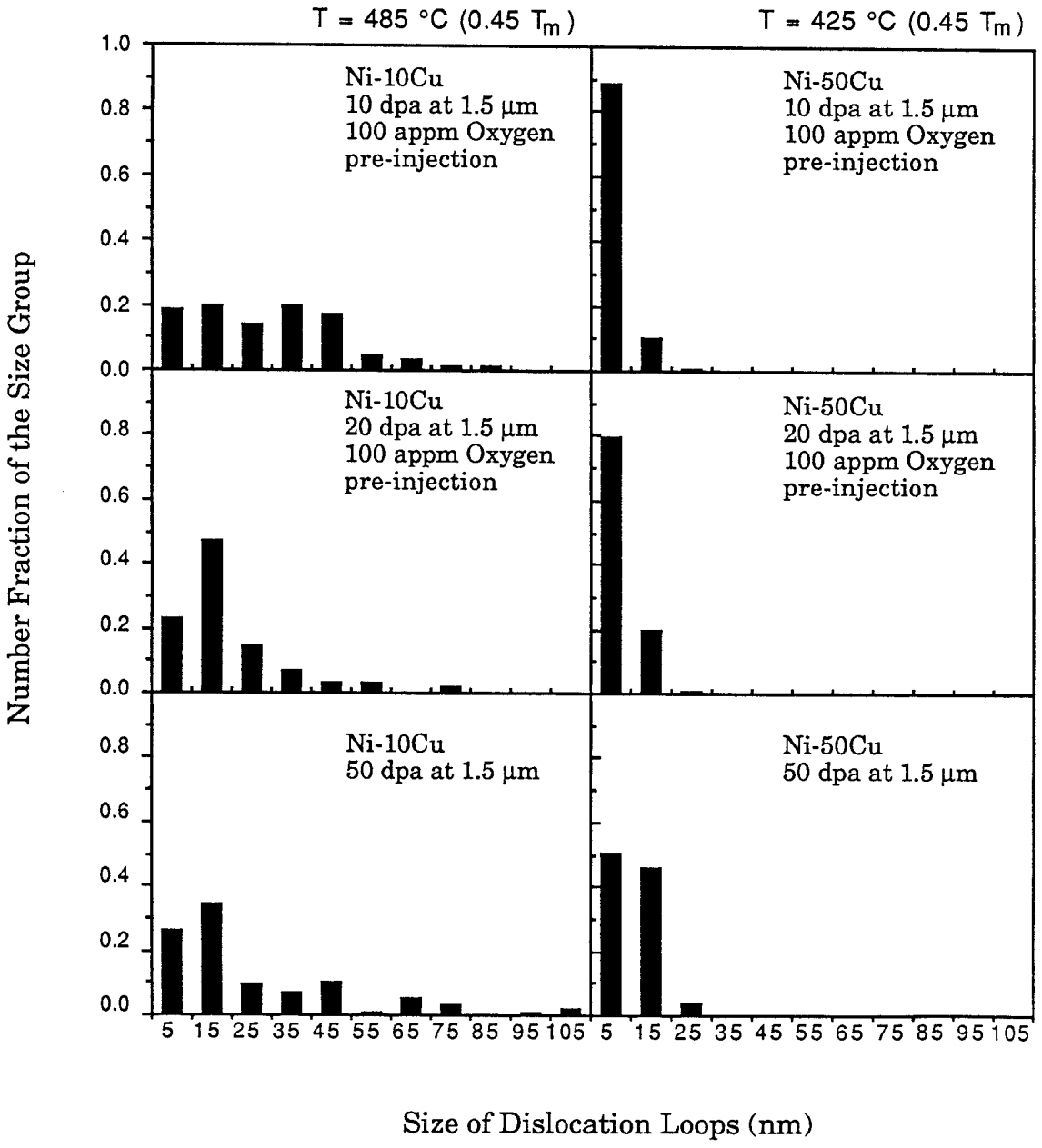

Figure 5.20 Comparison of size distributions of dislocation loops in 14 MeV Ni ion irradiated Ni-10Cu and Ni-50Cu.

sample No. 18 has been irradiated to 100 dpa at the peak depth without oxygen pre-injection. The cross-section TEM micrographs which show the entire ion damage range in the two specimens are presented in Figure 5.21 (A) and (B). Figure 5.22 compares the dislocation structures in several different regions of the irradiated alloy with that of the unirradiated region at higher magnifications. The damage structure in the irradiated Ni-25Cu alloy is very similar to that observed in the irradiated Ni-50Cu alloy, which consists of a high density of small dislocation loops. However, the loop size is slightly larger (average diameter is 10-14 nm) and the loop density is slightly lower (average density is $3\text{-}4\text{x}10^{21}$ m^{-3}) than those measured from the irradiated Ni-50Cu specimens. No voids have been found in either of the two irradiated Ni-25Cu specimens.

The defect characteristics of all the eight irradiated Ni-Cu alloy samples, which are mentioned in this section, are summarized in Table 5.2 along with the result obtained from the irradiated nickel sample with 75 appm oxygen pre-injection (No. 10). The void densities, void sizes and dislocation loop densities listed in the table were all counted from the region of about 1.5 (1.3-1.8) μm from the irradiated surface unless noted in the table. This is the region where the injected oxygen ions come to rest and the effect of the injected Ni interstitials[4] would not be significant. It should be noticed that the dpa level at that depth is about half the peak level.

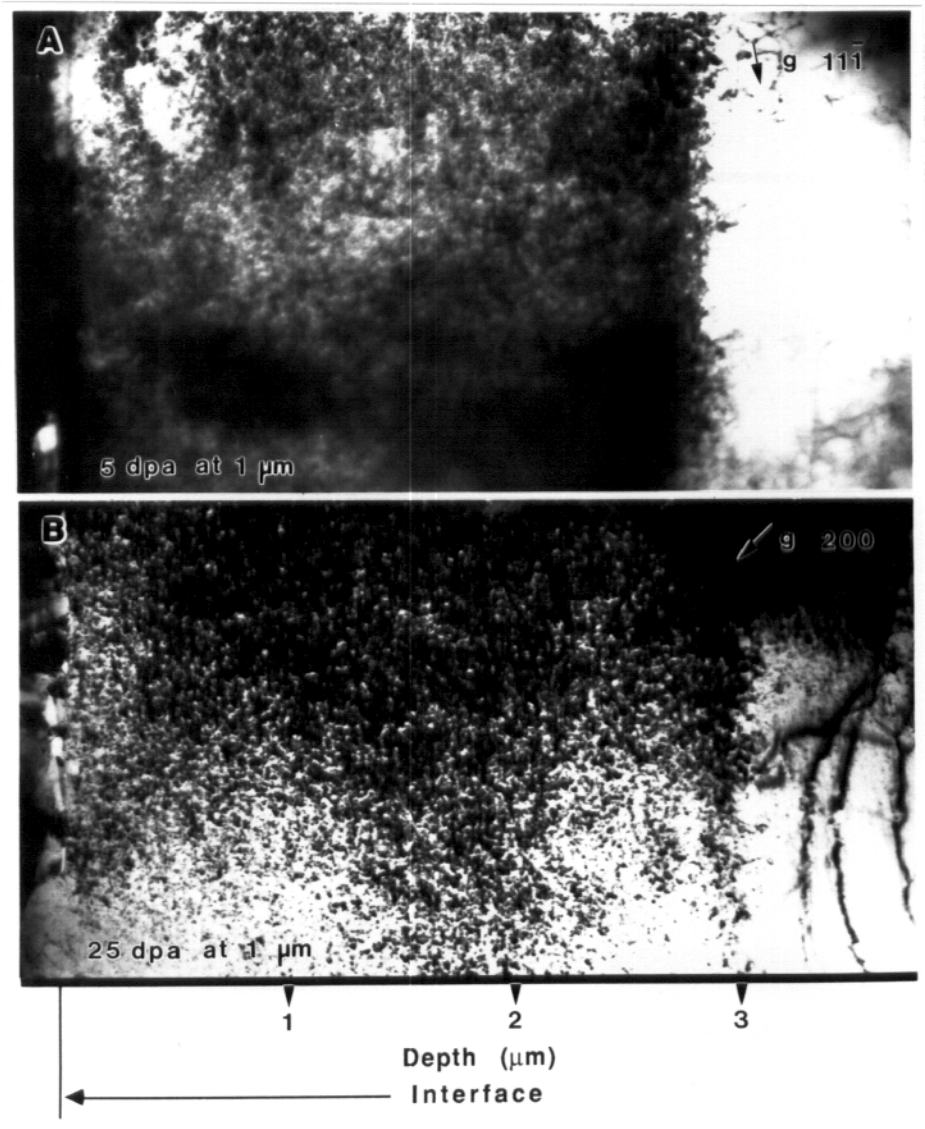

Figure 5.21 Entire ion damage region in Ni-25Cu irradiated with 14 MeV Ni ions at 465 °C. (A) 100 appm oxygen pre-injection, 5 dpa at 1 μm (No. 17); (B) 25 dpa at 1 μm (No. 18).

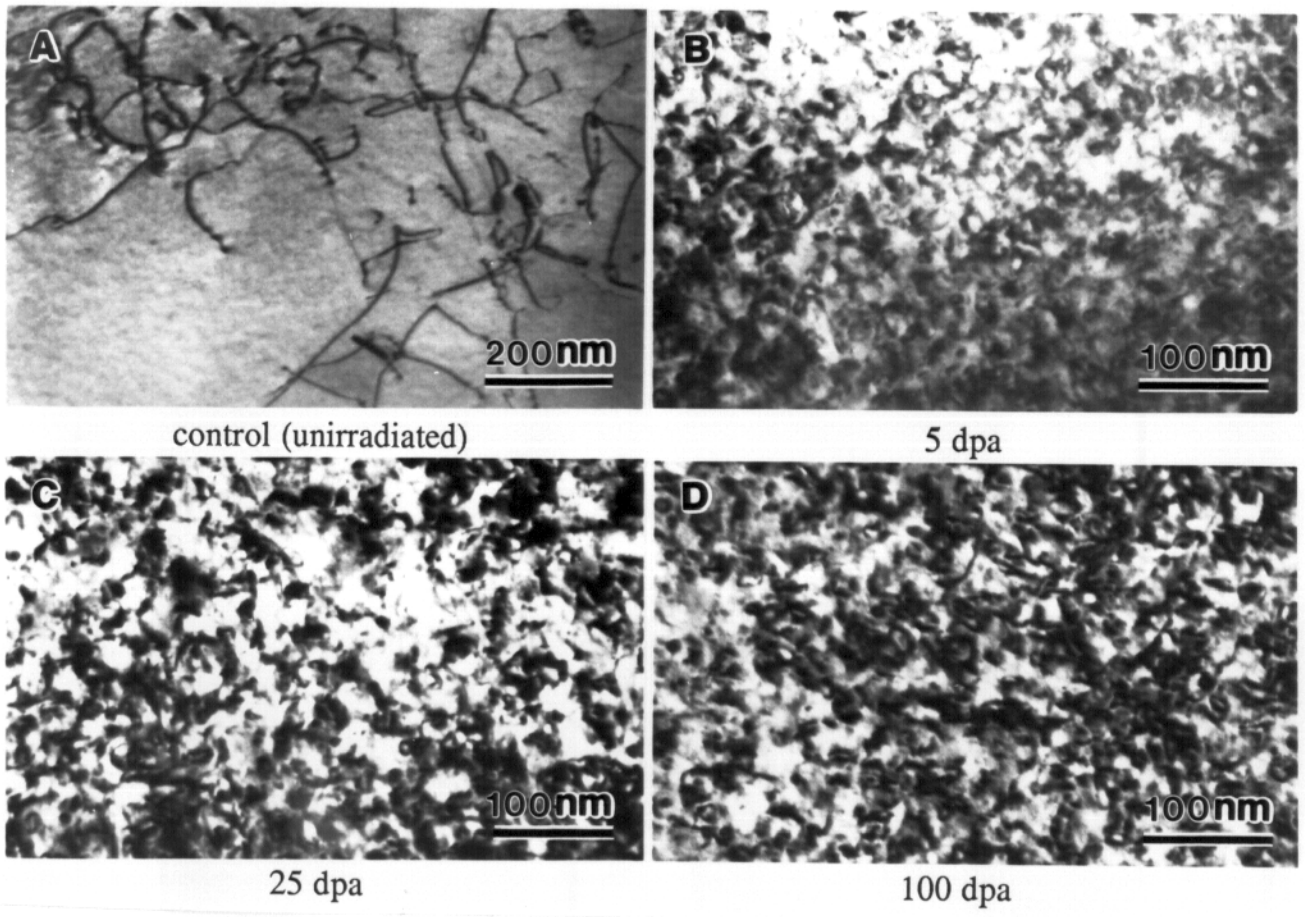

Figure 5.22 Comparison of the dislocation structures in Ni-25Cu with various irradiation conditions at 465 °C. (A) control region (unirradiated); (B) 5 dpa; (C) 25 dpa; (D) 100 dpa. (B), (C) were taken from a depth of ~ 1 μm in samples No. 17 and 18 respectively, and (D) was taken from the peak damage region of sample No. 18.

Table 5.2 Defect characteristics of 14 MeV Ni ion irradiated Ni and Ni-Cu alloys with or without oxygen pre-injection

Sample No.† (Material)	Irradiation Temp. (°C)	Oxygen pre-injected (appm)	Dose at 1.5 μm (dpa)	Dose at peak (dpa)	Voids* density (m^{-3})	Voids* average size (nm)	Dislocation loops* density (m^{-3})
10 (Ni)	500	75	10	20	~$1x10^{21}$	29	~$5x10^{19}$
13 (Ni-10Cu)	485	100	10	20	~$7x10^{19}$	12	~$1x10^{21}$
14 (Ni-10Cu)	485	100	20	40	~$1x10^{20}$	5 (90%) 53 (10%)	~$1x10^{21}$
16 (Ni-10Cu)	485	none	50	100	not observed at 1.5 μm ~$9x10^{19}$ (peak damage region)	14	~$1x10^{21}$
17 (Ni-25Cu)	465	100	10	20	not observed		~$4x10^{21}$
18 (Ni-25Cu)	465	none	50	100	not observed		~$3x10^{21}$
19 (Ni-50Cu)	425	100	10	20	not observed		~$7x10^{21}$
20 (Ni-50Cu)	425	100	20	40	not observed		~$5x10^{21}$
22 (Ni-50Cu)	425	none	50	100	not observed		~$5x10^{21}$

* Voids and dislocation loops were counted in a region of 1.5 (1.3~1.8) μm deep from the irradiated surface unless noted

† See Table 4.1 for the pre-irradiation and irradiation conditions of the samples

C. Comparison of Effects of Pre-injected Helium in Irradiated Nickel and Ni-Cu Alloys

To compare the effects of pre-injected helium on defect structure evolution in irradiated nickel and Ni-Cu alloys, three samples (one pure nickel, one Ni-10Cu and one Ni-50Cu) were first pre-injected with 50 appm helium at room temperature and then irradiated with 14 MeV nickel ions at the same homologous temperature of 0.45 T_m, i.e. 500°C, 485°C and 425°C for pure nickel, Ni-10Cu and Ni-50Cu respectively. The pure nickel specimen received 3 dpa with nickel ion irradiation at the depth of 1 μm, while the Ni-Cu alloy samples received 5 dpa at the same depth. The calculated helium ion distribution in the pre-injected pure nickel and Ni-50Cu has been shown in Figure 4.2.

Figure 5.23 (A), (B) and (C) are the cross-sectional TEM micrographs showing the entire ion damaged range in the three irradiated samples (Nos. 08, 15 and 21). The micrographs in Figure 5.24 were taken at a higher magnification from each specimen at the actual depth of 0.6-1.0 μm, where the pre-injected helium is present.

The defect structures in the three irradiated materials are distinctly different. In the irradiated pure nickel, the most obvious defect clusters are voids, although prismatic dislocation loops are also present. Comparing the result reported in section A on the nickel containing the same amount of residual oxygen (75 appm) but without helium pre-injection (No. 06), it appears that the relatively high density of voids in

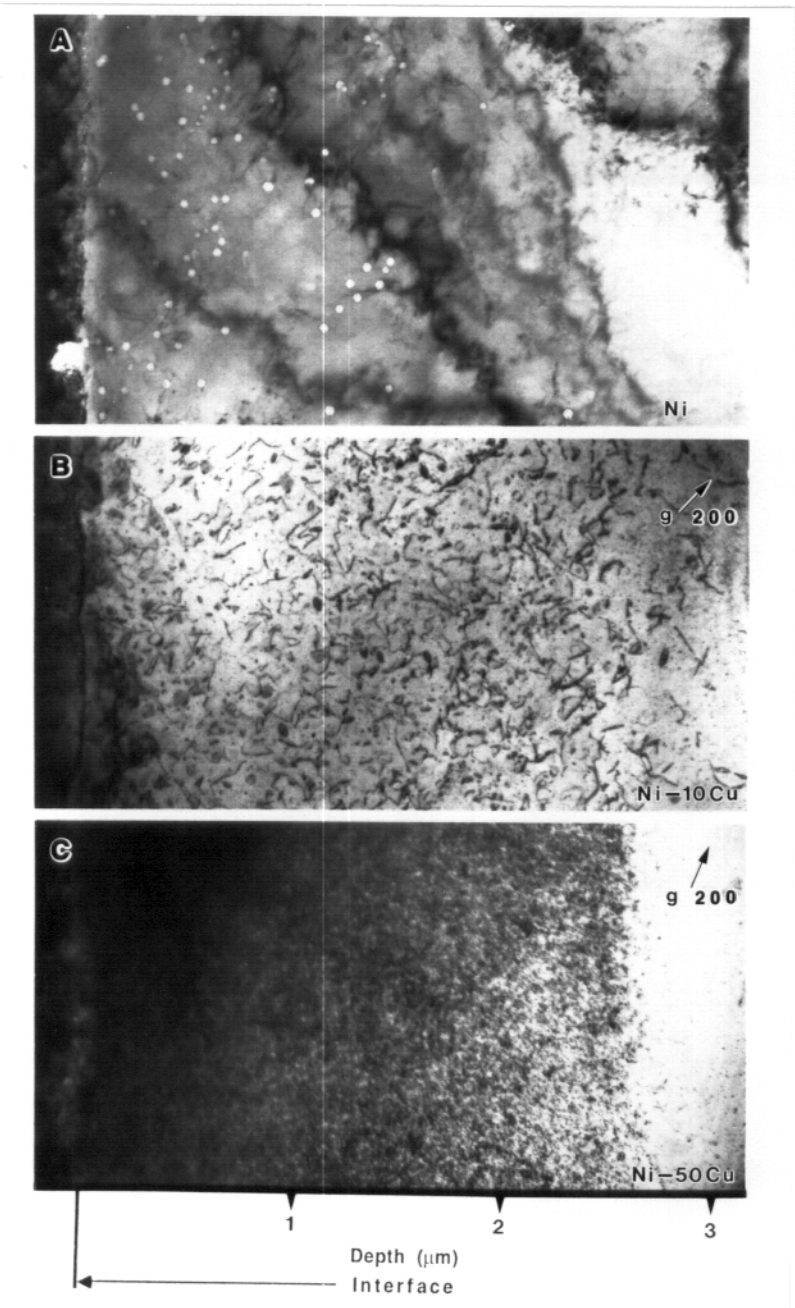

Figure 5.23 Entire ion damage region of 14 MeV Ni ion irradiated samples with 50 appm helium pre-injection. (A) Ni (No. 08, 3 dpa at 1 μm, 500 °C); (B) Ni-10Cu (No. 15, 5 dpa at 1μm, 485 °C) and (C) Ni-50Cu (No. 21, 5 dpa at 1 μm, 425 °C).

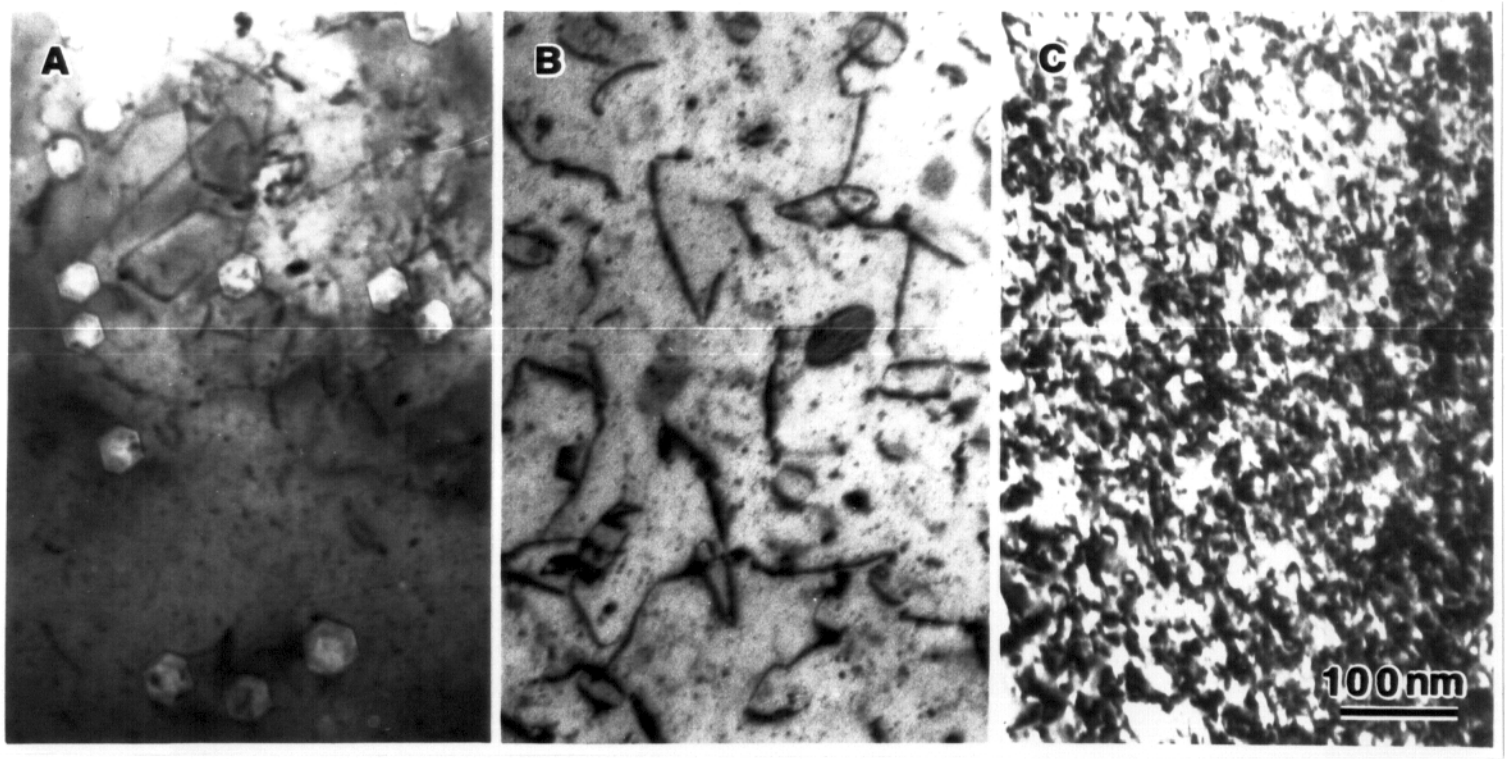

Figure 5.24 TEM micrographs showing the comparison of major defect clusters in 14 MeV Ni ion irradiated (A) pure Ni (No. 08, 3 dpa, 500 °C), (B) Ni-10Cu (No. 15, 5 dpa, 485 °C) and (C) Ni-50Cu (No. 21, 5 dpa, 425 °C), all with 50 appm He pre-injection. The micrographs were taken from the region of 0.6-1 μm below the irradiated surface (g=[200]).

the first 1.5 μm of the nickel specimen shown in Figure 5.23 (A) is due to the presence of pre-injected helium in that region.

In the two irradiated Ni-Cu alloy samples, as shown in 5.23 (B) and (C), dislocation loops constitute the major defect cluster. The loop density increased dramatically with the copper content, while the loop size decreased concomitantly. Again, perfect loops on {111} planes with $\vec{b}$ = a/2 <110> and Frank loops enclosing a stacking fault with $\vec{b}$ = a/3 <111> were both identified in Ni-10Cu, but only perfect loops have been identified in Ni-50Cu. The density and size distribution of the loops are almost the same as the result for the irradiated Ni-Cu alloys with 5 MeV oxygen ion pre-injection shown in the previous section. Since the 5 MeV oxygen was implanted deeper into the samples, the similarity in the loop distribution means that the pre-injected helium did not have the power to alter the defect characteristics in the alloys under the experimental conditions. However, when dislocations are tilted out of contrast, e.g. the specimen is tilted away from the strong diffracting orientation, small bubbles with diameters less than 5 nm are observed at the helium injected depth in both Ni-10Cu and Ni-50Cu as shown in Figure 5.25. Figure 5.26 shows both under-focus and over-focus images of the bubbles observed in the helium injected region of irradiated Ni-10Cu. The density of the helium bubbles in Ni-50Cu is an order of magnitude higher than that in Ni-10Cu, and the bubble size is larger in the latter. When comparing the size of the bubbles in the Ni-Cu alloys with the size of

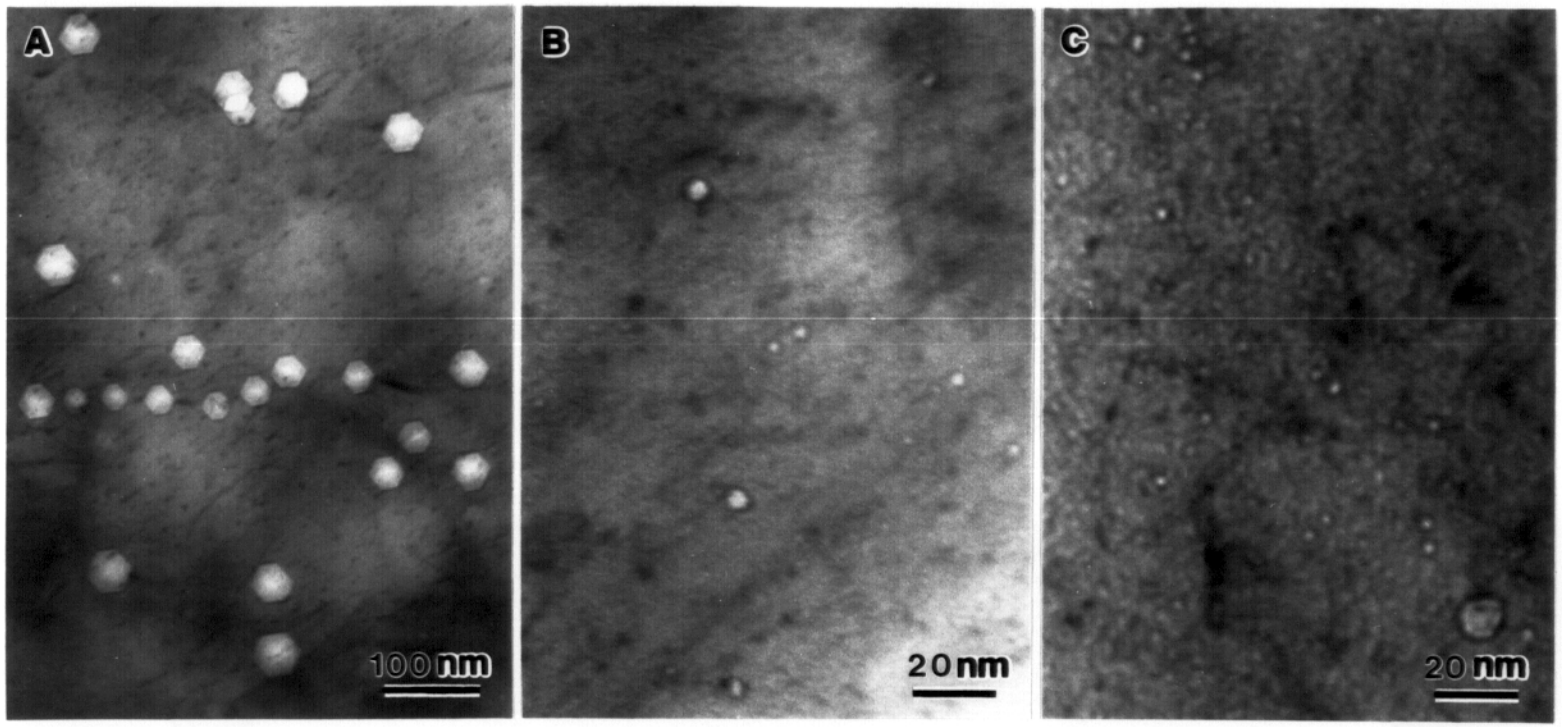

Figure 5.25 Low contrast TEM micrographs showing the comparison of the effect of 50 appm pre-injected He in 14 MeV Ni ion irradiated (A) pure Ni (No. 08, 3 dpa, 500 °C), (B) Ni-10Cu (No. 15, 5 dpa, 485 °C) and (C) Ni-50Cu (No. 21, 5 dpa, 425 °C). The micrographs were taken from the region of 0.6-1 μm below the irradiated surface.

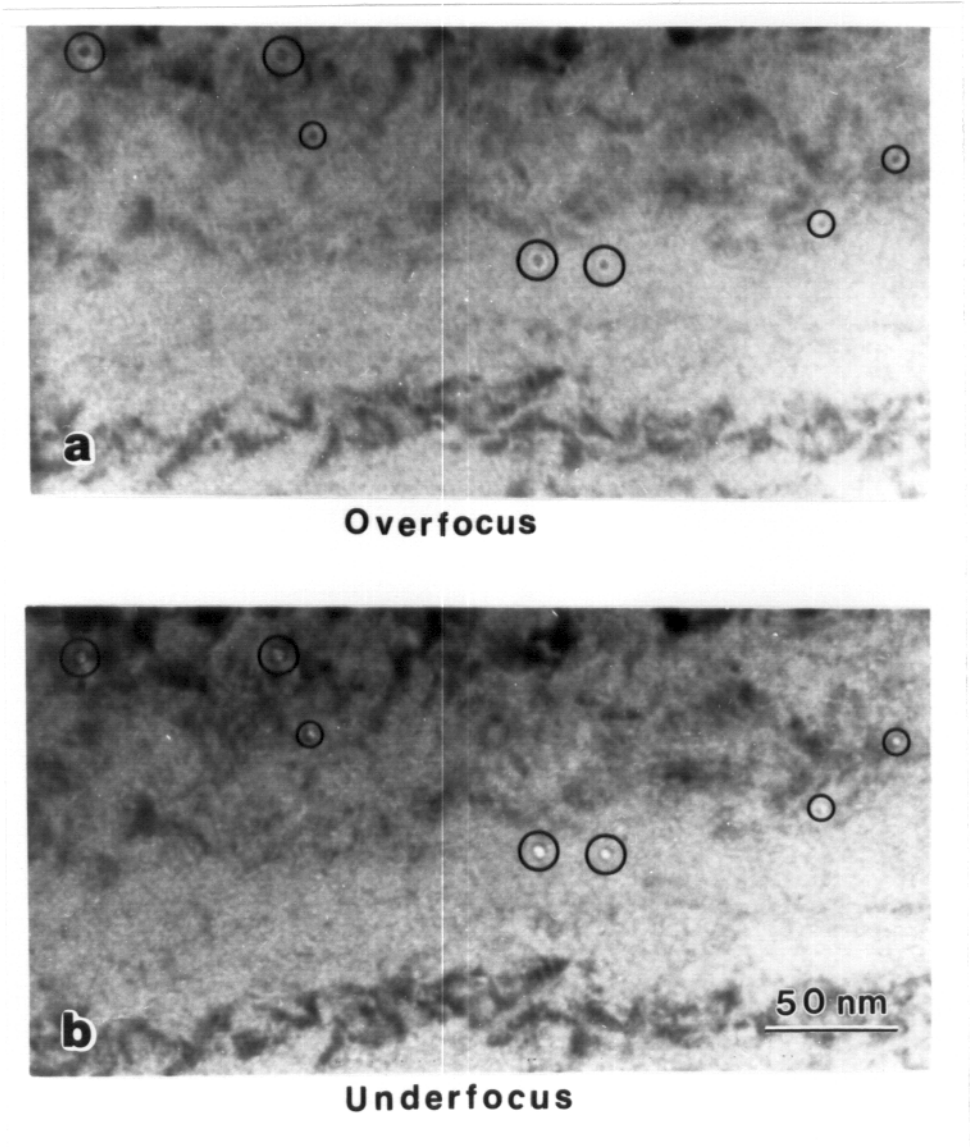

Figure 5.26 TEM image of helium bubbles formed in 50 appm helium pre-injected Ni-10Cu after 14 MeV Ni ion irradiation (No. 15, 5 dpa, 485 °C).

voids in pure nickel as shown in Figure 5.25 (A), note that Figure 5.25 (B) and 5.25 (C) have a much higher magnification.

Table 5.3 summarizes the major defect characteristics in the helium injected region of the three specimens compared in this section. The volume swelling in the helium pre-injected region of the nickel specimen is about $3.5x10^{-3}$, while the swelling due to the formation of small bubbles in the Ni-Cu alloys is estimated to be at least one order of magnitude lower, even though the Ni-Cu samples were irradiated to a higher displacement damage level. Based on the data tabulated in table 5.3, the residual vacancy/helium ratio in the voids or bubbles has been estimated to be 70 for the pure Ni sample, 1.5 for the Ni-10Cu sample and 3.5 for the Ni-50Cu sample.

Table 5.3 Major defect characteristics* in 50 appm helium pre-injected Ni and Ni-Cu alloys following 14 MeV Ni ion irradiation

Sample No.† (Material)	Dose at 1 μm (dpa)	Irradiation Temperature (°C)	Dislocation Loop density (m^{-3})	Dislocation Loop average size (nm)	Helium Bubble (or Void) density (m^{-3})	Helium Bubble (or Void) average size (nm)
08 (Ni)	3	500	$1x10^{20}$	15.3	$1.5x10^{20}$	35 (void)
15 (Ni-10Cu)	5	485	$1x10^{21}$	27.5	$3.0x10^{21}$	3.5
21 (Ni-50Cu)	5	425	$7x10^{21}$	6.5	$3.0x10^{22}$	2.3

* Defect parameters in the table refer to the region about 1 μm below the irradiated surface

† See Table 4.1 for the pre-irradiation and irradiation conditions of the samples

D. Effect of Small Amount of Implanted Copper on Void Formation in 14 MeV Copper Ion Irradiated Nickel

It has been shown in the previous sections that the copper content in Ni-Cu alloys plays an important role on altering the structure of radiation-induced defect clusters. To study the effect of a small amount of implanted copper on void formation, two degassed nickel specimens (Nos. 11 and 12), were irradiated with either 14 MeV nickel ions or 14 MeV copper ions respectively at 500 °C. Since copper and nickel have slightly different energy deposition characteristics, different ion fluences are required to reach the same displacement damage level. The sample irradiated with nickel ions (No. 11) received a total dose of 6.5×10^{20} ions/m^2, while the sample irradiated with 14 MeV copper ions received a total dose of 6×10^{20} ions/m^2, so that the damage level at 1 μm depth equals 25 dpa for both samples according to the Monte Carlo calculations performed using the TAMIX code.

The low contrast cross-section TEM micrographs showing void distributions in the nickel-ion-irradiated and copper-ion-irradiated nickel specimens are shown in Figure 5.27 and 5.28 respectively. Figure 5.29 is a cross-section TEM micrograph of the copper-ion-irradiated specimen taken under a strong diffraction condition ($g = [\bar{1}1\bar{1}]$). While voids were the only significant defect clusters observed in the nickel-ion-irradiated specimen, and they formed throughout the entire damage range (as shown in Figure 5.27), both voids and a high density of dislocation loops were seen in the copper ion irradiated specimen (as

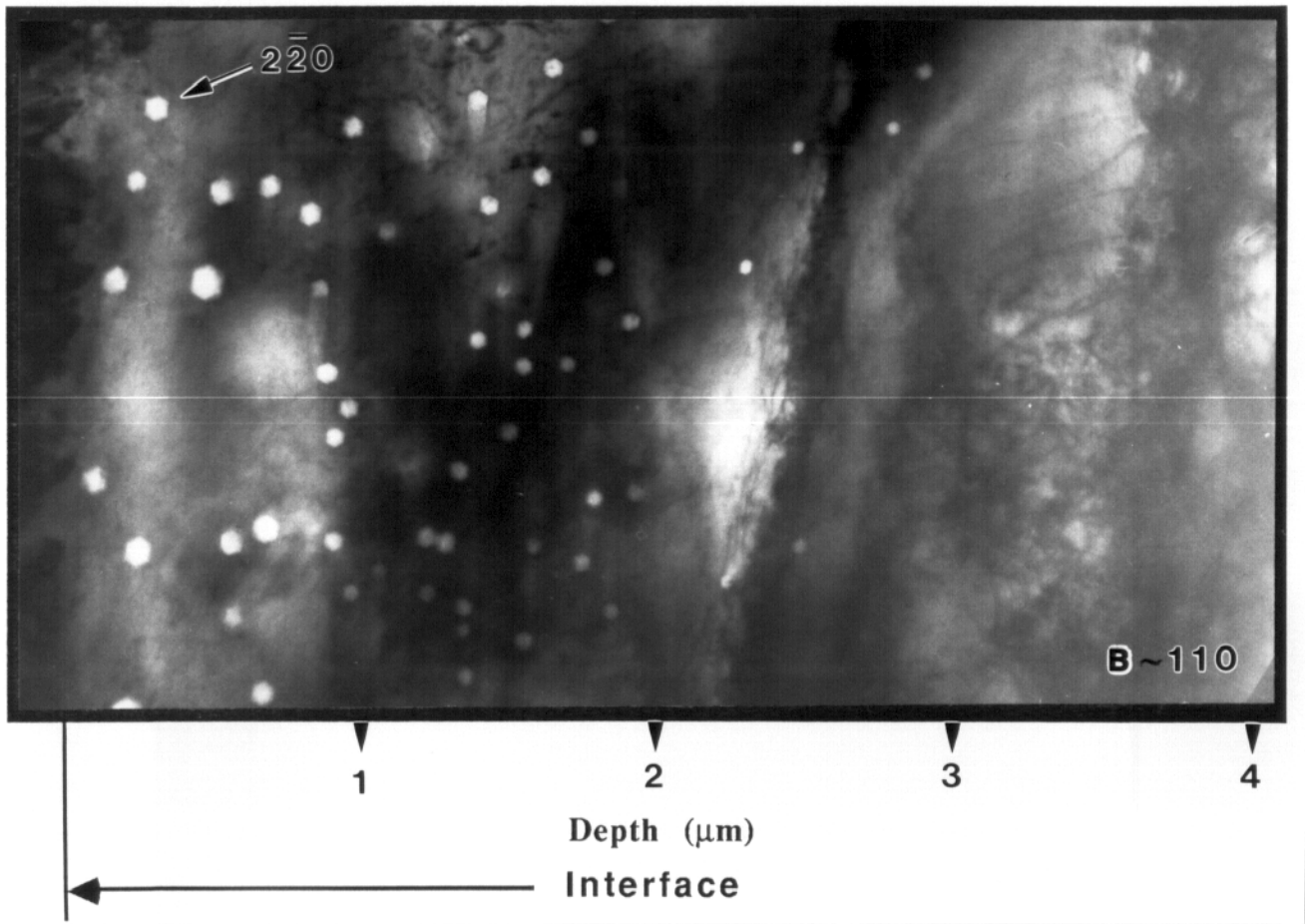

Figure 5.27 Cross-section TEM micrograph showing void distribution in 14 MeV Ni ion irradiated Ni (No. 11, 75 appm oxygen, 25 dpa at 1 μm, 500 °C).

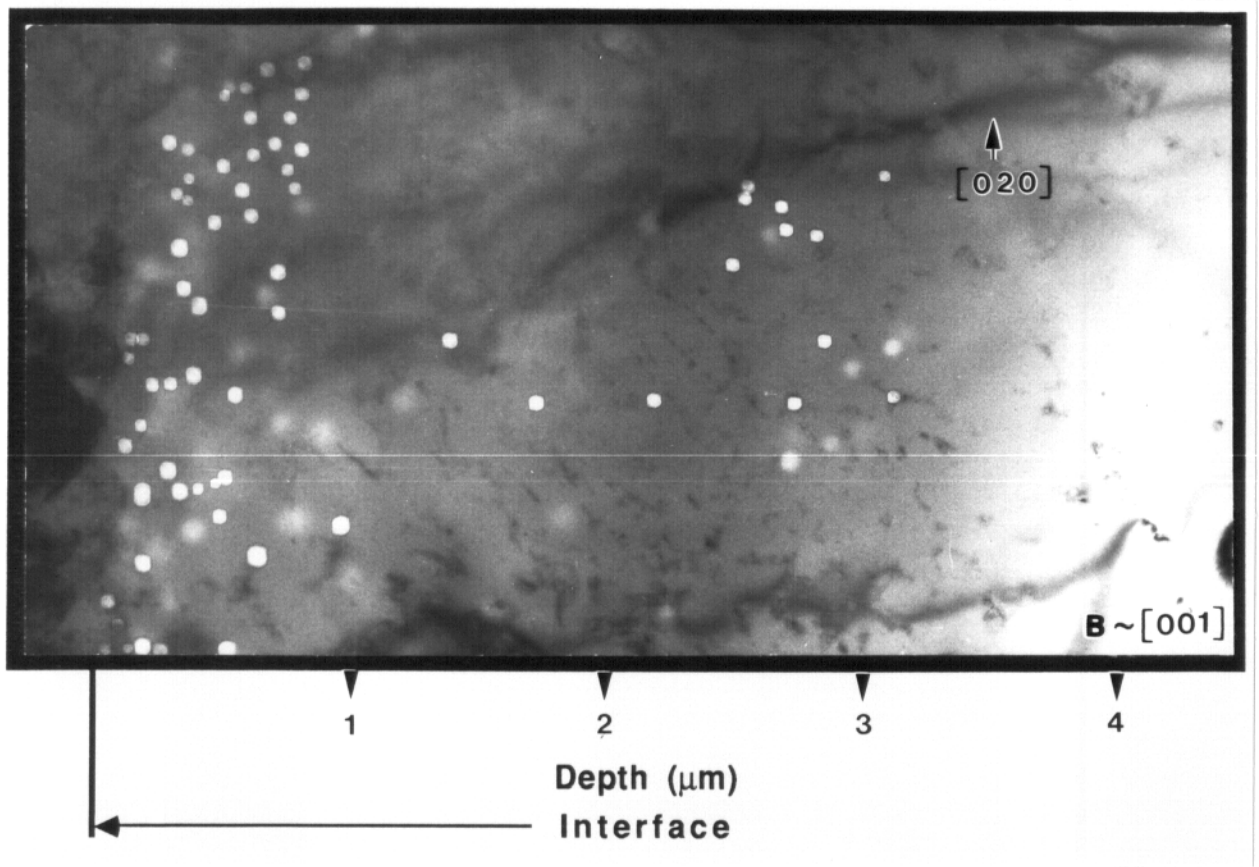

Figure 5.28 Cross-section TEM micrograph showing void distribution in 14 MeV Cu ion irradiated Ni (No. 12, 75 appm oxygen, 25 dpa at 1 μm, 500 °C).

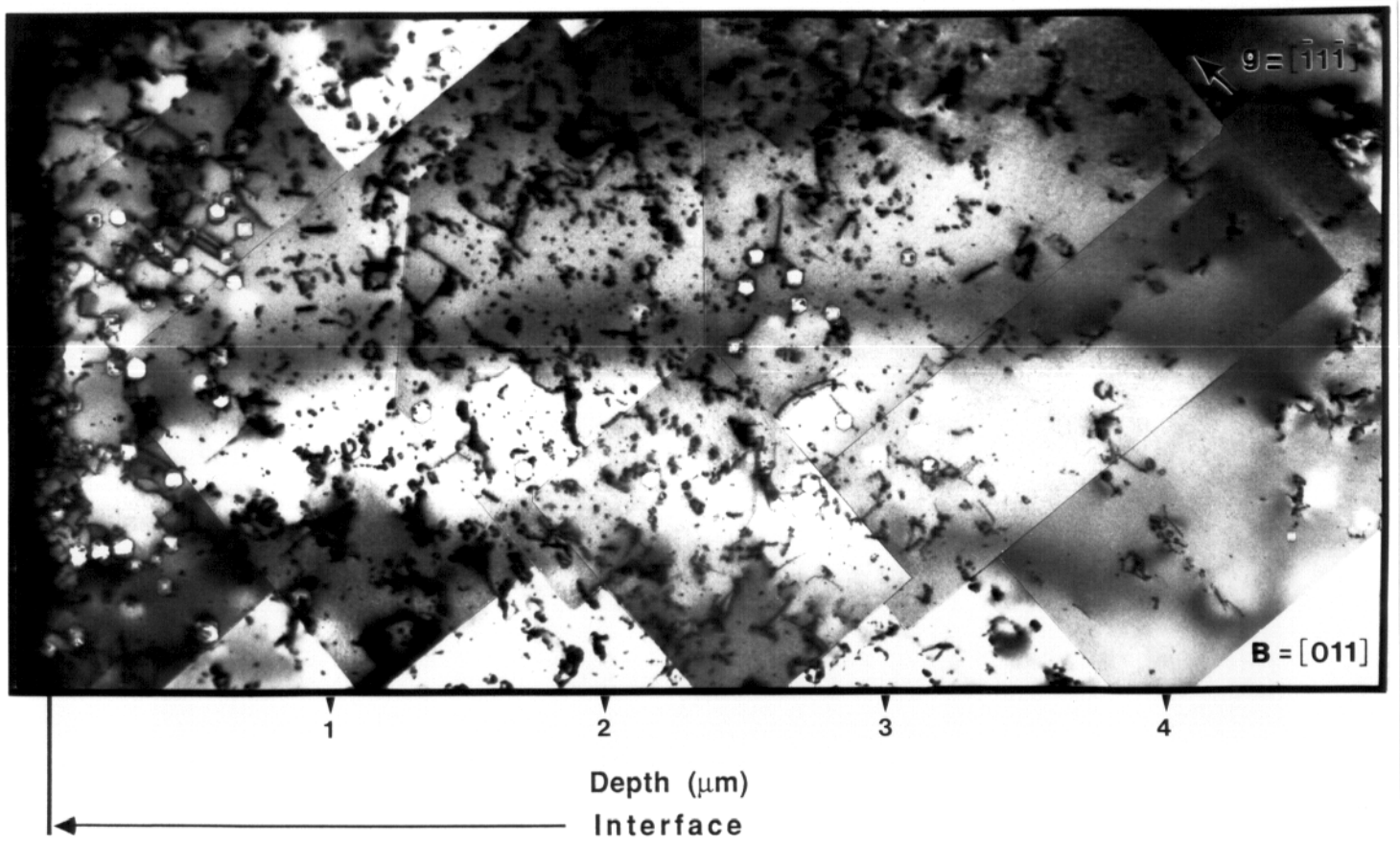

Figure 5.29 Cross-section TEM micrograph showing both void and dislocation loop distribution in 14 MeV Cu ion irradiated Ni (No. 12, 75 appm oxygen, 25 dpa at 1 μm, 500 °C).

shown in Figures 5.28 and 5.29). The voids in the latter were mainly located in a region near the surface and in another region that was about 2.75-3 μm deep from the original irradiated surface (remember that the actual distance from the original surface is the distance marked in the cross-section micrographs plus ~ 0.3 μm). The dislocation loops observed in the copper-ion-irradiated specimen are mostly perfect loops with the Burgers vector of $\vec{b}$ = a/2 <110>. Figure 5.30 shows the typical dislocation loop images at various depths in the-copper-ion irradiated sample with higher magnification. At both the surface and at the end of damage range, some larger loops (~ 50 nm in diameter) were observed. In between, a high density of smaller loops (≤ 10 nm in diameter) was found. The density and average diameter of the voids and swelling in both samples, as well as the dislocation loop density in the copper ion irradiated specimen, have been plotted against the depth from the irradiated surface, and they are shown in Figures 5.31 and 5.32 respectively. From Figure 5.31, it is very clear that there is a void suppression region, which extends from a depth of ~ 1 μm to a depth of ~ 3 μm, in the copper-ion-irradiated specimen. Also in that region, a high density of dislocation loops was formed, which is shown in Figure 5.32. The void density and swelling peak at the depth of ~ 3 μm for the same sample is believed to be the correspondent of the damage peak, where the point defect production rate has a sharp increase. It may be noticed that compared to the calculated peak damage location, which is about 2.2 μm below the surface of irradiation according to a TAMIX calculation for 14

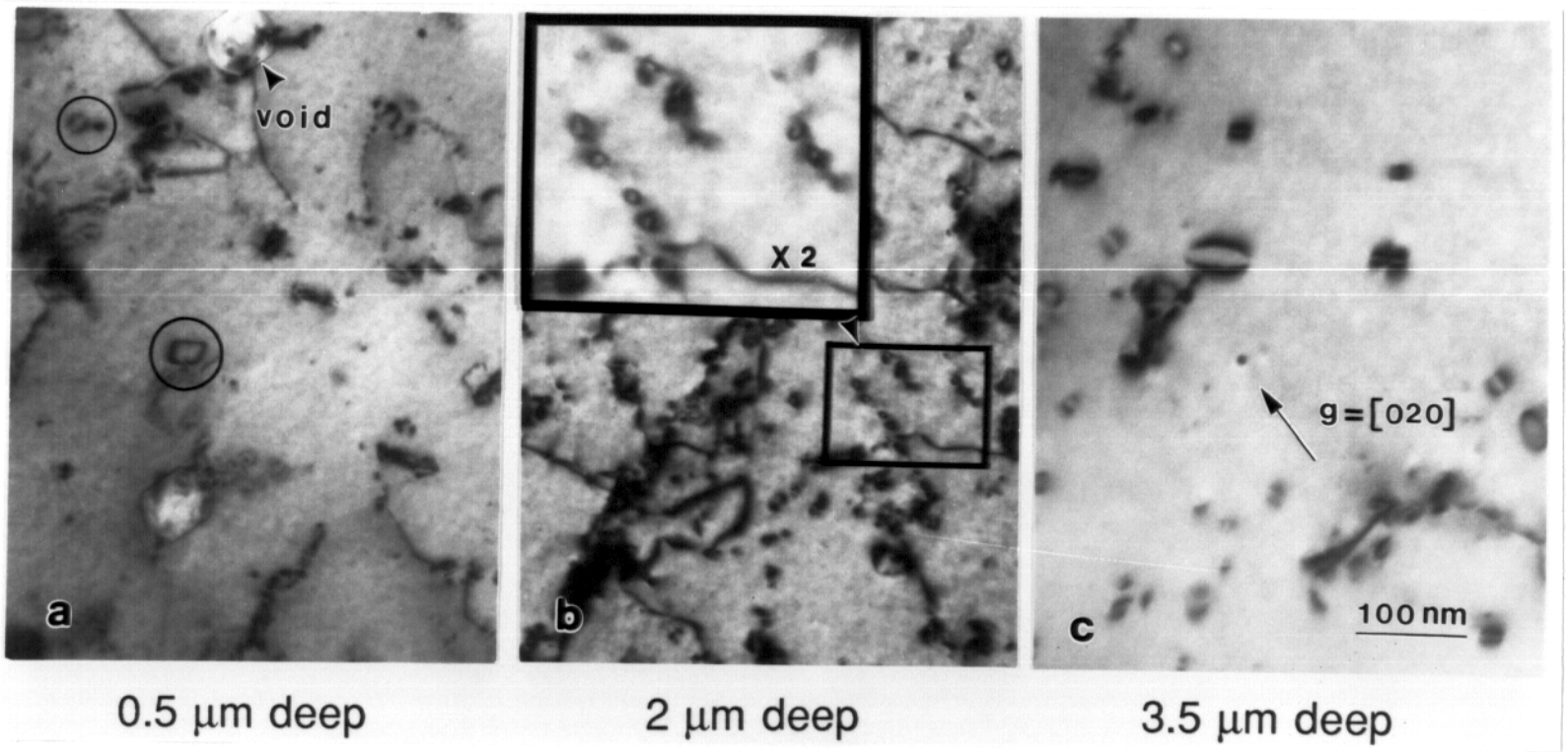

Figure 5.30 Dislocation loop images taken from various depths in the 14 MeV Cu ion irradiated Ni (No.12, 75 appm oxygen, 25 dpa at 1 μm, 500 °C). (a) 0.5 μm deep; (b) 2 μm deep; (c) 3.5 μm deep.

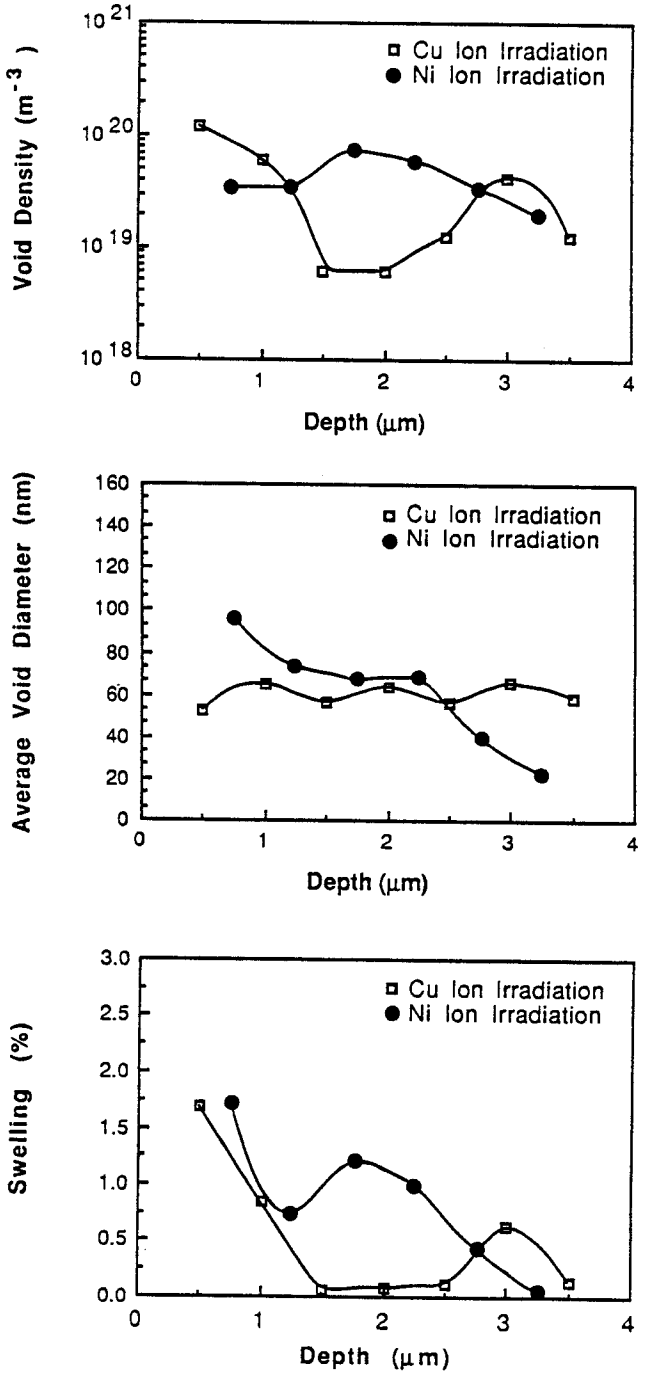

Figure 5.31 Void parameters and swelling versus depth in 14 MeV Cu and Ni ion irradiated Ni (No. 11 and 12, 75 appm oxygen, 25 dpa at 1 μm, 500 °C).

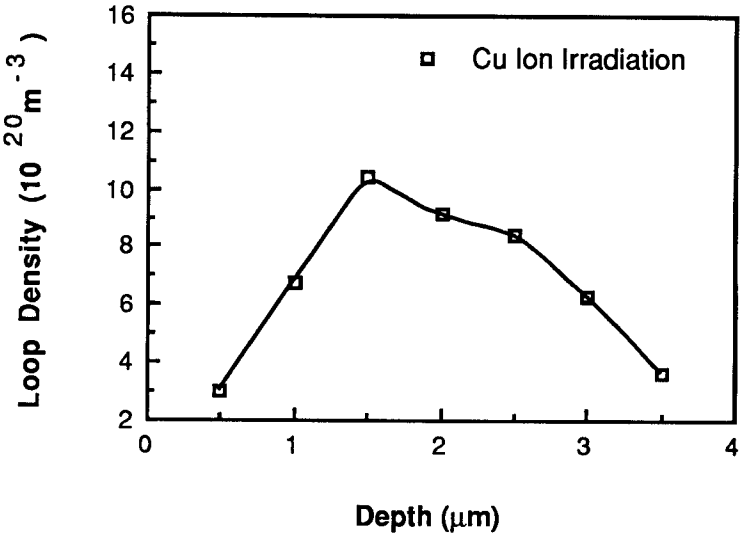

Figure 5.32 Dislocation density versus depth in 14 MeV Cu ion irradiated pure Ni (No. 12, 75 appm oxygen, 25 dpa at 1 μm, 500 °C).

MeV copper ion irradiation on nickel, the observed damage peak location is much deeper. Similar discrepancies have been noted for a long time in the literature[1,5,6], and have also been seen in the other specimens irradiated to high doses in this study. This discrepancy will be discussed in the next chapter.

In addition to the TEM analysis, Analytical Electron Microscopy (AEM) analysis has been conducted on sample No. 12 to measure the implanted copper concentration profile. The AEM analysis was performed in STEM mode of the 200 CX microscope with a beam spot size of ≤ 20 nm using a TN-2000 energy dispersive X-ray spectroscopy (EDXS)

system. During the AEM analysis, a series of points lying on a line which is normal to the interface between the plated and irradiated nickel in the cross-section TEM disc, i.e. parallel to the direction of incident ions and covering the entire damage range, was analyzed. To prevent the interference of copper signals from the brass sample holder, a graphite holder was used during the AEM study; this appeared to be very effective. Because the implanted copper content is very low and the copper K_α (8.04 keV) and the nickel K_β (8.26 keV) are close to each other, great care must be taken to distinguish copper in the AEM compositional study. To detect the small copper K_α signal which may be hidden beneath the nickel K_β peak, two regions of interest were selected, one covering the energy range between 7.9 and 8.4 keV (both nickel K_β and copper K_α are included) and the other only covers nickel K_α peak as shown in Figure 5.33. The counting on each point was continued until a constant height (4096 counts) for the nickel K_α peak had been reached. The ratio of the two peak integrals (copper K_α + nickel K_β divided by nickel K_α) was then calculated and plotted against the depth. Finally, the curve was normalized to copper concentration versus depth by fitting the total number of implanted copper ions, which is known from the beam current during irradiation, into the area underneath the peak integral ratio curve. That normalized copper concentration versus depth curve is shown in Figure 5.34 along with the copper distribution curve calculated by the Monte Carlo method for the irradiation fluence. To determine the height of the error bar, the measurement at several depths was repeated

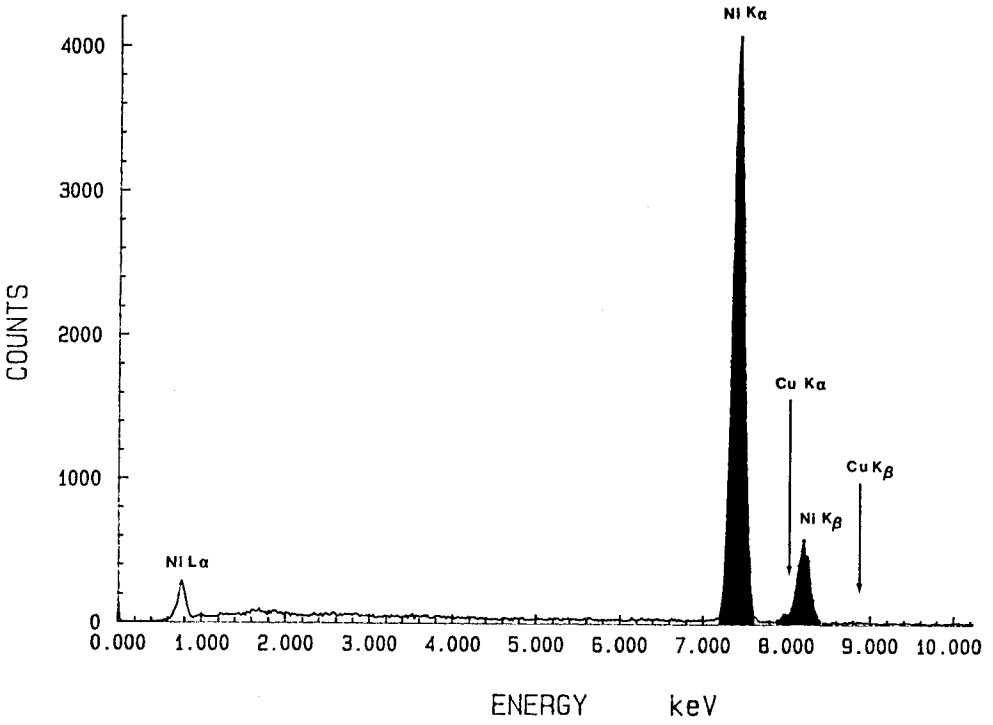

Figure 5.33 EDX spectrum recorded from the Cu ion implanted region of an irradiated Ni specimen (No. 12) with the two regions of interest indicated.

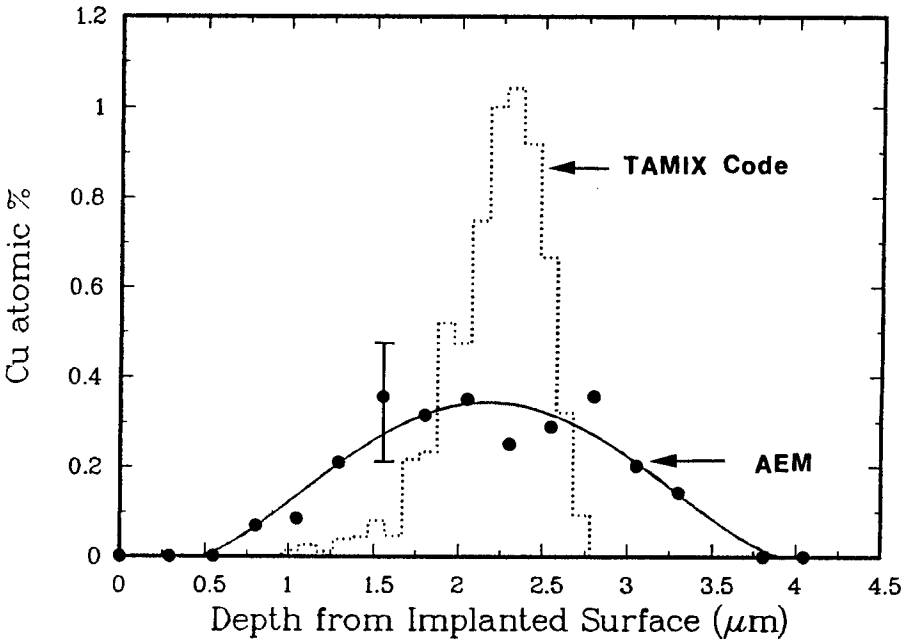

Figure 5.34 Comparison of measured and calculated Cu content profile for 14 MeV Cu ion implanted Ni (No. 12, 6×10^{20} ions/m^2, 500 °C).

three times. Although the scattering of the data is relatively large, the increase of copper signal in the region of 1.5 to 2.75 μm below the implanted surface is distinct. Comparing Figure 5.34 with Figures 5.31 and 5.32, it is quite clear that the implanted copper suppressed void formation and promoted dislocation loop formation. One can also see a relatively large discrepancy between the calculated and measured copper range and concentration in Figure 5.34. The measured values are lower and cover a wider region. This is partly due to radiation-enhanced diffusion, because the diffusional spreading was not considered in the Monte Carlo calculation. There is evidence showing that the diffusion coefficient of copper in Ni-Cu alloy could be increased by two orders of magnitude by ion bombardment below ~ 550 °C[7]. In addition to the normal vacancy diffusion mechanism, one should note that the copper ions are the injected interstitials in the sample. The diffusional spreading of migrating interstitials before they annihilate with the vacancies could be very significant. A recent TAMIX calculation by S. Han, which included the diffusional spreading consideration, showed a result very close with that of the AEM measurements[8]. Another possible reason for the measured large copper spreading is due to the beam broadening during AEM measurements. The area analyzed has a thickness of ~ 140 nm. A primary interaction volume with a diameter ≤ 200 nm could be created by the incident 200 keV electrons. Nevertheless, the measured profile of dislocation loop density matched quite well with the measured copper profile in this study.

References for Chapter 5

1. D.B. Bullen, Ph.D. Thesis, University of Wisconsin-Madison (1984).

2. J.W. Edington, Monographs in Practical Electron Microscopy in Materials Science, Vol. 3, Interpretation of Transmission Electron Micrographs, Philips, Eindhoven (1974), p. 26.

3. K.-H. Leister, Ph.D. Thesis, Kernforschungszentrum Karlsruhe (1983).

4. B. Badger, Jr., D.L. Plumton, S.J. Zinkle, R.L. Sindelar, G.L. Kulcinski, R.A. Dodd and W.G. Wolfer, ASTM STP 870 (1985) p. 297.

5. J.B. Whitley, Ph.D. Thesis, University of Wisconsin-Madison (1978).

6. R.L. Sindelar, Ph.D. Thesis, University of Wisconsin-Madison (1985).

7. N.Q. Lam, H.A. Hoff, H. Wiedersich and L.E. Rehn, Surface Science, 149 (1985) 517.

8. S. Han, Ph.D. Thesis, University of Wisconsin-Madison (1988).

CHAPTER 6
DISCUSSION

A. Gas Effects on Void Formation

The effect of both helium and oxygen on void formation has been clearly demonstrated by the results shown in Chapter 5. Although, theoretically, the mechanisms of void stabilization by helium and by oxygen are quite different (cavity pressurization by helium suppresses thermal vacancy emission[1]; surface energy reduction by oxygen makes voids energetically more stable[2]), their observed ultimate effects are roughly the same. Higher content of either gas gives a higher void density but smaller void size in the irradiated pure nickel. Furthermore, the void density observed in this study varies with the sum of the two gas concentrations which existed in the sample, provided other irradiation conditions were kept constant. This indicates either that large fractions of the two kinds of gas work separately on different void embryos when they coexist in the irradiated material, or that when they work on the same void embryo, the number of gas atoms of each kind required for the embryo to grow is reduced compared to the case when only one kind of gas is present. However, accurate quantitative analysis on this topic is impossible from the results of this study, because of the uncertainty in knowing the fraction of residual oxygen which was tied up at grain boundaries, dislocations or other binding sites, and which therefore did not participate in void nucleation.

Comparing the data presented in Figure 5.7 (a), it is interesting to notice that reducing the residual oxygen content from 180 appm to 75 appm (a 58% reduction in oxygen content) results in void density drop by almost two orders of magnitude (from ~ 10^{21} m^{-3} to 10^{19} m^{-3}). This means that the oxygen which was removed in the hydrogen reduction degassing treatment (see Chapter 4) seems to be much more effective in promoting void nucleation than the oxygen retained after the treatment. Similarly, pre-injection of only 75 appm oxygen into a sample (No. 10) which already contains 75 appm residual oxygen (a 100% increase) increased void density also by about two orders of magnitude (as shown in Figure 5.9 and Table 5.1). This indicates that the pre-injected oxygen is more effective than the residual oxygen in the outgassed nickel in promoting void nucleation. The above observations could be explained as follows. The residual oxygen which was eventually removed by the hydrogen reduction treatment and the pre-injected oxygen are free in the matrix, and once irradiation starts, it is able to partition to void embryo surfaces. In contrast, a large fraction of the 75 appm residual oxygen, which remained in the material after the degassing treatment, is probably tied up at grain boundaries, dislocations, internal oxides, or other binding sites, being unable to partition to void embryos during irradiation. Although bombarding or knock-on atoms may free some of these bound atoms, it is not expected that the density of these liberated oxygen atoms will be high enough to stabilize many embryos. The chance of such an event is greater near large oxide particles as shown in Figure 5.2. In

other words, although the degassed nickel foil used in this study still contained about 75 appm residual oxygen, the free oxygen content in the foil, which is important for void nucleation, might be very low. The trend of void density change with the oxygen content observed in this study supports the recent theoretical model[2,3] which predicts that oxygen can stabilize voids by reducing the metal surface energy, and that gas is necessary for voids to form in nickel.

B. Void Suppression Mechanism for Irradiated Ni-Cu Alloys

The results on the irradiated Ni-Cu alloys of this study support the previous findings that voids are increasingly more difficult to form with increasing copper content for the Ni-based Ni-Cu alloys[4, 5]. The reason for the void suppression is of great interest.

From energetic considerations[6,7], a system which has a lower stacking fault energy favors the formation of faulted dislocation loops or stacking fault tetrahedra rather than voids. However, the possibility of void suppression in Ni-Cu alloys due to a stacking fault energy effect has been excluded[8], because the stacking fault energy is 50% higher in Ni-50Cu as compared to pure copper[9] while voids are easy to form in irradiated pure copper as long as a certain concentration of gas atoms are present (as shown in Chapter 3). Since the effective migration energies of point defects in the Ni-Cu alloys have been determined to change monotonically and continuously between values for pure nickel and pure copper[10], the void suppression in the alloys due to differences

in diffusion between the alloys and the pure metals has also been excluded[8]. As mentioned in Chapter 3, the mechanism of point defect trapping by single solute atoms in the solution due to the size difference, which was proposed by Brimhall and Kissinger[8], is hardly likely to be responsible because the size difference between a nickel atom and a copper atom is too small and the explanation apparently breaks down for the Ni-50Cu alloy. Mazey and Menzinger[4], in 1973, proposed the possibility of trapping vacancies and interstitials at the boundaries of fine-scaled clusters having compositions different from the matrix. Their explanation seems more plausible, but they did not give further elaboration of the mechanism. The extended discussion on this mechanism based on the more recent experimental results, including the results from this study, is given as follows.

In a binary solid solution composed of elements A and B, local clustering is defined in terms of a reduced number of unlike nearest neighbors, or A-B pairs compared with the number in a random solution[11]. The essential condition for that to happen is that similar atoms must attract each other more than dissimilar atoms in order to lower the free energy upon clustering, although the interaction is not strong enough for precipitation. In terms of interaction energies between pairs of atoms of the two atomic species, this condition can be expressed as $E_{AB} > 1/2\ (E_{AA}+E_{BB})$[11,12]. The positive value of the heat of mixing of the Ni-Cu system[13] suggests that the above condition is met[14]. When clustering occurs, the heat of mixing (ΔH_m) is reduced, which in turn

reduces the free energy of the system. On the other hand, upon clustering the mixing entropy (ΔS_m), i.e. the number of ways of arranging atoms in the lattice, is decreased and thus increases the free energy of the system. Since $\Delta G = \Delta H - T\Delta S$, the entropy term will be less important at lower temperatures. Eventually, an optimum value of *short-range order* (here it means local clustering) will be attained, reflecting a balance between ΔH_m and the $T\Delta S_m$ contributions. That value is measured by the short range order parameter, α_1[14], and the parameter is defined as follows:

$$\alpha_1 = 1 - \frac{P_{(AB)}}{ZN_0X_AX_B} , \qquad (6.1)$$

where $P_{(AB)}$ is the probability of finding an A-B pair in the solid solution of A and B, Z is the coordination number, N_0 is Avogadro's constant, and X_A or X_B is the atomic fraction of component A or B. In a complete random solution, the probability of finding an A-B pair equals $ZN_0X_AX_B$, thus $\alpha_1 = 0$. For short-range order in which there is a preference for A-B pairs, $\alpha_1 < 0$, and for clustering $\alpha_1 > 0$. Figure 6.1 illustrates the three different arrangements with their corresponding values of α_1 in two dimensions.

More information has now become available in the literature which provides strong evidence suggesting that clustering takes place in Ni-Cu alloys. Vrijen and Radelaar[15], in 1978, systematically studied the short range order parameters for the Ni-Cu system using diffuse neutron scattering. Their results from the alloys quenched at 450°C,

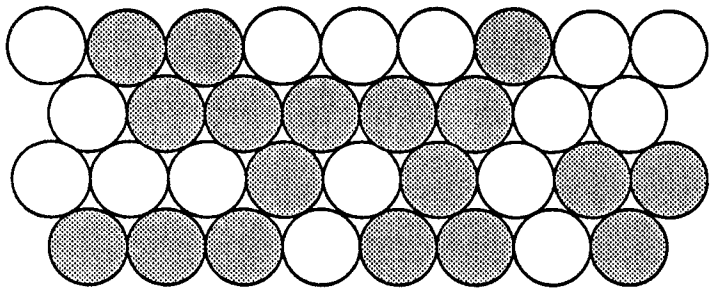

Average Number of Unlike Neighbors = 3

$$\alpha_1 = 0$$

Random Solution

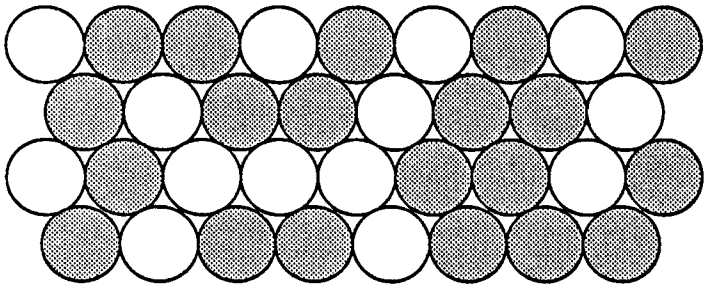

Average Number of Unlike Neighbors = 4

$$\alpha_1 = -\frac{1}{3}$$

Short Range Order

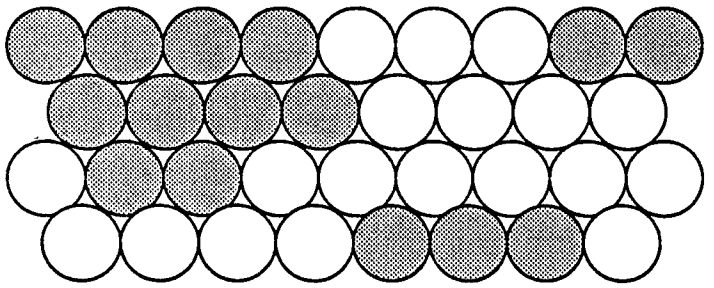

Average Number of Unlike Neighbors = 2

$$\alpha_1 = +\frac{1}{3}$$

Clustering

Figure 6.1 Illustration of local atom arrangement in a binary alloy with various short range order parameters in two dimensions

along with some of the measurements made by Aldred et al. in 1973[16] and Medina et al. in 1977[17], are plotted in Figure 6.2. The data indicated not only that local clustering does occur in the Ni-Cu alloys but also that the tendency for clustering is higher in a more concentrated Ni-Cu solid solution than in a dilute solution.

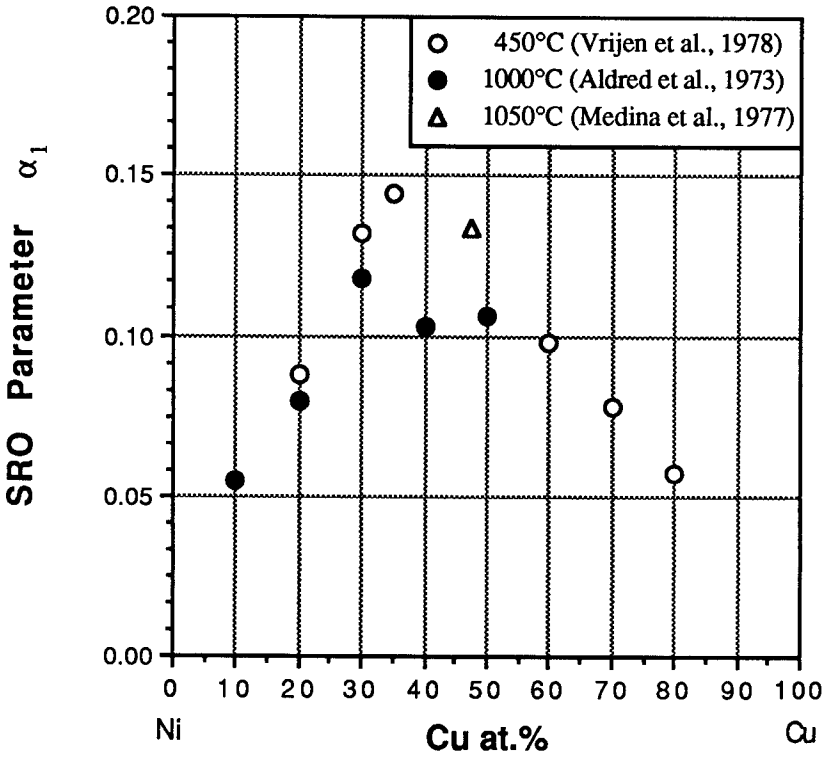

Figure 6.2 Short range order parameter α_1 for Ni-Cu alloys measured by Vrijen et al.[15], Aldred et al.[16] and Medina et al.[17] with diffuse neutron scattering after quenching from various temperatures.

The boundaries of the clusters might trap vacancies and gas atoms to reduce the high binding energy as well as the strain energy. These traps can also operate as nucleation sites for vacancy clusters. When a high density of this kind of trap is present, the arrival rate of irradiation-produced vacancies at each site will be low, so the small vacancy clusters will not grow fast enough to reach the critical size of the void embryo before collapsing into dislocation loops. This inhibits void formation in the alloys. It is apparent that Ni-50Cu will contain more fine-scaled clusters of like atoms than Ni-10Cu; in other words, more vacancy traps are present in Ni-50Cu than in Ni-10Cu. Therefore, the major trend in defect cluster formation with increasing copper content observed in this study, i.e. higher resistance to void formation and higher density of dislocation loops in the more concentrated Ni-Cu alloys (as shown in Figure 6.3), can be explained.

The formation of helium bubbles in the helium pre-injected Ni-Cu alloys is expected, because there are theoretical and experimental indications that helium tends to undergo spontaneous precipitation when implanted into metals, including the void resistant Ni-Cu alloys[18]. The interesting point of the results of this study is that the resistance to void swelling of the Ni-Cu alloys is maintained even in the presence of small helium bubbles during irradiation. Although a simple calculation based on the ideal gas law and the assumption of equilibrium bubble pressure indicated that some vacancies must have been trapped in those bubbles to achieve the bubble volume observed in this study,

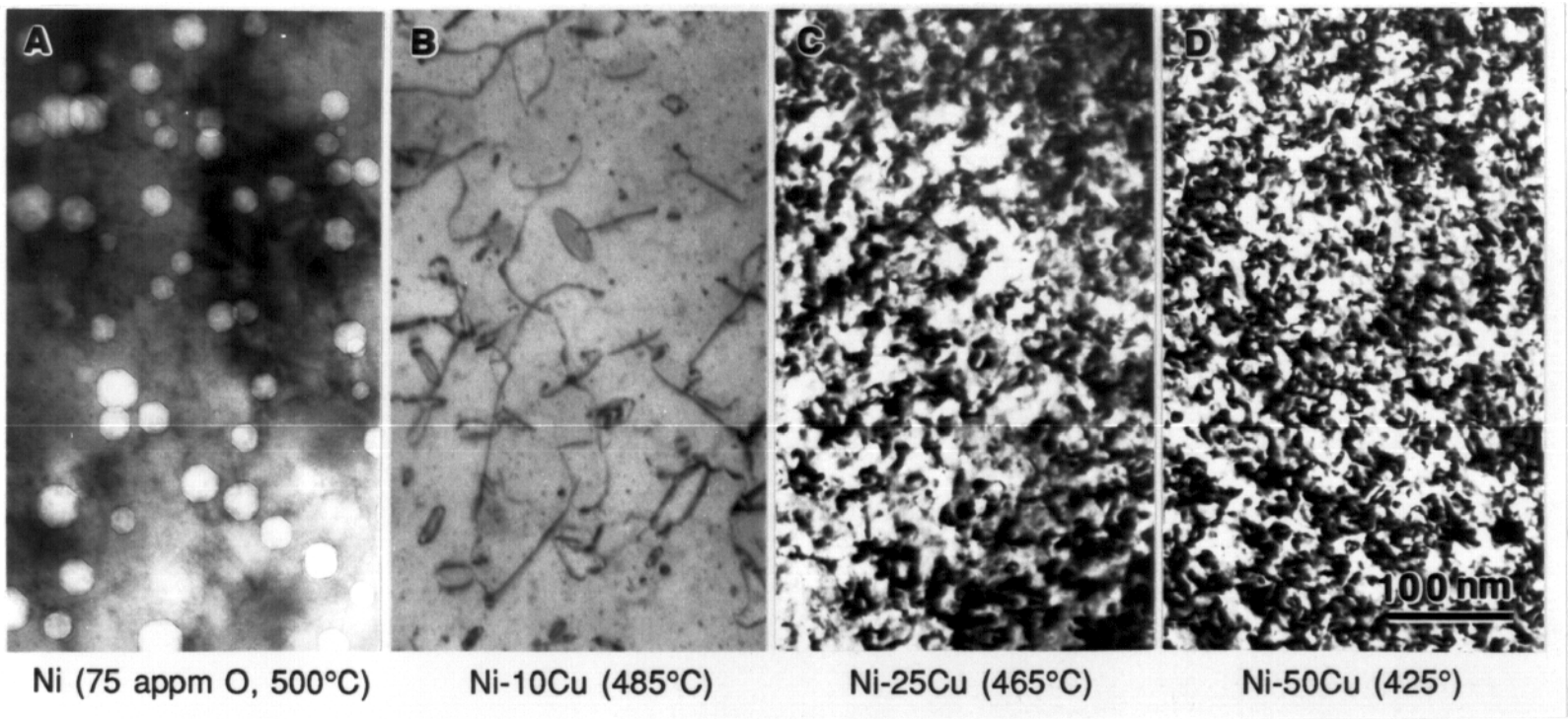

Figure 6.3 Comparison of major defect clusters observed in 14 MeV Ni ion irradiated (A) pure Ni, (B) Ni-10Cu, (C) Ni-25Cu and (D) Ni-50Cu (irradiated to 5 dpa at the same homologous temperature of 0.45 T_m. The pure Ni sample contains 75 appm pre-injected oxygen, the Ni-Cu samples contain 100 appm pre-injected oxygen).

nevertheless, the majority of the excess vacancies which survived recombination apparently did not go to the bubbles to cause growth into larger voids. Instead, they form dislocation loops just as if there is no helium available to help void nucleation. Obviously, that is because the presence of abundant vacancy traps makes each helium bubble unable to draw enough vacancies to grow into larger voids. The smaller size and higher density of bubbles in the irradiated Ni-50Cu versus the larger and lower density of bubbles in Ni-10Cu indicates that the helium bubbles are also trapped by the fine-scaled clusters of like atoms in the alloys. Since the tendency for clustering also increases with decreasing temperature[15] (smaller contribution of the $T\Delta S_m$ term) and during irradiation[19] (radiation-enhanced diffusion), the higher density of bubbles observed in this study versus the relatively low density and alloy composition independent distribution of helium bubbles observed by Zinkle et al.[18], after injecting helium at 0.65 T_m without subsequent irradiation, can also be understood.

In this study, the irradiation of Ni-Cu alloys has been carried out to the maximum peak damage level of ~ 100 dpa, while the damage level has only reached ~ 5 dpa in the helium pre-injected region of the Ni-10Cu and Ni-50Cu specimens. Whether or not the resistance to void formation of the Ni-Cu alloys will be retained under continuous irradiation to high dpa level is not certain. From the point of view of the existence of the high density of dislocation loops, the subsequent formation of voids is unlikely. The vacancies produced by continued irradiation would be more likely to

be incorporated into the loops to make them either grow (in the case of vacancy loops) or shrink (in the case of interstitial loops). However, along with the dislocation loops, small stacking fault tetrahedra (SFT) have also been been found in the irradiated Ni-50Cu samples of this study by weak-beam dark-field TEM, as shown in Figure 6.4; and there has been experimental evidence showing that the stacking fault tetrahedra in the irradiated material can be converted to voids under continuous irradiation[20].

It has been shown in Chapter 5 that the void suppression zone observed in the copper-ion-irradiated nickel specimen (No. 12) overlaps the injected copper range. It is believed that the void suppression is due to the effect of injected copper in the nickel sample, but not due to the simple injected interstitial effect[21]. There are two reasons for that. First, in the nickel-ion-irradiated nickel specimen with the same damage level (No. 11), voids formed throughout the entire damage region; secondly, previous calculations and experiments have shown that the injected interstitial effect is important only at the temperatures $\leq$ 450 °C in 14 MeV heavy-ion irradiated nickel[22]. Although the copper concentration in the ion stopping range of the 14 MeV copper-ion-irradiated nickel specimen is quite low (see Figure 5.34), it is still able to provide sufficient copper clusters to serve as vacancy traps and the nucleation sites for the observed dislocation loops, because the observed loop density is only about five orders of magnitude lower than the density of copper atoms in that region. Whitley irradiated several nickel

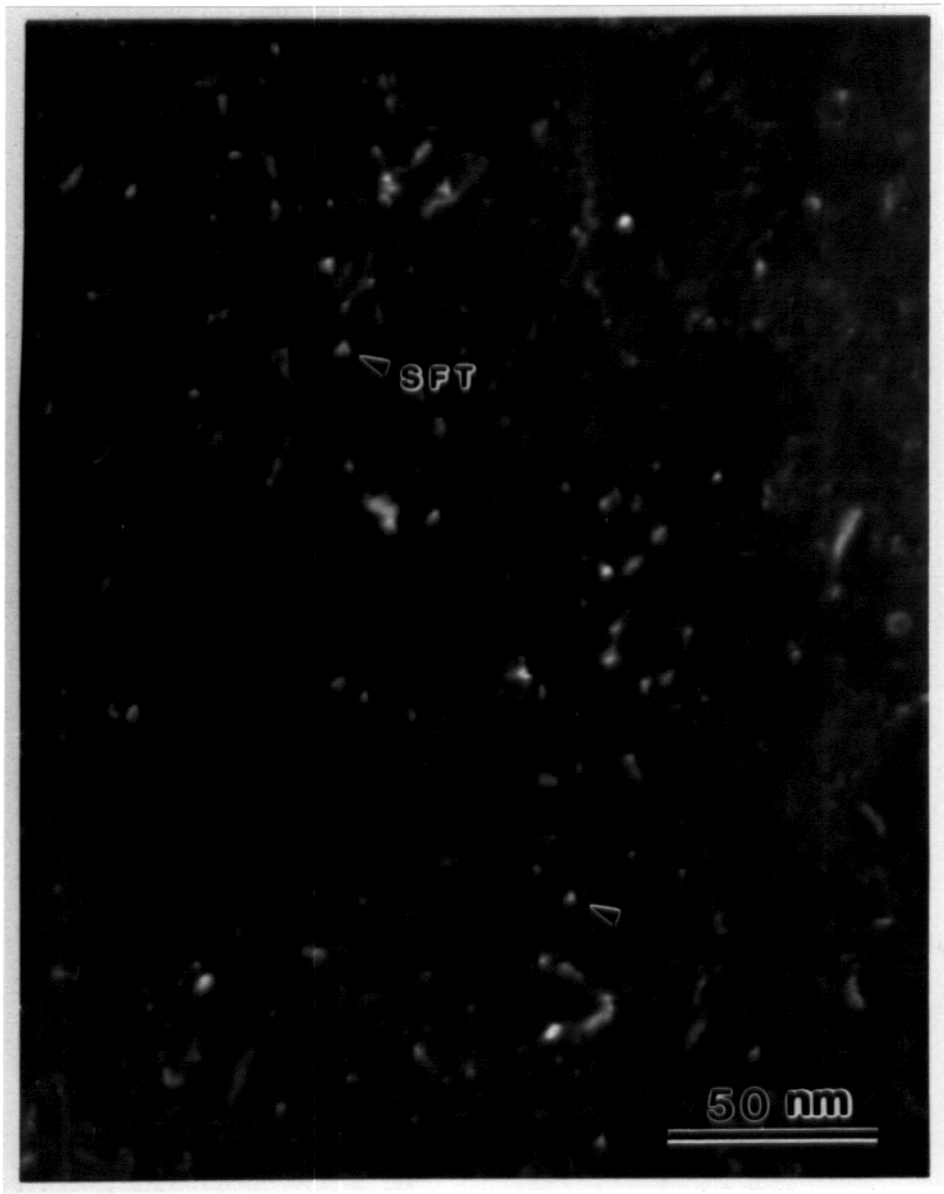

Figure 6.4 Weak-beam dark-field micrograph showing the presence of stacking fault tetrahedra (indicated as SFT) in 14 MeV nickel ion irradiated Ni-50Cu (No. 21, 5 dpa, 425 °C) with 50 appm helium pre-injection.

specimens with 14-19 MeV copper ions at 525 °C[23], but did not see the void suppression in the copper-injected region as noted in this study. That is because all his samples were electropolished before irradiation, and the hydrogen introduced during this process[23] was probably able to help void nucleation and growth even at the very early stage of irradiation. During that same early period not enough copper ions were introduced into his samples for forming clusters to trap vacancies.

C. Extended Ion Damage Range

Most of the end of damage range depth measured from the cross-section micrographs exceed the calculated value, if the ~ 0.3 μm layer, which was removed from the irradiated sample surface during cross-section TEM sample preparation to assure good bounding at the interface, is included in the consideration. Typical radiation damage microstructures, i.e. voids and faulted dislocation loops, were observed in some irradiated samples at depths as far as 0.8 μm (~ 30 %) beyond the calculated end of damage range depth shown in Figures 2.1 and 2.2. The same discrepancy has been reported in many previous cross-section studies on heavy-ion irradiated materials[22-26]. The discrepancy is not believed due to any experimental errors[23-24].

There have been a number of explanations made to account the discrepancy. Farrell et al.[25] have proposed that the discrepancy between observed and calculated damage profiles is primarily due to the neglect of diffusional spreading of point defects in the calculations.

Whitley[23] addressed diffusional spreading also, but argued that it could not account for the magnitude of the discrepancy noted. Whitley[23], Fenske et al.[26] and Bullen[22] have all attributed the extended range observations in nickel to the possible overestimation of the electronic stopping data used to calculated range profiles, because the choice of the available electronic stopping powers is somewhat arbitrary[27], and calculations by Fenske et al.[28] and Attaya[29] have shown that by reducing the electronic stopping value one could explain the anomalous ranges. It is believed that diffusional spreading may be further enhancing this discrepancy[24].

A unique observation from the present study, which seems to be evidence for the diffusional spreading explanation, is that the end of the damage range depth is dependent on the dose of nickel ion irradiations. This is shown in Figure 6.5 for the six 14 MeV nickel ion irradiated Ni-10Cu or Ni-50Cu samples. All these samples were irradiated with an ion flux of ~ $3x10^{16}$ Ni^{3+}/m^2s and at a homologous temperature of 0.45 T_m, i.e. 485 °C for Ni-10Cu and 425 °C for Ni-50Cu. Of course, the length of time during which the irradiation was completed is proportional to the dose which the sample has received. For example, the Ni-10Cu sample which has received an ion dose of $14x10^{19}/m^2$ has been irradiated for 1.5 hrs., while the irradiation for the Ni-10Cu sample which has received $70x10^{19}$ ions/m^2 was completed in about 7.5 hrs. A maximum error of ± 0.15 μm was estimated for the measured depth, as represented by the error bars in the figure, this error is mainly due to the uncertainty in the

thickness which was removed before nickel plating by making the sample anodic in the plating solution. Although no diffusion coefficients are available to justify the arguments, the trend shown in Figure 6.5 at least reinforces the explanation of diffusional spreading qualitatively.

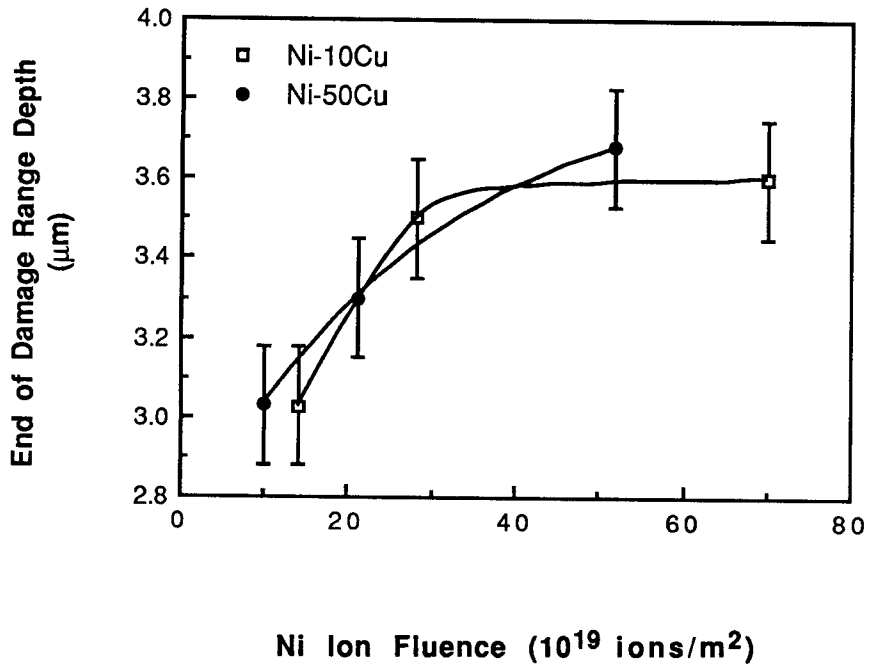

Figure 6.5 The dependence of the end of damage range depth on 14 MeV Ni ion fluence for the irradiated Ni-10Cu and Ni-50Cu (note: the 0.3 μm surface layer, which has been removed during cross-section sample preparation, is included in the depth data of this figure). Irradiation temperature: 485 °C for Ni-10Cu, 425 °C for Ni-50Cu. Ion flux: ~ $3x10^{16}$ Ni^{3+}/m^2s.

References for Chapter 6

1. L.K. Mansur, in Kinetics of Nonhomogeneous Processes, Edited by G. R. Freeman, John Wiley & Sons, Inc., 1987, Ch. 8, p. 430.

2. S.J. Zinkle, L.E. Seitzman and W.G. Wolfer, Phil. Mag. A55 (1987) 111-125.

3. L.E. Seitzman, L.M. Wang, G.L. Kulcinski and R.A. Dodd, J. Nucl. Mater. 141-143 (1986) 738-742.

4. D.J. Mazey and F. Menzinger, J. Nucl. Mater. 48 (1973) 15.

5. P. Barlow, Ph.D. Thesis, University of Sussex (1977).

6. F. Kroupa, Czech. J. Phys. 10B (1960) 284.

7. T. Jossang and J.P. Hirth, Phil. Mag. 13 (1966) 657-670.

8. J.L. Brimhall and H.E. Kissinger, Radiat. Effects 15 (1972) 259.

9. P.J.C. Gallaggher, Met. Trans. 1 (1970) 2429.

10. F. Lihl and H. Wildhack, Z. Metallk. 62 (1971) 143.

11. W.R. Hibbard, Jr., in: Strengthening Mechanisms in Solid, American Society for Metals, Metals Park, OH, 1962, Ch. 1, p. 24.

12. T.B. Massal, in: Physical Metallurgy, R.W. Cahn and P. Haassen, eds., Elsevier Science Publishers B. V., 1983, Ch. 4, p. 213.

13. INCRA Monograph on the Metallurgy of Copper, I. Selected Thermodynamic Values and Phase Diagrams for Copper and Some of Its Binary Alloys (International Copper Research Association, Inc., 1971, Eds. R. Hultgren and P.D. Desai), p. 126.

14. R.A. Swalin, Thermodynamics of Solids, Jhon Wiley & Sons, Inc., 1972, p. 146.

15. J. Vrijen and S. Radelaar, Physical Review B17 (1978) 409-421.

16. A.T. Aldred, B.D. Rainford, T.J. Hicks and J.S. Kouvel, Physical Review B7 (1973) 218-229.

17. R.A. Medina and J.W. Cable, Physical Review B15 (1977) 1539-1551.

18. S.J. Zinkle, R.A. Dodd, G.L. Kulcinski and K. Farrell, J. Nucl. Mater. 117 (1983) 213-217.

19. R. Poerschke and H. Wollenberger, Radiat. Eff. 49 (1980) 225-232.

20. S. Kojima, Y. Sano, T. Yoshiie, N. Yoshida and M. Kiritani, J. Nucl. Mater. 141-143 (1986) 763-766.

21. B. Badger, Jr., D.L. Plumton, S.J. Zinkle, R.L. Sindelar, G.L. Kulcinski, R.A. Dodd and W.G. Wolfer, ASTM STP 870 (1985) 297-316.

22. D.B. Bullen, Ph.D. Thesis, University of Wisconsin-Madison (1984).

23. J.B. Whitley, Ph.D. Thesis, University of Wisconsin-Madison (1978).

24. S.J. Zinkle, Ph.D. Thesis, University of Wisconsin-Madison (1985).

25. K. Farrell, N.H. Packan and J.T. Houston, Radiat. Effect 62 (1982) 39-52.

26. G. Fenske, S.K. Das, M. Kaminsky and G.H. Miley, J. Nucl. Mater. 85 & 86 (1979) 707-711.

27. J. Narayan et al., J. Nucl. Mater. 71 (1977) 160.

28. G. Fenske et al., J. Appl. Phys. 52 (1981) 3618.

29. H. Attaya, Ph.D. Thesis, University of Wisconsin-Madison (1981).

CHAPTER 7

SUMMARY AND CONCLUSIONS

Pure nickel and three concentrated Ni-Cu alloys, namely, Ni-10Cu, Ni-25Cu and Ni-50Cu, with various oxygen (residual or pre-injected) and helium (pre-injected) contents have been irradiated with 14 MeV heavy-ions at the same homologous temperature of 0.45 T_m. The radiation-induced damage microstructures in the irradiated specimens have been analyzed by cross-section transmission electron microscopy.

The specific observations noted in this study and the conclusions that have been drawn from these observations are listed as follows:

1. The residual oxygen plays an important role in promoting void nucleation in ion irradiated nickel. Lowering the oxygen content from 180 appm to 75 appm reduces the void density and increases void size remarkably. For comparative radiation-induced void formation (or swelling) studies, the amount of residual oxygen content should be specified in all future specimens.
2. Voids tend to form in regions with high dissolved oxygen content. The heterogeneity in void distribution observed in as-received (cold-worked) nickel could be attributed mainly to the heterogeneous oxygen distribution.
3. Pre-injection of a small amount (10 appm) of helium enhances the void nucleation significantly in both high (180 appm) and

low (75 appm) oxygen content nickel irradiated to ~ 3 dpa, but the void density in the low oxygen content sample is still much lower compared to that in the high oxygen content sample in the same region with pre-injected helium.

4. Pre-injection of a relatively large amount (30 appm) of helium reduced the observable void density in the high oxygen content nickel (contains 180 appm residual oxygen) irradiated to 3 dpa, by over-nucleating small-sized cavities.
5. Pre-injection of outgassed nickel (still containing 75 appm residual oxygen) with an additional 75 appm of oxygen dramatically increases the void nucleation rate in a region irradiated to ~ 5 dpa.
6. Pre-injected oxygen seems to be more efficient in promoting void formation in irradiated outgassed nickel because it is thought that the injected oxygen is mostly unbound and able to partition readily to void embryos, while most of the residual oxygen left in the outgassed nickel is probably tied up at various kinds of binding sites such as dislocations and grain boundaries.
7. The experimental results on the effect of oxygen in this study support the theoretical model which predicts that oxygen can stabilize voids by reducing the metal surface energy and that gas is necessary for voids to form in nickel.

8. The resistance to void formation of concentrated Ni-Cu alloys is confirmed by 14 MeV nickel ion irradiation of Ni-10Cu, Ni-25Cu and Ni-50Cu, and the results support the previous observations that voids are progressively harder to form with increasing copper content in nickel-rich Ni-Cu alloys.
9. Without oxygen pre-injection, voids formed in irradiated Ni-10Cu (contains ~ 100 appm residual oxygen) only at a dose at ~ 100 dpa with 14 MeV nickel ion irradiation, but no voids were observed in Ni-25Cu and Ni-50Cu (both contain ~ 100 appm residual oxygen) even at that damage level.
10. Pre-injection of 100 appm oxygen promotes void formation in Ni-10Cu at ~ 10 dpa, but showed no effect on Ni-25Cu and Ni-50Cu.
11. Pre-injection of 50 appm helium into Ni-10Cu and Ni-50Cu has little effect on promoting void formation as a result of irradiation with 14 MeV nickel ions to 5 dpa, while pre-injection of 50 appm helium results in copious voids in pure nickel (contains 75 appm residual oxygen) by irradiation to 3 dpa.
12. Small helium bubbles (< 5 nm in diameter) are formed in the region of 50 appm helium pre-injection in both Ni-10Cu and Ni-50Cu, but they did not grow into larger voids during the subsequent nickel ion irradiation. The density of the bubbles increases with the increasing copper content, while the size of

the bubbles decreases concomitantly with the increasing copper content.

13. Most excess vacancies precipitate into dislocation loops in irradiated Ni-Cu alloys regardless of the presence of pre-injected oxygen or small helium bubbles.
14. The density of dislocation loops in the irradiated Ni-Cu alloys increases with increasing copper content and their size decreases with increasing copper content in the investigated composition range.
15. A small amount of implanted copper promotes dislocation loop formation and suppresses void formation in the low oxygen content nickel sample (75 appm residual oxygen) irradiated by 14 MeV copper ions to ~ 100 dpa at the damage peak.
16. The special swelling resistance of Ni-Cu alloys appears to be the result of trapping of gas atoms and vacancies by fine-scaled clusters of like atoms during irradiation.
17. The results of this study support the predictions and observations that there is a tendency for local clustering of like atoms to occur in the Ni-Cu alloys, that the tendency is stronger in a more concentrated Ni-Cu alloy, and that ion irradiation would enhance the clustering process.
18. Radiation induced defect clusters have been observed at depths up to ~ 30% beyond the calculated end of damage range. The observed ion damage range extended to a greater depth when

the irradiating ion dose was increased, and this seems to be an indication of the diffusional spreading of the point defects during continuous irradiation.

The overall conclusions are: (1) both oxygen and helium promote void formation remarkably in ion irradiated pure nickel; (2) addition of copper into nickel promotes dislocation loop formation and suppresses void formation by providing traps for gas atoms and point defects.

Due to the limitations of the experimental conditions of this research, the following future work is suggested for gaining a more thorough understanding on the major topics covered in this thesis:

1. Ultrahigh purity nickel foil which contains less than 5 appm residual oxygen should be irradiated and analyzed to verify the theoretically predicted minimum oxygen level for void stability in nickel.
2. High resolution transmission electron microscopy and analytical electron microscopy should be performed in the irradiated Ni-Cu alloy samples to directly show the local clustering of like atoms and its relationship with the dislocation loop formation.